REPORT DOCUMENTATION PAGE

Form Approved
OMB No. 0704-0188

Public reporting burden for this collection of information is estimated to average 1 hour per response, including the time for reviewing instructions, searching existing data sources, gathering and maintaining the data needed, and completing and reviewing the collection of information. Send comments regarding this burden estimate or any other aspect of this collection of information, including suggestions for reducing this burden, to Washington Headquarters Services, Directorate for Information Operations and Reports, 1215 Jefferson Davis Highway, Suite 1204, Arlington, VA 22202-4302, and to the Office of Management and Budget, Paperwork Reduction Project (0704-0188), Washington, DC 20503.

1. AGENCY USE ONLY (Leave blank)	2. REPORT DATE	3. REPORT TYPE AND DATES COVERED
	2/20/97	Final Tech Report 1 Jul 94, 30 Sep 96

4. TITLE AND SUBTITLE

On a Rational Analysis Methodology for 3-D Braided Fibrous Composites

5. FUNDING NUMBERS

AFOSR - 94 - 0318

6. AUTHOR(S)

Dr. A.S.D. Wang

7. PERFORMING ORGANIZATION NAME(S) AND ADDRESS(ES)

Drexel University, Philadelphia, PA 19104

8. PERFORMING ORGANIZATION REPORT NUMBER

N/A
AFOSR-TR 97-0129

9. SPONSORING/MONITORING AGENCY NAME(S) AND ADDRESS(ES)

AFOSR/NA Bolling AFB Washington, DC 20332 NA

10. SPONSORING/MONITORING AGENCY REPORT NUMBER

94-1-0318

11. SUPPLEMENTARY NOTES

19970314 058

12a. DISTRIBUTION/AVAILABILITY STATEMENT

Distribution Unlimitted

13. ABSTRACT *(Maximum 200 words)*

This final technical report summarizes the research results obtained under the Air Force Office of Scientific Research Grant F-49620-94-0318, which covered the duration from 1 July 1994 to 30 September 1996.

The main objective of this research is to develop a rational analysis approach which compliments the rapidly advancing technology in Textile Composite Materials. Key results rendered are grouped and discussed in seven categories: (1) Modeling yarn architecture in preforms; (2) Local unit-cells and global cell-composition structures; (3) Mechanics modeling for local and global properties; (4) Geometric mapping of fiber architecture due to shape change;(5) Preform braidability and deformability; (6) Experiment and testing; and (7) Correlations between model prediction and test results. Detailed development in each of the categories is contained in the seven papers which are appended as a part of this report.

14. SUBJECT TERMS	15. NUMBER OF PAGES	16. PRICE CODE
	97	

17. SECURITY CLASSIFICATION OF REPORT	18. SECURITY CLASSIFICATION OF THIS PAGE	19. SECURITY CLASSIFICATION OF ABSTRACT	20. LIMITATION OF ABSTRACT
Unclassified			

NSN 7540-01-280-5500

Standard Form 298 (Rev. 2-89)
Prescribed by ANSI Std. Z39-18

DTIC QUALITY INSPECTED 1

DISCLAIMER NOTICE

THIS DOCUMENT IS BEST QUALITY AVAILABLE. THE COPY FURNISHED TO DTIC CONTAINED A SIGNIFICANT NUMBER OF PAGES WHICH DO NOT REPRODUCE LEGIBLY.

1. INTRODUCTION

This final technical report presents a summary of results obtained in the course of research, entitled "On A Rational Analysis Methodology for 3-D Braided Fibrous Composites". The research is conducted under the Air Force Office of Scientific Research Grant AFOSR F-49620-94-0318, for the duration from 1 July 1994 to 30 September 1996.

1.1 Research Objective.

The main objective of this research is to develop a rational analysis approach which compliments the rapidly advancing technology in "Textile Composite Materials".

Of the frontier technological areas in advanced fiber-reinforced composites, development of light-weight, high-strength and high-toughness composites for structural application in extreme temperatures has not been successfully rendered. Despite the recent advances in metallic, intermetallic and ceramic matrix composites, cost-effective manufacturing poses a high order of challenge. In this regard, "textile preforming" as a viable and complimenting solution to cost-effective manufacturing has attracted increased attention. In particular, "preforming" by three-dimensional (3-D) braiding has been seriously explored, as it can produce near-net-shape preforms with an integrated fiber architecture; and the resulting composites are endowed with exceptional mechanical properties. At the present time, however, there exist still many scientific and engineering issues that need intensive research and development. Among the basic and scientific issues are:

(1) Science-based rather than craft-based design methodology by which 3-D preforms with the prescribed near-net shape and the desired fiber architecture can be produced;

(2) The analytical description of the fiber architecture in braided preforms before and after matrix consolidation, especially when the shape of preform is altered during consolidation; and

(3) The realistic modeling of the consolidated preforms for the elementary properties at the local level and the functional performance at the global level.

A related issue concerns two inverse design problems: (a) the braidability of a certain prescribed preform shape; and (b) the deformability of preform from one shape to another shape.

The main objective of this research is to investigate these issues rationally, as it is felt that they will play a vital role in the developing textile composites technology.

1.2. Research Scope.

The present research is both analytical and experimental in scope. It aims to investigate the above-

mentioned basic issues with generic and practical results. The investigation attempts to accomplish the following tasks:

(1) To develop a descriptive method for the general topology of the fiber architecture in 3-D braided preforms. The description must be based on the initial preform design and the steps in the ensuing braiding cycles. The developed method will thus serve as the necessary first link between preform design and the fiber architecture in the as-designed preform. When the as-design preform is actually braided with the specified braiding details, a second link is also needed between the as-braided preform and the fiber architecture endowed within;

(2) To extend the descriptive method developed in (1) in order to account for the fact that braided preforms are often deformed from their initial shape during matrix consolidation. An analytical link between the fiber architecture in the initial shape and that in the final shape must be formulated;

(3) To develop a micromechanics modeling approach to reliably characterize the mechanical properties of matrix consolidated preforms. A unified approach, taking into account the fully described fiber architecture, must be provided for predicting both the local properties and the global responses of the final composite under the applied load;

(4) To validate the descriptive methods developed in (1-3) through a comprehensive experimental correlation study. To this end, preforms of various shapes will be designed, braided, matrix consolidated, mechanically tested and analyzed in correlation with the developed methods; and

(5) To utilize the validated analytical interrelations developed in (1-3) and investigate the inverse design problems of preform braidability and deformability as mentioned above in section 1.1.

Accordingly, the present research is aimed at developing analytical links that connect preform design, braiding and processing, fiber architecture, property characterization and mechanical performance in a closed-loop format.

2. RESEARCH RESULTS.

Key results rendered in the course of the present research are grouped in the following seven categories: (1) Modeling yarn architecture in preforms; (2) Local unit-cells and global cell-composition structures; (3) Mechanics modeling for local and global properties; (4) Geometric mapping of fiber architecture due to shape change; (5) Preform braidability and deformability; (6) Experiment and testing; and (7) Correlations between model prediction and test results.

2.1. Modeling Yarn Architecture In Preforms.

A "control space" method is developed to describe the topology of the braiding yarns in as-de-

signed preforms. This is essentially a simulation of the braiding process in abstract. The method requires the details of the braiding design, including the exact deployment of yarn carriers on the braiding machine, and the specific braiding steps in each braiding cycle. A "control space" is defined as a chosen space above the yarn carriers; during each simulated braiding cycle, yarns are tracing geometrically as they enter into and/or exit from the "control space". The yarns that remain inside the control space after a complete braiding cycle thus form a 3-D skeletal structure; the general topology described by a set of parameters, the values of which remain free at this simulated stage.

Once a preform is actually braided according to the prescribed design and braiding steps, the topology of the resulting fiber architecture is first determined according to the 'control space" simulation as described above. Since the topology is characterized by a set of value-free parameters, the actual fiber architecture in the as-braided preform is yet to be determined. In this regard, the size of the braiding yarns and the degree of yarn jamming during braiding are all important physical factors in defining the actual dimension of the braided preform. A procedure is developed to determine the values of the topology-characterizing parameters based on the final dimensions of the as-braided preform. Consequently, the exact fiber architecture in the final preform is fully described geometrically.

The above 2-stage development provides the necessary linkage from the initial braiding design to the yarn architecture in as-braided preforms.

The "control space" concept was first conceived by Wang [1, 1992]. That conception was a key feature in the proposed study which was later to become the present research. The concept was then implemented in the Ph.D dissertation by Mohajerjasbi [2, 1994] who considered 3-D preforms of Cartesian rectangular cross-sections; and it was further refined and generalized by Wang and Wang [3, 4, 1994; 5, 1995] to include preforms of tubular and more complex cross-sections, such as cross-sections with a curvilinear contour.

2.2. Local Unit-Cells And Global Cell-Composition Structures.

A "convective" approach is developed to identify the smallest representative cells in the braided preform. By "convective" it is meant that the geometric shape of each unit-cell is defined by the yarns which shape the cell's outline. Only then, the shape of the cell will be describable by the same topology-characterizing parameters as that for the overall fiber architecture in the preform. This is important in that when a preform is finally consolidated and the values of the topology-characterizing parameters are determined, it will follow that the geometry of the unit-cells and the yarns in them will be fully described by these parameters as well.

Other important findings in this development include: (a) unit-cells in the preform interior are different from those on the bounding surfaces, although they are related geometrically and are all

characterized by the same set of topology-characterizing parameters; (b) in preforms of curvilinear cross-sections, the unit-cells are spatially variable in shape and the values of the topology-characterizing parameters are also spatially variable; (c) a given preform has a unique composition of the unit-cells; generally the composition is consisted of a core of interior cells and a surface layer which encloses the core, the surface layer being formed by surface cells.

The significance of the unit-cell and cell-composition representation is that the unit-cell provides the basis for extracting local properties of the consolidated preform, and that the cell-composition structure provides the basis for extracting global responses of the consolidated preform to externally applied loading. This is analogous to a local "finite element" in relation to a large structure composed of a mesh of the finite elements.

The above development has been presented in various degree of details in the publications [1-5].

2.3. Mechanics Modeling For Local And Global Properties.

A unified approach was followed to forecast the mechanical properties for preforms after matrix-consolidation. A micromechanics model was applied to extract the local properties for each of the 3-D unit-cells. The model takes into account the exact yarn structure in the cell.

It should be noted that the micromechanics model essentially homogenizes each of the cells; but it does retain the "effective" anisotropic properties. In addition, in preforms of Cartesian rectangular cross-sections, the geometry of the unit-cells are invariant in space, while the geometry of the unit-cells are spatially variant in preforms of curvilinear cross-sections. In essence, each of the cells can be treated as a "3-D finite element" in the conventional sense and the local stiffness matrix can thus be formulated accordingly.

The global properties are structural responses of a particular consolidated preform to the applied loading condition. For example, the bending rigidity of a preform loaded as a beam member, the torsional rigidity of a preform serving as a transmission shaft, etc., are such global properties. The approach taken to forecast this level of response properties is based on the exact cell-composition structure of the consolidated preform at hand. Here, the cell-composition of the overall preform is analogous to a mesh of "3-D finite elements", the elements being the local unit-cells.

The above approach has been applied to model two classes of preforms: preforms of Cartesian rectangular cross-sections and preforms of tubular cross-sections. Major results have been presented in several publications [5], [6, 1995] and [7, 1996].

2.4. Geometric Mapping Of Fiber Architecture.

There exist two situations where the yarn architecture in a preform becomes too laborious and diffi-

cult to describe: to braid a preform of curvilinear cross-section directly in its near-net shape; and to deform a preform of cross-section into complex (curvilinear) ones. The latter is usually achieved during matrix consolidation. Of course, complex shapes can come in ways of direct braiding, post-braiding deformation and both.

To address the issues explained above, a "geometric mapping" concept has been developed. The concept is derived from the analogy that the yarn architecture topology is similar to a system of partial difference equations whose general solutions are provided by the exact braiding procedure; the topology characterizing parameters represents the particular solutions which must be furnished by the preform exterior (boundary) geometric conditions. Thus, the task here is to find the permissible "mapping" which can take the yarn architecture topology from one exterior geometry to another.

Accordingly, in the case where a preform of complex cross-section must be braided directly by a certain braiding procedure, the target shape is given. The issue here is to find the permissible "mapping" function which can take the complex shaped cross-section to one which is simple (say, a Cartesian rectangular one). When this is done, the general yarn architecture topology in the simple cross-section is found using the "control space" method; and that in the complex (target) shape is then determined by the "mapping" function.

Similarly, in the case where a preform of simply shaped cross-section is deformed into a complex shape, the "mapping" to be found is one which can link the geometries of the initial (simple) and the final (complex) shapes.

Detailed mathematical developments for the geometric "mapping" functions between preforms of rectangular and tubular cross-sections has been presented in [3] and more extensively in [8, 1995].

The geometric mapping concept developed here serves as the necessary and analytical linking between the yarn architecture in one shape to that of another shape, provided that certain physical conditions are met by the "mapping" function. These conditions are central to the "braidability" and "deformability" issues. More specifically, preforming of complex shape by direct braiding is an issue of initial braiding design, the heart of which being the "braidability" of the intended shape; preforming by post-braiding deformation is an issue of "deformability", that being to deform the as-braided shape to another (complex) shape.

2.5. Preform Braidability And Deformability.

As explained above, the geometric mapping can provide the analytical determination of yarn architecture in preforms of a complex shape - be it directly braided or post-braiding deformed. In the process, only the permissible mapping function is useful. Thus the issues of preform braidability and/or deformability arise. Both these issues are inverse design problems, as each is concerned with the possibility whether or not preform of a certain prescribed shape could be fabricated by 3-D

braiding at all. Determining such a possibility would require a converging iteration process in which the braiding design, braiding procedure, selection of yarns, control of braiding angles and yarn jamming, the condition of matrix consolidation, etc. are among major influencing factors. The subject was first explored in [8]; it was further investigated in [9, 1996]. Both developments had to make use the topology mapping technique, resulting in a complex optimization process.

2.6. Experiment And Testing.

The experimental study involved three separate phases. The first phase is concerned with the experimental validation of the yarn architectures determined by the "control space" method as described above in section 2.1. Here, several preforms were first braided by the "4-step 1x1" procedure; all were braided with tracer yarns of different colors in order to show the yarn trajectories in space during successive braiding cycles. The helped to establish the accuracy of the "control space" method. Next, the braided preforms were cast in an epoxy matrix in room temperature; and they were sectioned in selected orientations in order to reveal the interior and surface yarn architecture and the cell-composition. The experiment helped to validate the predicted unit-cells and cell-composition structures. This work, however, was not published in the open literature but has been documented in a Drexel University Technical Report [10, 1994].

The second phase is concerned with fabrication and testing of quality specimens for a "baseline" understanding of the local and global properties in matrix consolidated preforms. To this end, six preforms were braided by the 4-step 1x1 method on a semi-automated braiding track at Drexel's Fibrous Composites Laboratory. Three of these were braided using the AS4-G2 12K graphite yarn; and the other three were braided using a 12K E-glass yarn. It should be noted that the size of the glass yarn is an order of magnitude larger than that of the graphite yarn. All the braided preforms were matrix consolidated by the resin transfer molding (RTM) process. This was conducted in collaboration with Boeing Defense & Space Group, Helicopter Division. The matrix consolidated preforms were cut into 16 test specimens suitable for the thermal expansion test and 16 specimens suitable for the 4-point bending test.

In the thermal expansion test, data were collected in the form of the global thermal expansion of the consolidated preforms, and these were used in extracting the thermoelastic constants of the various unit-cells by the predictive models as described above in section 2.3. Determination of the local thermal expansion constants is essential for a realistic estimation of the thermal residual stresses in the cells. The latter is important in delineating the stress states, the mechanisms of deformation and failure.

The 4-point bending specimens were loaded in room temperature all the way to failure. Both local strains on the specimen's surfaces and global responses in the form of bending deflection were recorded as a function of the applied load. Post-mortem examination of the failed specimens was then conducted by sectioning and examining under the scanning electronic microscope (SEM) in

order to delineate the mechanisms of failure at the fiber architectural level. This understanding was essential for the formulation of a failure criterion in the correlation study to be discussed next in section 2.7 below.

The third phase of the experiment was focussed on the design, braiding and matrix consolidation of preforms in various structural shapes. Here, ten (10) preforms were designed and braided using the 12K graphite yarns: four (4) preforms of L-section (each with a certain % of axial yarns); three (3) preforms of U-section (each with a certain % of axial yarns); One (1) preform of I-section (with axial yarns in the flanges; one (1) preform of hollow square section; and one (1) preform with a cross-section resemble an integrated turbine with 8-fans. Each of these preforms are approximately 24 inches long and their cross-sectional areas are between 1 to 2 inch square. These preforms are being matrix consolidated at the time of this reporting.

2.7. Correlations Between Model Predictions And Test Results.

Most of the test results in the Phase-II experiment have been correlated with the pertinent model predictions. Here, two major correlations were undertaken: correlation of the elastic (pre-failure) properties; and correlation of the failure (post-failure) properties.

Correlation of the pre-failure properties followed the approaches outlined in sections 2.1 and 2.2. First, the fiber architecture, unit-cells and cell-composition for each of the specimens tested were determined; the thermoelastic constants in the unit-cells are then calculated following the mechanics modeling approaches outlined in section 2.3. With the above, prediction of the global responses (e.g. deflections under the 4-point bending) was finally rendered for the specimen under the applied load. Both the global thermal expansion and bending deflection in each of the specimens tested could be correlated in this manner. Results were described in detail in [11, 1995].

The post-failure study culminated the formulating a failure criterion, with the help of the failure mechanisms and failure modes observed during the tests. Clearly, the understanding of the yarn architecture, the 3-D local stress and deformation states and the extensive post-mortem SEM work were all necessary in order to reach this point. A full account of this development has been presented in [12,1996].

3. PERSONNEL ASSOCIATED IN THIS RESEARCH

1. Dr. Albert S. D. Wang, Principal Investigator. Albert & Harriet Soffa Professor of Mechanical Engineering, Drexel University.

2. Dr. You-Qi Wang, Research Associate (supported 1 July 1994 to 30 September 95). Dr. Wang continues to collaborate in the research after she became an Assistant Professor of Mechanical Engineering at Kansas State University.

3. Miss Amrita Kumar, Graduate Research Assistant (supported since 1 October 94). Miss Kumar is a full-time graduate student in Mechanical Engineering, Drexel University.

4. Dr. Soheil Mohajerjasbi, Boeing Helicopters Division. Dr. Mohajerjasbi oversees a Boeing in-house program on 3-D braided composites; Boeing collaborates with Drexel in several technical areas, including braiding design of structural shapes, RTM consolidation of braided preforms, etc.

4. PUBLICATIONS STEMMING FROM THIS RESEARCH

(Listed in the order of reference in the text above)

[1] A. S. D. Wang,"The Yarn Structure in 3-D Braided Composites and Evaluation of Their Mechanical Properties," Fiber-Tex '92 - the 6th Conference on Advanced Engineering Fibers and Textile Structures for Composites. October 1992. Philadelphia.

[2] Soheil Mohajerjasbi, "Structure and Mechanical Properties of 3-D Braided Composites," Ph. D. Thesis, Drexel University, 1994 (Thesis Advisor: A. S. D. Wang).

[3] Y. Q. Wang and A. S. D. Wang, "On Topological Mapping of Yarn Structures in 3-D Braided Composites," Proc. American Society for Composites, 9th Technical Conference, Technomic Publishing, 1994. pp. 869-876.

[4] Y. Q. Wang and A. S. D. Wang, "On the Topological Yarn Structure in 3-D Rectangular and Tubular Braided Preforms," J. Composites Science & Technology , Vol. 51, 1994. pp. 575-586.

[5] Y. Q. Wang and A. S. D. Wang, "Spatial Distribution of Yarns and Thermomechanical Properties in 3-D Braided Tubular Composites:, Proc. ICCM-10, Canada. Vol. 4, 1995. pp. 285-292.

[6] Y. Q. Wang and A. S. D. Wang, "Geometric Mapping of Yarn Structures in 3-D Braided Composites due to Shape Change", J. Composite Science & Technology, Vol. 54, 1995.pp. 359-370.

[7] Y. Q. Wang and A. S. D. Wang, "Spatial Distribution of Yarns and Mechanical Properties in 3D Braided Tubular Composites,"Journal of. Applied Composite Materials, Vol. 1, 1996. pp.1-12.

[8] Y. Q. Wang and A. S. D. Wang, "Microstructure-Property Relationships in 3-D Braided Composites," Proc. 1st International Meeting on Mesostructure and Mesomechanics A Specialty Volume, Univ. Toronto, 1994. pp.174-196. Also in Composites Science & Technology, Vol. 53, 1995. pp. 213-222.

[9] Y. Q. Wang and A. S. D. Wang,"Formability of 3-D Braided Composites," Proc. ICAM-96, Beijing, China. 1996. pp.160-167.

[10] A. S. D. Wang,"The Yarn Structure Topology in #-D Braided Preforms," Drexel University Technical Report. 1994.

[11] A. S. D. Wang and S. Mohajerjasbi, "Thermoelastic Properties of 3-D Braided Composites: Predictions and Experiment", Proc. Int'l. Symp. on Innovative Processing and Characterization of Composite Materials", AMD Vol. 211, ASME 1995. pp.275-293.

[12] A. S. D. Wang and A. Kumar, "Stiffness and Strength Properties in 3-D Braided Structural Shapes," to appear in Proc. ICCM-11, Australia, 1997.

5. INTERACTIONS AND TRANSITIONS

5.1. Presentations And Seminars.

* International Mesomechanics and Mesostructures Specialists Meeting, Toronto, CANADA 1994.
* Ninth Technical Conference, American Society for Composites, U. of Del. Sept. 1994
* State University of New York at Stoneybrook, November 1994.
* Workshop on 3-D braided composites, Boeing Helicopters, Eddy Stone, PA. January 1995.
* ASME AMD-MD Summer Conference, UCLA, June 1995.
* International Conference on Composite Materials -10, CANADA, 1995.
* ASME Symp. Innovative Processing and Characterization of Composites, San Francisco, 1995
* Invited Seminar at Drexel University (Chemical Engineering), April 1995.
* Invited Seminar at Industrial Technology and Research Institute, TAIWAN, July 1995.
* Invited Seminar at China Academy of Sciences, Beijing, CHINA, July 1995.
* ASME Mechanics and Materials Conference, John Hopkins U. June 1996.
* International Conference on Advanced Materials -96. Beijing, CHINA 1996.
* ASME Winter Annual Meeting, Atlanta, November, 1996.
* Invited Seminar at Arizona State University, November 1996.
* Invited Seminar at Boeing Helicopters, Eddy Stone, PA. January 1996.
* International Conference on Composite Materials, Australia, 1997 (paper accepted in 96).

5.2. Transitions.

Some key braiding design, analysis methods and experimental results have been made available to Boeing Helicopters. These results have proven useful in evaluating the potentials of 3-D braided composites in helicopter structures applications. Boeing's contact is Dr. Soheil Mohajerjasbi. Close technical collaboration between Boeing and Drexel researchers has been cultivated in other forms,

such as undergraduate co-op at Boeing and Drexel Senior Design Projects with Boeing's technical inputs. The cooperation is being continued.

6. APPENDICES

All papers referred in the text above are available upon request to the Principal Investigator. In order to avoid possible topical duplication, only the key papers are appended in this report for propose of orderly referencing. The appended papers are listed below:

[4] Y. Q. Wang and A. S. D. Wang, "On the Topological Yarn Structure in 3-D Rectangular and Tubular Braided Preforms," J. Composites Science & Technology , Vol. 51, 1994. pp. 575-586.

[6] Y. Q. Wang and A. S. D. Wang, "Geometric Mapping of Yarn Structures in 3-D Braided Composites due to Shape Change", J. Composite Science & Technology, Vol. 54, 1995.pp. 359-370.

[7] Y. Q. Wang and A. S. D. Wang, "Spatial Distribution of Yarns and Mechanical Properties in 3D Braided Tubular Composites," Journal of. Applied Composite Materials, Vol. 1, 1996. pp.1-12.

[8] Y. Q. Wang and A. S. D. Wang, "Microstructure-Property Relationships in 3-D Braided Composites," Composites Science & Technology, Vol. 53, 1995. pp. 213-222.

[9] Y. Q. Wang and A. S. D. Wang,"Formability of 3-D Braided Composites," Proc. ICAM-96, Beijing, China. 1996. pp.160-167.

[11] A. S. D. Wang and S. Mohajerjasbi, "Thermoelastic Properties of 3-D Braided Composites: Predictions and Experiment", Proc. Int'l. Symp. on Innovative Processing and Characterization of Composite Materials", AMD Vol. 211, ASME 1995. pp.275-293.

[12] A. S. D. Wang and A. Kumar, "Stiffness and Strength Properties in 3-D Braided Structural Shapes," to appear in Proc. ICCM-11, Australia, 1997.

ELSEVIER

Composites Science and Technology **51** (1994) 575–586
© 1994 Elsevier Science Limited
Printed in Northern Ireland. All rights reserved
0266-3538/94/$07.00

ON THE TOPOLOGICAL YARN STRUCTURE OF 3-D RECTANGULAR AND TUBULAR BRAIDED PREFORMS

Y. Q. Wang & A. S. D. Wang

Mechanical Engineering Department, Drexel University, Philadelphia, Pennsylvania 19104, USA

(Received 9 April 1993; revised version received 5 November 1993; accepted 17 January 1994)

Abstract

This paper presents an analysis method for the description of yarn structures in 3-D braided preforms. Initially, the general topology of the yarn structure in the preform is determined on the basis of the braiding procedure alone. Then, from the general topology, unit-cell-like substructures are identified in the preform interior and on the boundary. Thus, the total preform is represented as a structural composition of the unit cells.

A full description of the yarn structure topology is necessary for the determination of the final yarn structure after the preform is impregnated with matrix and consolidated into the final shape. In particular, if the final shape is not the same as the initial shape, the yarn structure in the final shape may be obtained by a particular topological mapping procedure.

Preforms of rectangular and tubular cross-section braided by the popular 4-step 1×1 procedure are analyzed as examples. The topology in the respective yarn structures is described in terms of some physically measurable parameters. It is shown that the topological characteristics in both preforms are the same; only the respective characterizing parameters are determined by the specifics in the respective geometric shapes.

Keywords: textile composites, preforming, fiber architecture, topology

1 INTRODUCTION

Fabrication of fiber-reinforced composites by textile braiding methods began to develop in the early 1970s.[1] The initial purpose was to improve the interlaminar property by providing a three-dimensional reinforcement in the composites.[2] Typically, fiber strands or yarns are first braided into a 3-D fabric known as a preform; it is then impregnated with a matrix material and consolidated directly into a structure of the desired shape.

From the material processing point of view, there exists a unique connection between the braiding method used and the resulting yarn structure in the preform. Ideally, this manufacturing–microstructure relationship should be analytically obtainable. Ko,[3] who coined the term 'fiber architecture', was probably the first to study the yarn structure in preforms based on the braiding procedure. In the case of a rectangular preform braided by the 4-step 1×1 procedure, Ko found that a unit-cell–like substructure could be identified which represents the fiber architecture of the entire preform. Figure 1 shows the unit cell identified by Ko; it is a cuboid of square cross-section, oriented in the same reference frame as the preform cross-section, with the depth taken as the braiding pitch (denoted by h). There are four diagonally intersecting yarns in the cell; each is oriented to the braiding axis at an angle γ, known as the braiding angle.

Later, Li[4] performed an experiment using rectangular preforms braided by the same 4-step 1×1 procedure. Li concluded that the preform interior is spanned by four groups of parallel yarns which from two sets of parallel planes and interesect orthogonally (see planes labeled set-a and seb-b in Fig. 2(a)). On alternate planes of each set, parallel yarns are distributed with braiding angles γ and $-\gamma$, respectively, as shown in Fig. 2(b).

Using the two sets of yarn-formed planes as a natural (convected) reference frame, Li could describe the 3-D yarn structure in the interior more easily. For instance, Fig. 3(a) shows the cross-section of the yarn structure along a plane of set-a. From this structure, Li identified a representative unit-cell as shown in Fig. 3(b). The unit cell identified by Li is topologically different from the unit cell by Ko.[3] In particular, the orientation of Li's unit-cells differs from Ko's by a 45° rotation about the braiding axis.

In his experiment, Li also observed that yarn structure on the preform surface is not the same as that in the interior. In fact, subsequent studies conducted by Lei *et al.*[5] and Kostar and Chou[6] further observed that the yarn structure at the preform corners is also unique.

In the present paper, a method is developed to characterize yarn structures in 3-D braided preforms. The developed method involves two major steps. The first step is to establish the general topology of the

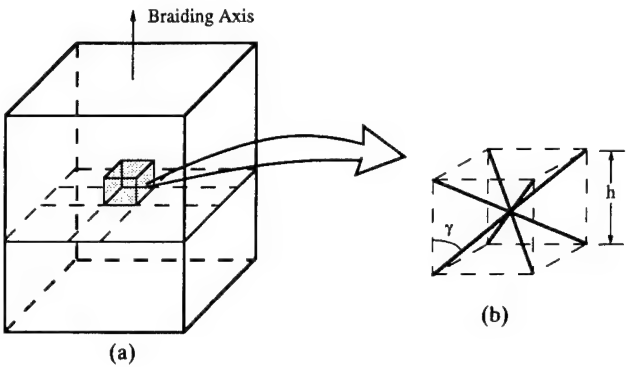

Fig. 1. Interior yarn structure in 4-step 1×1 cuboid preform identified by Ko.[3] (a) The preform; (b) the unit cell.

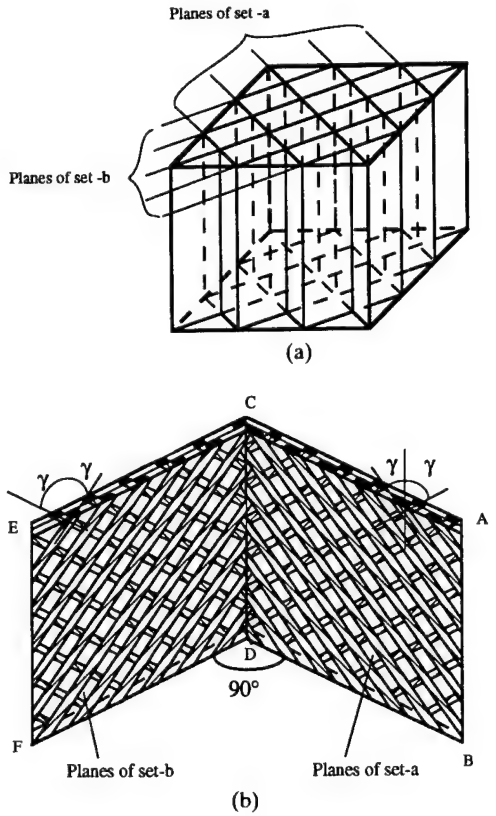

Fig. 2. Interior planes on which yarns distribute (identified by Li[4]). (a) Two sets of intersecting planes in the interior; (b) yarn distributions on alternating planes.

yarn structure based on the braiding procedure alone, the general topology being described in terms of some characterizing parameters. The second step is to relate the characterizing parameters to the final dimensions of the preform after consolidation. This then provides a full description of the yarn structure in the final shape.

It is noted that the topology of yarn structure in 3-D braids likens the skeletal bone structure of a certain animal species. In that context, all animals of the

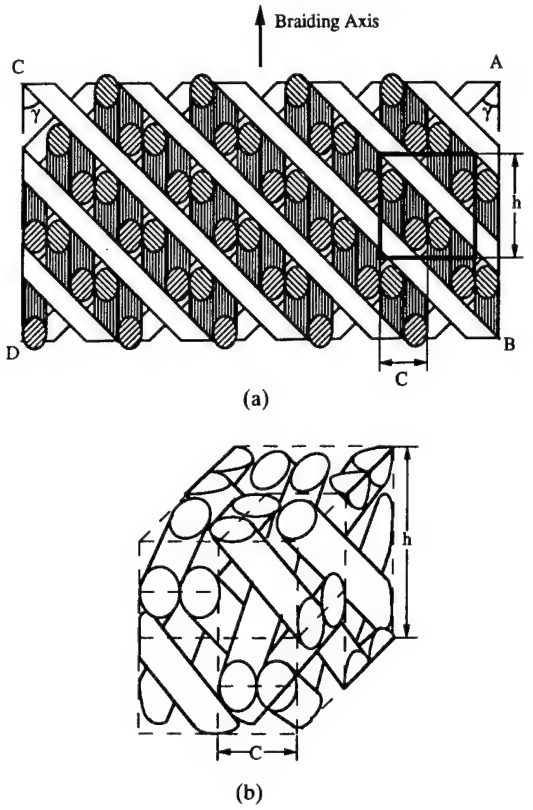

Fig. 3. Schematics of interior yarn structure and the unit cell (identified by Li[4]). (a) Yarn arrangement viewed from cross section-ABCD of Fig. 2(b); (b) the unit cell.

same species have the same skeletal characteristics in the bone structure. Of course, the physical detail in any one bone structure is unique by itself due to the specifics of that structure, such as size and shape. Likewise, the topology of the yarn structure is constitutionally governed by the particular braiding procedure, in that all preforms braided by the same procedure have the same topology. Additional factors such as yarn material, size, texture, and preform shape will influence the yarn structure details but not the general topology.

Thus, it is the purpose here to utilize this particular feature in braided preforms in order to systematically describe the yarn structure in preforms of more complex shapes.

In the interests of clarity, the 4-step 1×1 procedure is used to illustrate the method. Preforms of (solid) rectangular and tubular cross-section are analyzed and their yarn structures described. It is shown that the two preforms have the same yarn structure topology; only their respective characterizing parameters are subject to the specifics of their shapes. In each case, unit-cell–like substructures are identified in the interior, surfaces, and corners; and the total preform is represented by a structural composition of the unit cells.

It is further noted that if the initial shape of the

preform is distorted during consolidation, the resulting yarn structure in the final shape can be obtained by a topological mapping, the mapping being defined by the geometric relation between the initial and the final shapes. The details in the topological mapping procedure, however, are not included in this paper.

2 YARN STRUCTURE IN RECTANGULAR PREFORMS

2.1 The 4-step 1 × 1 braiding procedure

At the outset, it is useful to describe briefly the 4-step 1 × 1 braiding procedure and to introduce the associated terminology. Figure 4 is a schematic illustration of the braiding set-up. The preform being braided is hung above the machine bed on which yarn carriers are arranged in a prescribed pattern. Braiding is realized through the movements of the yarn carriers on the machine bed. In this Illustration, yarn carriers are arranged in a Cartesian column-and-row pattern; hence the resulting preform will have a rectangular (or square) cross-section. The yarn carriers can be arranged in a number of other patterns, such as an I-shape, a U-shape, a tubular shape, etc. In the case of a tubular shape, the carriers are arranged in a radial columns and circumferential rows pattern (see, e.g., Fig. 15).

There are four carrier movement steps in one braiding cycle; in each step, the carriers move only one position along the column or the row directions, hence the name '4-step 1 × 1'. To illustrate, consider the Cartesian pattern shown in Fig. 5. Here, the original carrier pattern is intended for a square cross-section. In the first braiding step, the carriers in the first and third rows move one position to the left,

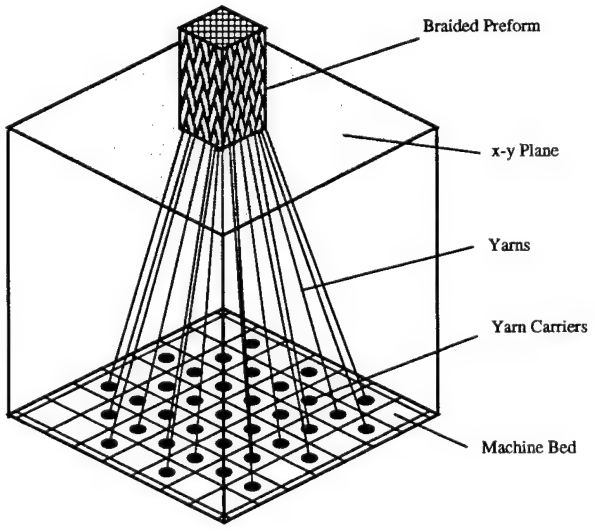

Fig. 4. Schematic of a 3-D braiding set-up.

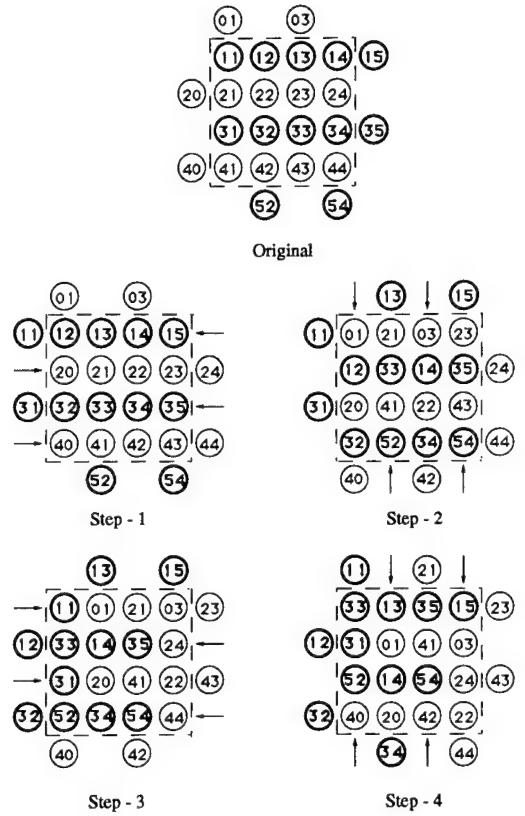

Fig. 5. Yarn carrier movement in one braiding cycle of the 4-step 1 × 1 procedure.

while the carriers in the second and fourth rows move one position to the right. In the second step, the carriers in the first and third columns move one downward, and the carriers in the second and fourth columns move one position upward. The third step reverses the row movements in step-1; the fourth step reverses the column movements in step-2. After these four steps, yarn carriers on the machine bed return to the original pattern, completing a single braiding cycle. During each cycle, the yarns are subjected to a certain 'jamming' action which will make the yarns more or less closely intertwined; the length of the preform so realized is known as the braiding pitch, denoted by h.

The size of the braiding carrier arrangement on the machine bed for a rectangular or a tubular braid is denoted by $[M \times N]$, M being the number of rows and N the number of columns. The actual size of the preform cross-section, however, depends on the size of the yarn used and the yarn-jamming action applied.

2.2 A control volume method

Consider the Cartesian braiding set-up in Fig. 5 and follow the yarn carrier movements for a complete cycle. Figure 6 shows the yarn trace in space during the first 2 steps, where the top plate shows the original carrier positions and the bottom plate shows their

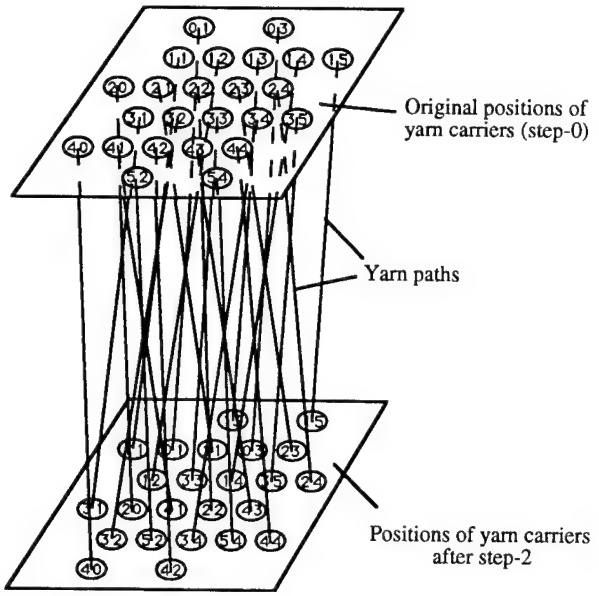

Fig. 6. Yarn paths formed during the first 2 steps.

positions after step-2. The lines connecting the yarn carriers labeled by the same numerals between the plates represent the yarn paths in space. To further obtain a geometric description of the yarns, it is necessary only to examine the yarn paths inside a selected 'control volume'. Specifically, let the space defined by the area enclosed by carriers 31–34 and 41–44 in the original pattern and the depth of four braiding steps be the selected control volume (see Fig. 7(a)). Note that carriers 41, 32 and 43, 34 exchange their respective positions after step-2; and carriers 31, 33, 42, 44 move to positions outside the control volume. Thus, after two steps, only four crisscrossing yarns remain in the upper half of the control volume. Similarly, during the next two steps, four crisscrossing yarns are found in the lower half of the control volume.

When a uniform yarn-jamming action is applied, the yarns will be straightened and repositioned in space. This, in effect, redefines a new control volume as illustrated in Fig. 7(b), i.e. the upper half of the new control volume (with the depth of $h/2$) now consists of two identical units; in each of which there are two crisscrossing yarns. Similarly, the lower half also consists of two identical units; and each contains two crisscrossing yarns.

2.3 Yarn topology in the interior

A close analysis of the units in the upper and the lower halves, see Fig. 8(a), shows that their respective yarn structures are not the same.

Thus, it follows from the above control volume analysis that the preform interior is spanned with four

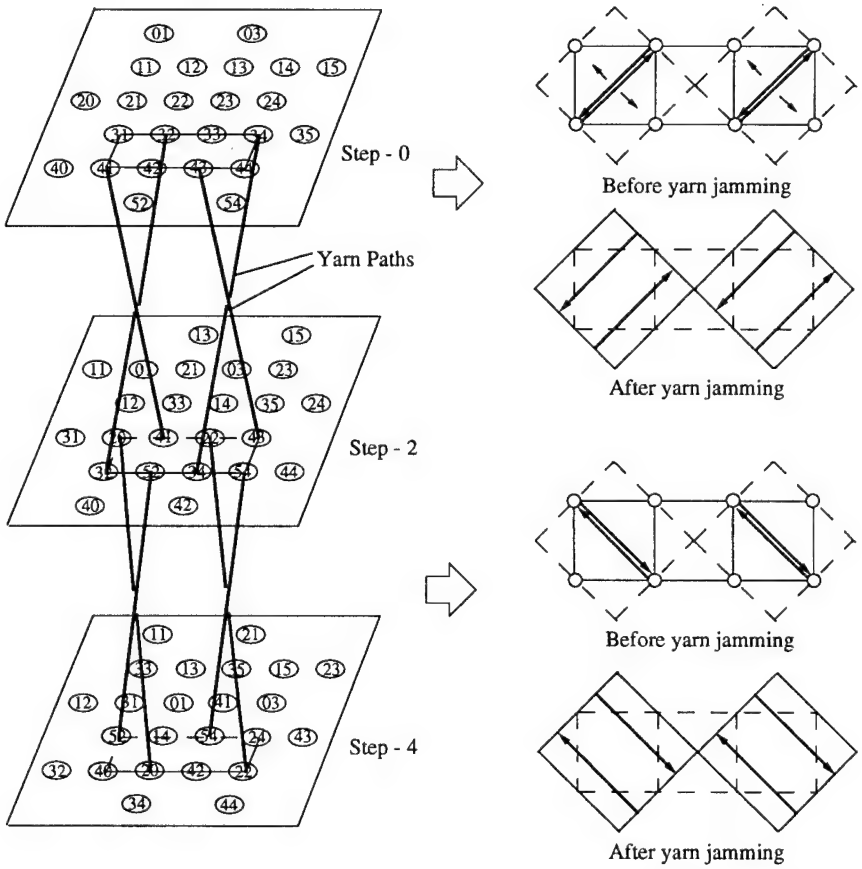

Fig. 7. Yarn trace in the control volume before and after yarn jamming.

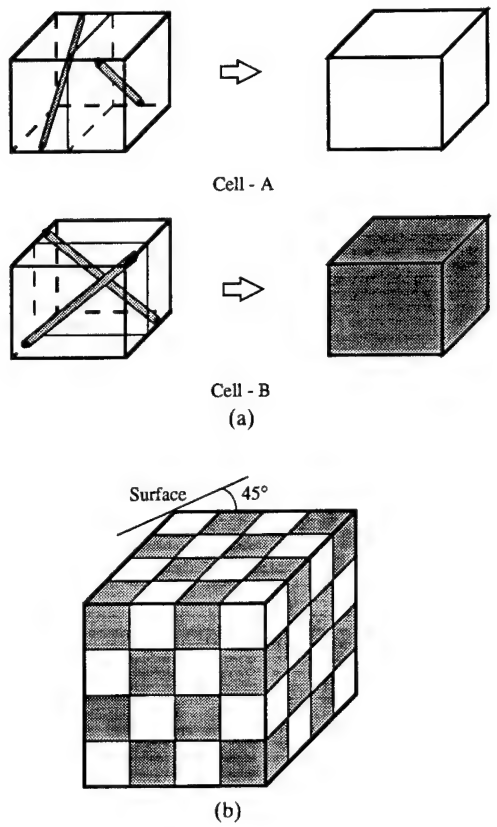

Fig. 8. Unit cells and their arrangement in the interior. (a) Yarn topology in cells A and B; (b) cell arrangement in the preform interior.

groups of yarns, distributed on two sets of parallel planes. These two sets of planes intersect each other at the right-angle, and at 45° with the boundary of the preform. On alternate planes of each set, parallel yarns are distributed with the braiding angle γ and $-\gamma$, respectively. Hence, the braiding pitch h and the braiding angle γ together characterize the topology of the preform interior.

The result above agrees with Li,[4] although the procedure used to reach it here is analytical.

Unit-cells in the interior

Each of the two identical units in the upper half of the control volume shown in Fig. 7(b) will now be designated as cell-A, while that in the lower half will be designated as cell-B. As mentioned, the yarn structure in each cell is unique (see Fig. 8(a)); hence cell-A and cell-B will be considered the smallest building units in the preform interior. Consequently, the preform interior can be represented as a structural composition of these two basic cells, arranged in the alternate pattern illustrated by Fig. 8(b).

The reference frame in which cells A and B are oriented follows the same convected coordinates adopted by Li.[4] However, the unit-cell identified by Li (Fig. 3(b)) is much larger, being composed of four cell-As and four cell-Bs, or 8-times larger than the basic cell identified here.

2.4 Yarn topology on the boundary

Now, focusing on the surface of the preform, an appropriate control surface will be selected instead of a control volume. Return to Fig. 5 and let the control surface be defined by the vertical plane containing carriers 41–44. Yarn carrier movements across the control surface during eight braiding steps are shown in Fig. 9(a). Follow the movement of carrier 42, for example: it exits the control surface from the interior at step-0 and re-enters at step-4. Similarly, carrier 34 exits the control surface after step-2 and re-enters at step-6. This leaves only two groups of crisscrossing yarns on the surface with the inclination angle at $\pm\theta_s$, as shown in Fig. 9(b).

The surface-cell

In actuality, yarns on the surface form a finite-thickness layer, depending on the size of the yarn used. Hence, a unit-cell on the surface can be defined as shown in Fig. 10(a), where the theoretical control surface (ABCD) is the mid-surface of the triangular cell. It can be shown (see Fig. 10(b)) that the yarn inclination angle θ_s is geometrically related to the braiding angle γ of the interior as follows:

$$\tan\gamma = 2\sqrt{2}(\tan\theta_s) \tag{1}$$

It can also be shown that, in preforms of a rectangular cross-section, the same surface cell is found on surfaces of opposing sides; the mirror-image

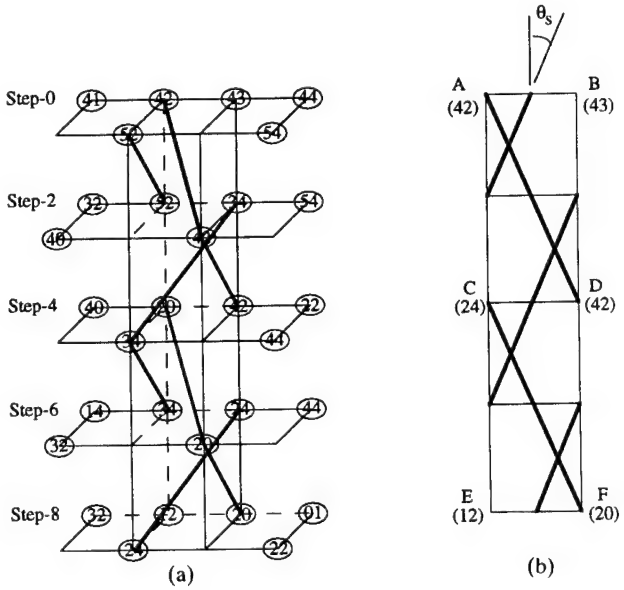

Fig. 9. Yarn trace on the control surface before yarn jamming. (a) Yarn paths on the surface during two braiding cycles; (b) surface yarn pattern on the control surface before yarn jamming.

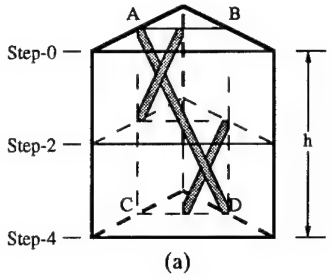

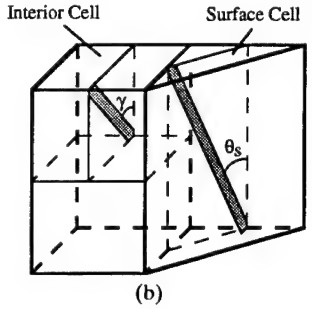

Fig. 10. Topological relationship between the surface and the interior cells. (a) The surface cell; (b) relationship between the inner braiding angle and the surface braiding angle.

of that surface cell is found on surfaces of the other pair of opposing sides.

The geometric yarn pattern on the surface

The yarn topology on the surface can provide an approximate physical look of the preform surface upon yarn jamming. For example, the first frame in Fig. 11 shows the theoretical yarn lines on the surface (thick lines) and the yarn lines in the interior cells behind the surface (thin lines). In the second frame, the yarn lines are replaced by yarns of a finite thickness. After yarn jamming, the yarns on the surface will close up and cover over the interior; then the geometric look of the surface is as shown in the last frame of Fig. 11.

In fact, the surface angle θ_s and the braiding pitch h are easily measured when the preform is finally consolidated. The braiding angle γ, being a quantity in the preform interior, can then be calculated using eqn (1).

Yarn trace at the corners

As already mentioned, the yarn trace at the corners of the preform is unique in itself. Theoretically, the corner is a 90° wedge formed by the bounding surfaces. In actuality, however, the corner is a rounded surface on which inclining yarns distribute. Now, return to Fig. 5 and select the control surface defined by the vertical plane containing carrier 44 and 54. Figure 12(a) shows the carrier movements across this control surface in six braiding steps. Note, for example, that carrier 44 comes onto the control surface from the interior at step-0; it moves outside the surface at step-2, remains outside the surface and shifts a position at step-4; it returns to the surface again at step-6. Upon yarn jamming, the yarn adjusts

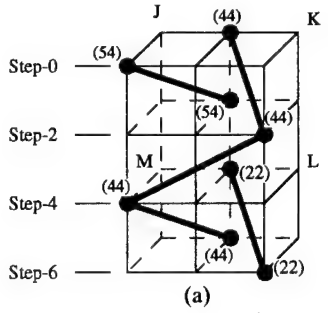

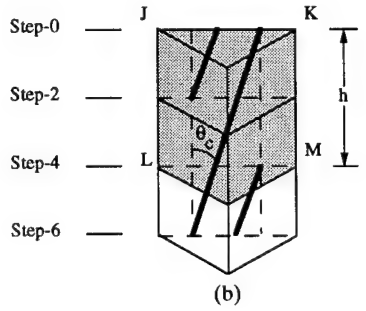

Fig. 12. Yarn trace at the corner and the corner cell. (a) Yarn trace at the corner; (b) the corner cell after yarn jamming.

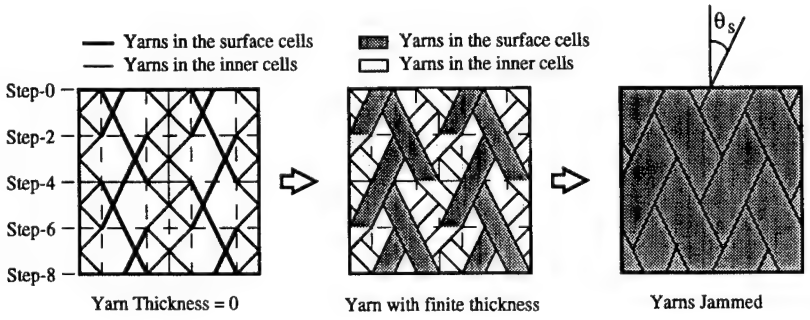

Fig. 11. Yarn structure on the surface before and after yarn jamming.

to the position shown in Fig. 12(b), where the straightened yarn on the control surface inclines with the braiding axis by the angle θ_c. A unit-cell in the form of a triangular prism can thus be defined at the corner as shown in Fig. 12(b).

When the triangular corner cell is fitted geometrically with its neighboring surface cells and interior cells, the following geometric relationship is obtained:

$$\tan \theta_c = (\tan \gamma)/6 \tag{2}$$

Again, due to the square symmetry, the same yarn trace is found at the diagonally opposing corners of the preform; the mirror-image of that yarn trace is found at the other diagonally opposing corners. In any event, it is rather difficult to measure θ_c in actuality, because the actual surface at the corners is curved. Equation (2) can be used to calculate θ_c from knowing γ.

2.5 Cell-composition in overall preform

At this point, the topology of the entire preform has been established, along with the various unit cells identified; all are expressed in terms of the free parameters γ and h. The values of the latter can be measured, given the final dimensions of the preform; so the yarn structure in the preform is fully described. Furthermore, the entire preform is a structural composition of the interior cells (A and B), surface cells, and corner cells. The exact cell composition is easily determined by the carrier arrangement on the machine bed. In the case of a rectangular solid cross-section, for instance, the integer values in $[M \times N]$ determine the exact cell composition. Figure 13(a), as an example, shows the cell composition in a $[6 \times 6]$ preform.

2.6 Topological mapping

The fact that the general topology of a preform is determined by the braiding procedure alone, and that the values of the characterizing parameters can be measured once the final dimensions (or shape) of the preform are established, can be utilized to determine yarn structures in preforms of complex shapes. In particular, if the final shape of the preform is distorted from the initial shape, then a geometric relation between the two shapes may be established. In that case, the characteristics of the topology may be mapped from one shape to the other. Accordingly, the yarn structure (and the unit cells) in the final shape can be obtained from that in the initial shape by a topological mapping.

Clearly, determination of the mapping function between two preform shapes requires a knowledge about the physical process in which one shape becomes the other. To relate the physical condition and to develop the associated mathematical connection are outside the scope of the present paper. A

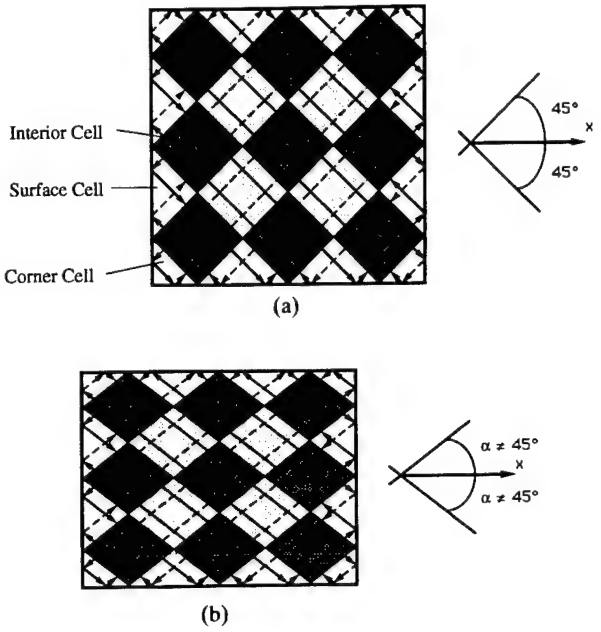

Fig. 13. Cell composition of a $[6 \times 6]$ preform before and after preform distortion. (a) Cell composition in the preform before distortion (top view); (b) cell composition in the distorted preform (top view).

detailed treatment focusing primarily on topological mapping of 3-D braids has been presented elsewhere.[7] In the following, a simple case involving preform deformation is examined just to illustrate the idea of topological mapping.

Consider the preform of square cross-section shown in Fig. 13(a). Upon consolidation, the preform cross-section is deformed into a rectangular cross-section as shown in Fig. 13(b). This is tantamount to a geometric mapping involving a distortion of the cross-sectional area. One result of the distortion is that the two sets of parallel planes, which intersected orthogonally in the interior before, will now intersect at the angle 2α ($\alpha \neq 45°$). So the interior is now characterized by three parameters: h, γ, and α. Another result is that the shapes (cross-section) of the interior cells, surface cells and corner cells will be distorted accordingly. Consequently, the surface cell on the long side will be different from that on the short side.

Now, on the distorted preform surfaces, let the yarn inclination angle on the long side (say, along the x axis) by denoted by θ_x and that on short side (along the y axis) by θ_y. Then, from the cell geometry shown in Fig. 14, the following relationships are obtained:

$$\tan \alpha = (\tan \theta_y)/(\tan \theta_x) \tag{3}$$

and

$$\tan \gamma = 2\sqrt{(\tan^2 \theta_x + \tan^2 \theta_y)} \tag{4}$$

Since the values of h, θ_x and θ_y are measurable

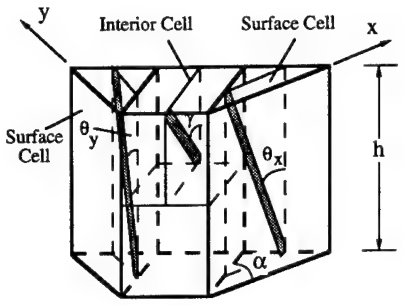

Fig. 14. Relationship between the interior braiding angle and the surface braiding angles.

from the distorted preform exterior, the values of α and γ can be calculated using eqns (3) and (4).

Finally, the fiber volume content in the interior of the consolidated shape can be estimated, given the fiber cross-sectional area A_f for the yarn. A simple computation of the fiber volume in the interior cell and the volume of the cell itself, gives

$$V_f = A_f/(h^2 \tan\theta_x \tan\theta_y \cos\gamma) \qquad (5)$$

It should be noted that, although a square can always be mapped into a rectangle geometrically, the mapping will be subjected to a certain limiting condition once the yarn used is assigned a finite size and limited extensibility. These and other factors influencing preform formability are discussed more fully in Ref. 7.

3 YARN STRUCTURE IN TUBULAR PREFORMS

The 4-step 1×1 braiding procedure can produce preforms of a tubular cross-section. A schematic illustration of the yarn carrier pattern and yarn movements is shown in Fig. 15. By the same control volume and control surface method discussed previously, yarn topology in the preform, along with its unit cells can be similarly established. This will be discussed briefly below.

3.1 Yarn topology in the interior

Figure 16 shows the first-quadrant top view of a $[5 \times 32]$ tubular braid with the yarn trace after one braiding cycle. Here, the yarn trace during the first two steps is indicated by solid lines and that of the last two steps by dahsed lines. After a complete cycle, the yarns in the interior form two families of parallel curved surfaces: one is labeled as surface-a and the other as surface-b. These two families of curved surfaces crisscross at an angle of 2β locally; the value of β varies radially. In order to define this local quantity, consider the circumferential surface of radius r; and let the angle between a curved surface and the cylindrical surface of radius r be denoted by α. Then, $\beta = \pi/2 - \alpha$ (see inset, Fig. 16).

On each curved surface, there is distributed a group of parallel yarns with an inclination angle γ; on the adjacent surface of the same family, there is distributed a group of parallel yarns with the angle $-\gamma$. Thus, yarns are distributed on the surfaces of family-a or family-b with alternating braiding angle γ and $-\gamma$. Since the curved surface spirals radially, γ will vary radially.

At this point, given h, α, and γ as free parameters, the interior yarn structure topology of the tubular preform is fully characterized. While the value of h can be measured from the preform exterior, the values of α and γ, which are functions of the radial position r, remains yet to be determined and related to quantities measurable from the preform surfaces.

Unit cells in the interior

Now, by observing the yarn distribution shown in Fig. 16, the crisscrossing planes of family-a and family-b form a natural (convected) coordinate system. From this reference frame, two basic unit cells are again identified: cell-A (dark shade) and cell-B (light shade). Figure 17(a) shows the yarn traces in cell-A and cell-B. The cell arrangement in the interior is shown in Fig. 17(b).

3.2 Yarn topology on the surfaces

By the same control surface procedure discussed earlier, yarn topology on the inner and the outer surfaces of the preform can be established. The unit cells on the inner and the outer surfaces are shown in Fig. 18(a), with the yarn inclination angle of the inner surface denoted by θ_{is} and that of the outer surface denoted by θ_{os}. When the inner (or the outer) surface cell is pitted against its neighboring interior cells, a certain topological relationship between the angle β and angle θ_{is} (or θ_{os}) exists (Fig. 18(b)). By specifying a finite thickness for the yarn and by applying yarn-jamming, an approximate geometric look of the surfaces can be obtained as illustrated in Fig. 18(c).

3.3 Evaluation of the characterizing parameters

At this point, the yarn structures in the interior and on the inner and outer surfaces are characterized in terms of five parameters: α, γ, h, θ_{is}, and θ_{os}. Of the five, only h is indepdent of the radial position r. In the following, an explicit expression for α and γ as a function of r will be determined, along with the definition for θ_{is} and θ_{os}.

Returning to Fig. 16, the cross-section of the tubular braid consists of a layer of inner-surface cells, a layer of outer-surface cells, and rows of the interior cells of type A and B. Now, let R_i and R_o be the inner and the outer radius of the tube, respectively; then, the thickness of the tube is $t = R_o - R_i$. It is further assumed here that each layer of the interior cells has a

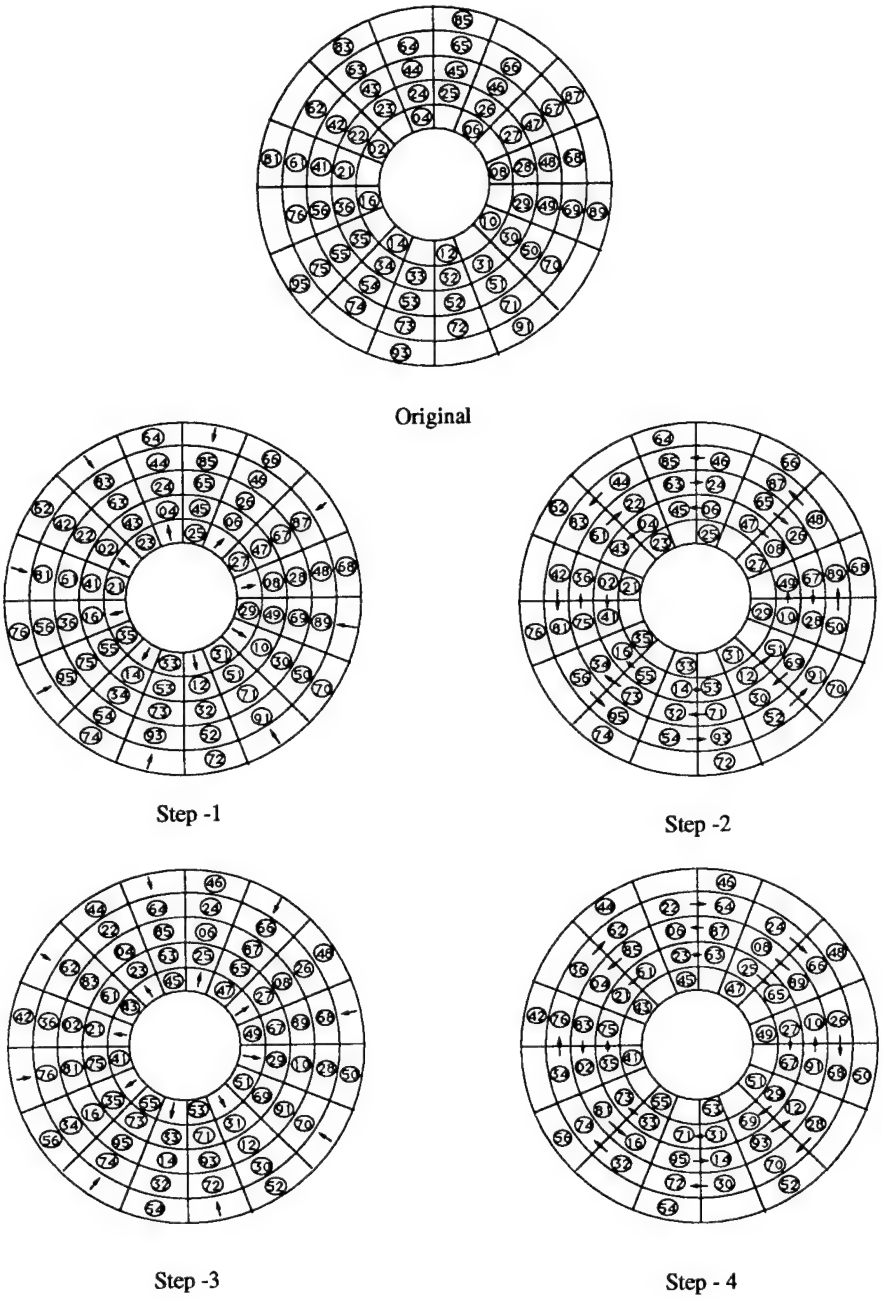

Fig. 15. Yarn carrier movement in one braiding cycle for a tubular braid.

thickness of $2\Delta r$ (the implication of this assumption vis-a-vis other similar assumptions is discussed in Ref. 7). Then the following can be written (see Fig. 19(a)):

$$t \approx M\Delta r \tag{6}$$

where M is referred to $[M \times N]$, being the number of circumference rows of the braiding carriers.

Yarn orientation angles: $\alpha(r)$ and $\gamma(r)$

Figure 19(a) shows the cross-section of an interior cell denoted as $ABCD$. The radial thickness of the cell is the length BD $(=2\Delta r)$; the circumferential width is the circular arc AC, whose radius is r. The angle facing are AC is denoted by $2\Delta\phi$, where $\Delta\phi = 2\pi/N$ (N is referred to $[M \times N]$, being the number of radial columns). The curved surface a–a', on which yarns distribute, intersects are AC at the angle $\alpha(r)$. The local geometry can be further simplified as shown in Fig. 19(b); then the following approximate relationship is obtained:

$$\tan(\alpha) = \Delta r/[r \sin(\Delta\phi)] \tag{7}$$

On the curved surface a–a', the yarns orientate with the braiding angle $\gamma(r)$ as shown in Fig. 19(c).

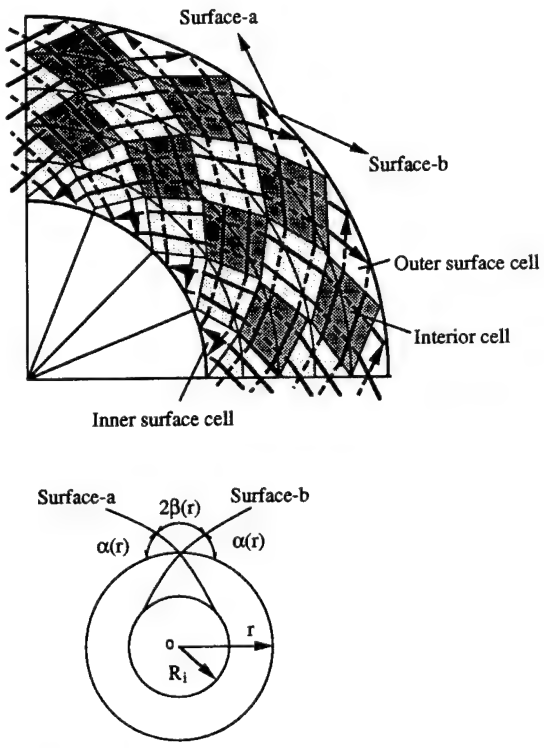

Fig. 16. Yarn topology and cell composition of a tubular braid.

Then

$$\tan(\gamma) = 2\Delta r/[h \sin(\alpha)] \tag{8}$$

Finally, yarn inclination angles on the inner and the outer surfaces can be expressed as

$$\tan(\theta_{is}) = 2\pi R_i/(Nh); \quad \tan(\theta_{os}) = 2\pi(R_o)/(Nh) \tag{9}$$

In summary, the yarn structure of the entire tube is now fully characterized; five external parameters must be given: M, N, R_i, R_o, and h. From them, explicit expressions for $\alpha(r)$, $\gamma(r)$, θ_{is}, and θ_{os} can be calculated using eqns (7), (8), and (9).

Fiber volume content $V_f(r)$

Given the solid cross-sectional area of the yarn, A_f, the fiber volume content in the interior cells can be estimated. From Fig. 19, the cross-sectional area of the cell is $(2r)(\sin\Delta\phi)(2\Delta r)/2$. The fibers in the cell have the total cross-sectional area $2A_f/\cos\gamma$. Thus, the fiber volume content of the cell, or that of the interior, is

$$V_f(r) = A_f/[r \sin\Delta\phi\ \Delta r \cos\gamma] \tag{10}$$

3.4 Radial characteristics of α, γ, and V_f

The parameters α, γ, and V_f vary radially. This implies that the properties of the preform also vary radially. For this reason, a brief investigation of the radial characteristics of these three parameters is given below.

Let the following be defined at the mid-thickness of the tube at $r_m = (R_i + R_o)/2$:

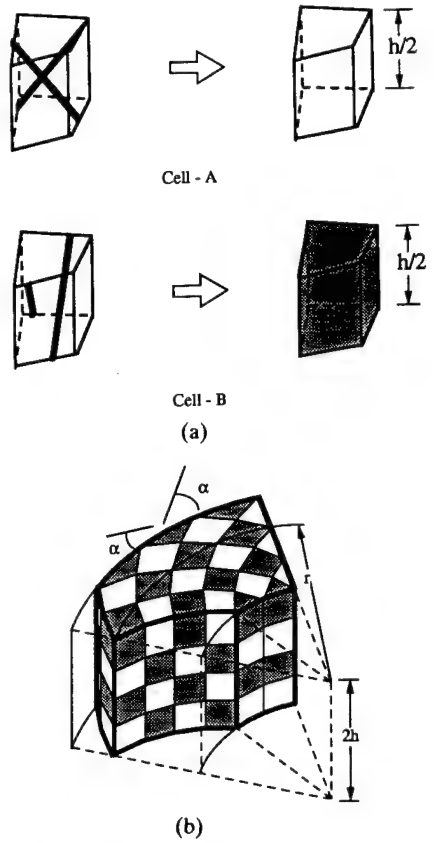

Fig. 17. Unit cells and their arrangement in the interior of the tubular braid. (a) Yarn topology in cells A and B; (b) cell arrangement in preform interior.

$$\alpha_m = \alpha(r = r_m); \quad \gamma_m = \gamma(r = r_m); \quad V_{fm} = V_f(r = r_m) \tag{11}$$

where the expressions for α_m, γ_m, and V_{fm} can be obtained using eqns (7), (8), and (10), respectively.

Introducing the non-dimensional numbers

$$\begin{aligned} K &= (Nt)/(Mr_m); \\ J &= (tr_m)/(MNh^2); \\ G &= (MNA_f)/(tr_m) \end{aligned} \tag{12}$$

it follows from eqns (7), (8), (10), and (11) that for very large N

$$\tan(\alpha_m) \approx K/2\pi; \quad \tan(\gamma_m) \approx 2\sqrt{[(4\pi^2/K) + JK]} \tag{13}$$

$$V_m \approx 2G\sqrt{[(JK/4\pi^2) + (J/K) + (1/16\pi^2)]} \tag{14}$$

The variation of α, γ, and V_f with the variable r can be expressed in terms of their respective mid-thickness values as:

$$\begin{aligned} &\tan(\alpha)/\tan(\alpha_m) = (r_m/r) \\ &\tan(\gamma)/\tan(\gamma_m) = (r/r_m)\{\sqrt{[(2\pi/K)^2 + (r_m/r)^2]}/ \\ &\qquad [\sqrt{(2\pi/K)^2 + 1}]\} \\ &V_f/V_{fm} = (r_m/r)\{\sqrt{[JK + (\tfrac{1}{4}) + (4\pi^2 J/K)(r/r_m)^2]}/ \\ &\qquad \sqrt{[JK + (\tfrac{1}{4}) + (4\pi^2 J/K)]}\} \end{aligned} \tag{15}$$

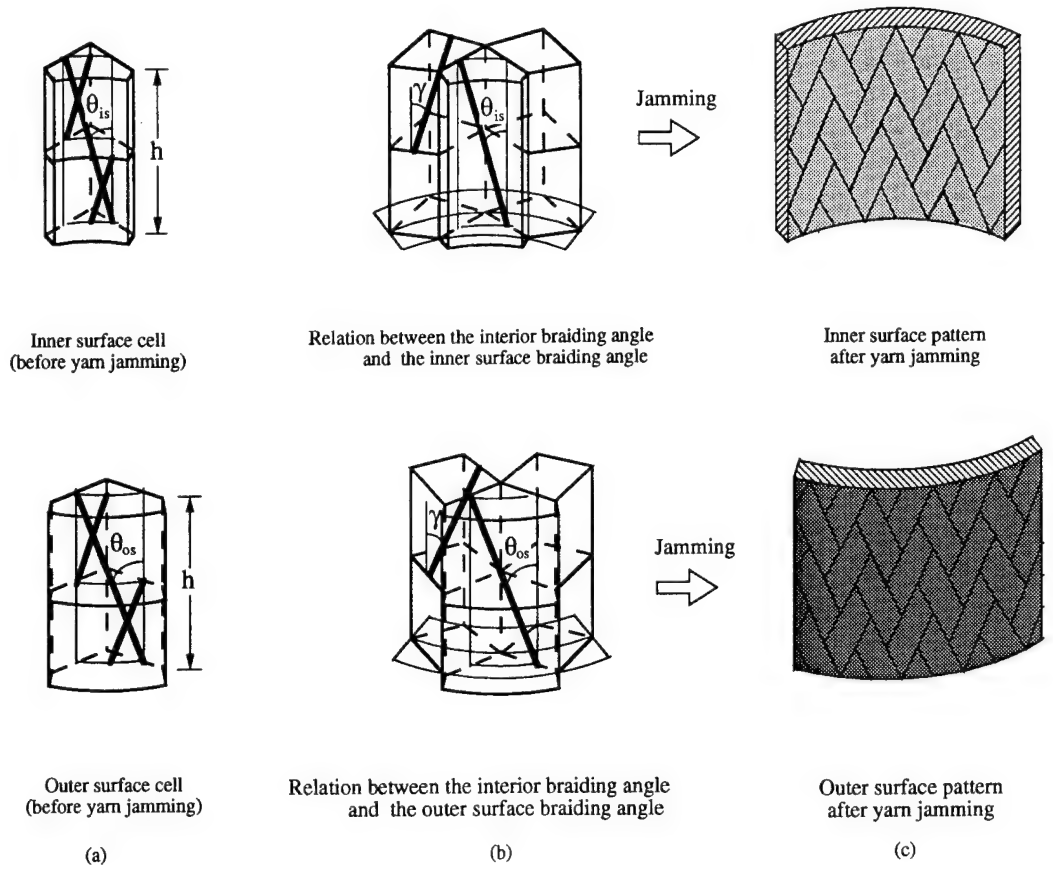

Fig. 18. Yarn structure on the surfaces of the tubular braid.

From the first term in eqn (15), it is readily seen that $\tan(\alpha)$ varies inversely with r; or α has the largest value near the inner surface of the tube and it decreases outwardly with r. Variation of $\tan(\gamma)$ and V_f as a function of r is shown in Fig. 20. Generally, the braiding angle γ increases radially and V_f decreases radially from the inner to the outer surface, roughly as the inverse of r.

In the plots in Fig. 20, the non-dimensional parameters K and J are assigned a range of values to show the dependence of γ and V_f on K and J. It is seen that K and J impose very little effect on γ and V_f over a wide range of r.

4 CONCLUDING REMARKS

In this paper, a general method is presented to describe the yarn structure inside 3-D braided preforms. This is done by determining first the topological structure formed by the yarns in space during the braiding process. A control volume and/or control surface procedure is adopted to trace the yarn positions in space. It is demonstrated that the braiding method alone determines the yarn structure topology; the values of the characterizing parameters are dependent on the specifics of the preform, including the preform shape, the yarn used, yarn jamming, preform consolidation, and the final dimensions of the preform.

It is observed that preforms having the same topological characteristics may be mapped from one shape to another. This subject bears the importance of the formability of preforms in actual use. Some specific cases involving topological mapping and conditions of formability have been discussed in Ref. 7.

From the overall yarn structure in the preform, distinctive unit cells can be defined in the preform interior and on its boundary; so the preform as a whole is a structural composition of the various cells. It should be noted that substructuring of a 3-D preform in terms of small unit cells is essential for property characterization. A treatment of this subject has been reported elsewhere.[8]

As illustrative examples, 3-D preforms of rectangular and tubular cross-section braided by the 4-step 1×1 method are analyzed in detail. As these are braided by the same procedure, the yarn structure topologies in both are shown to be the same, although the square corners in the rectangular sections require a special treatment, and the curvilinear nature of the tubular section causes the characterizing parameters

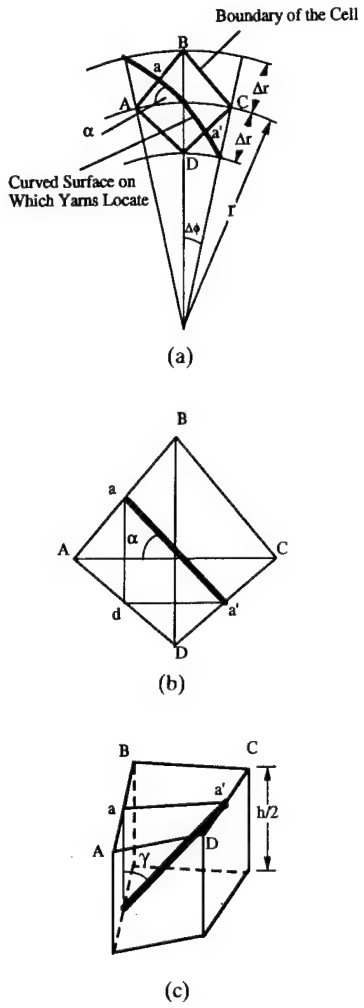

Fig. 19. Orientations of yarns in the interior cell. (a) Geometric relation of an interior cell (ABCD); (b) approximate relationships inside the cell (top view); (c) approximate relationships inside the cell (isometric view).

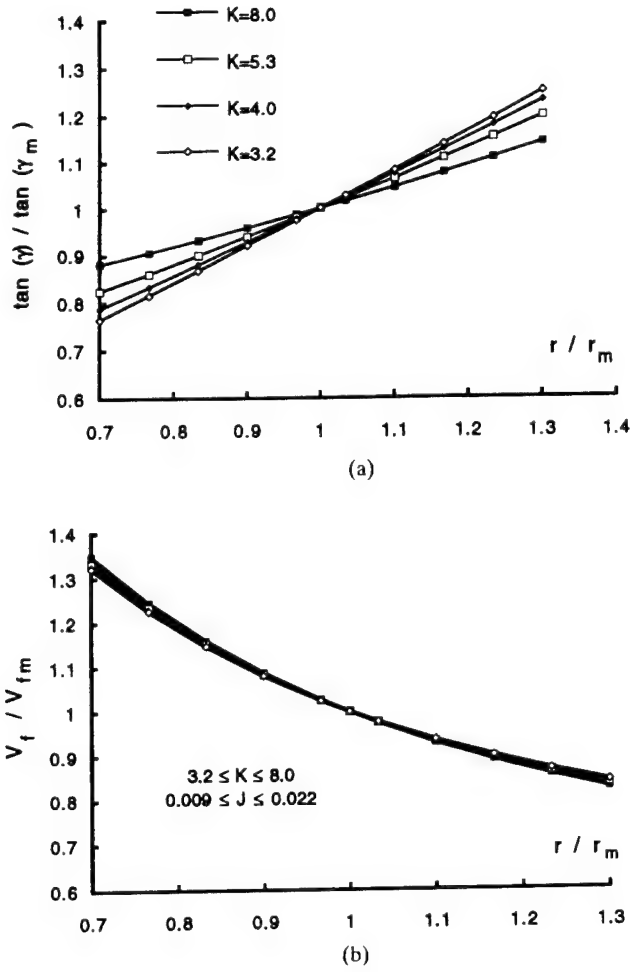

Fig. 20. Radial dependence of γ and V_f on r. (a) The variation of $\gamma(r)$; (b) the variation of $V_f(r)$.

to vary radially. From these results, the existence of a geometric mapping between the two preforms is quite evident; for further exploration into this subject, see elsewhere.[7]

REFERENCES

1. Stover, E. R., Mark, W. C., Marforwitz, I. & Mueller, W., Preparation of an omniweave reinforced carbon–carbon cylinder as a candidate for evaluation in the advanced heat shield screening program. AFML-TR-70-283, Wright-Patterson AFB, Ohio, March, 1971.
2. Popper, P. & McConnell, R. F., A new 3-D braid for integrated parts manufacturing and improved delamination resistance—The 2-step process. *Proc. 32nd Int. SAMPE Symp. & Exhibition,* **32** (1987) 92.
3. Ko, F. K., Three dimensional fabrics for composites—An introduction to the Magnaweave structure. *Proc. ICCM-4, Japan Soc. Composite Materials,* Tokyo, Japan, 1982, p. 1609.
4. Li, W., On the structural mechanics of 3-D braided preforms for composites. PhD Thesis, North Carolina State University, USA, March, 1990.
5. Lei, C., Cai, Y. J. & Ko, F. K., Finite element analysis of 3-D braided composites. *Advances Engineering Software and Workstations.* Elsevier Science Publishers, 1992, p. 187.
6. Kostar, T. D. & Chou, T. W., Design and automated fabrication of 3-D braided preforms for advanced structural composites. In *Composite Materials Technology III,* Elsevier Science Publishers, 1992, p. 63.
7. Wang, Y. Q. & Wang, A. S. D., On topological mapping of yarn structures in 3-D braided preforms. In *Proc. 9th Annual Meeting, American Society for Composites.* Technomics, 1994.
8. Wang, Y. Q. & Wang, A. S. D., Microstructure–property relationships in 3-dimensionally braided fiber composites. *Proc. Mesostructure & Mesomechanics Specialist Meeting,* ed. M. R. Piggott. Univ. Toronto, Toronto, Canada, 1994, p. 174.

ELSEVIER

0266-3538(95)00059-3

Composites Science and Technology **54** (1995) 359–370
Elsevier Science Limited
Printed in Northern Ireland

GEOMETRIC MAPPING OF YARN STRUCTURES DUE TO SHAPE CHANGE IN 3-D BRAIDED COMPOSITES

Y. Q. Wang* & A. S. D. Wang

Department of Mechanical Engineering, Drexel University, Philadelphia, Pennsylvania 19104, USA

(Received 12 October 1994; revised version received 27 March 1995; accepted 10 April 1995)

Abstract

The internal yarn structure in 3-D braided preforms possesses a certain topological character which is unique to the braiding method used. Hence, preforms of different shapes but braided by the same method have topologically similar yarn structures. This unique property offers the possibility that the yarn structure in preform of one shape may be geometrically mapped to that in another shape, and vice versa.

This study discusses a geometric mapping methodology, the objective of which is to obtain the appropriate mapping which analytically links the yarn structures in two preforms of different shapes; if the yarn structure in one preform is known, the yarn structure in the other can be determined by the derived geometric mapping.

Two broad classes of mapping are discussed. The first concerns mapping between two preforms that are braided directly in two different shapes; the second concerns mapping between the initial and final shapes of one single preform which is deformed after braiding. In each case, the mathematical forms of the desired mapping functions are obtained, satisfying the geometric constraints imposed by the internal yarns in the respective preforms. The determined mapping functions are then used to investigate the braidability and/or deformability of the considered preforms. Specifically, limiting windows for the braiding parameters that insure the braidability and/or deformability of the preforms are obtained using the appropriately derived mapping functions.

The 4-step 1 × 1 braiding method is used throughout this paper to illustrate the general mapping procedure; rigorous and explicit geometric relationships are derived leading to mapping functions between preforms of rectangular and curvilinear cross-sections. Numerical examples involving mapping between preforms of rectangular and tubular cross-sections are investigated in detail, along with examination of the preform braidability and/or formability.

*Present address: Department of Mechanical Engineering, Kansas State University, Manhattan, Kansas 66506, USA.

Keywords: 3-D braided preforms, yarn structure topology, geometric mapping, preform braidability and formability

1 INTRODUCTION

In recent years, modern textile technologies have been applied to the manufacture of near-netshape composite structures and/or components. Typically, a fabric preform is first produced with the desired near-netshape from yarns or fibers by a certain textile procedure; the preform is then impregnated with a binding material and consolidated to form and function as a structure or a structural part. Yarns made of advanced fibers (glass, carbon, Kevlar, SiC, etc.) have been used to produce simple and complex shaped preforms; binding materials of polymeric, metallic and ceramic nature have been used to consolidate the preforms into composites.[1]

Three-dimensional (3-D) braiding can produce preforms with spatial distribution of yarns in all directions; the exact yarn structure (distribution and orientation) depends on the procedures of braiding as well as on the details of composite consolidation. From the standpoint of preform design and property characterization, knowledge of the precise yarn structure in the final composite is an essential first requirement.

A series of recent articles[2,3] have detailed a method for geometrically describing the yarn structure in 3-D braided preforms. First, the general topology of the yarn structure is determined based on the actual braiding procedure alone; the topology is characterized by a set of physical but value-free parameters. Then, given the exterior dimensions of the preform, the values of the topology characterizing parameters can be determined by measuring certain physical features on the preform exterior.

For preforms of simple geometric shapes, the method described above is fairly easy to follow. In engineering practice, however, 3-D braided composites can have complex shapes. There are two basic

ways of making complex shapes: namely, to braid and consolidate the preform directly into the desired complex shape, and to braid the preform with a simple shape and then consolidate it into a complex shape. In either case, it can be a cumbersome task to describe the exact yarn structures in these preforms.

In fact, braided composites shaped in these different ways have distinct internal yarn structures, even if their final shapes and exterior dimensions are exactly the same. This is due to the difference in the internal yarn constraints during the shaping process. Specifically, preforms braided directly are subjected to a uniform yarn jamming, a condition of yarn tightening during braiding. This makes the yarns more or less uniformly spaced inside the preforms. On the other hand, preforms that are deformed after braiding are subjected to readjustment of yarn positions in space, resulting in non-uniform yarn spacing.

These yarn constraining factors also play a vital role in the braidability and/or deformability of a preform with a certain shape. These concerns arise during the early stage of preform design, as factors of yarn selection, braiding set-up, matrix consolidation, yarn distribution and composite property tailoring must be considered integrally.[4]

In has been shown[2] that preforms braided by the same procedure but with different shapes have topologically similar yarn structures; the question was raised as to whether the yarn structure topology in preform of one shape can be geometrically mappable to that of another shape. Such a mapping, if it exists, can then facilitate the determination of yarn structures in preforms of complex shapes.

Thus, the main objective of the present paper is to develop a general methodology for the determination of the permissible mapping between two preforms that have topologically similar yarn structures but with different shapes. In what follows, preforms braided by the 4-step 1×1 procedure will be used to develop the logical steps in specific terms that lead to the determination of the desired mapping functions. The focus is placed on mappings between preforms of rectangular and curvilinear cross-sections. Explicit results are then generated for special cases, involving preforms of rectangular and tubular cross-sections. With the aid of the determined mapping functions, the related issues of preform braidability and deformability are examined in some detail.

2 BRAIDING, YARN STRUCTURES AND GEOMETRIC MAPPING

2.1 Braiding procedure and yarn structure

The unique relationship between a braiding method and the resulting yarn structure topology in preforms will be briefly discussed; the 4-step 1×1 method is chosen due to its being widely discussed in the literature.[1]

Figure 1 shows a schematic set-up for the 4-step 1×1 braiding. The preform being braided is hung above the machine bed, on which yarn carriers are arranged in a row-and-column pattern. The pattern is customarily denoted by $[M \times N]$, M being the number of carriers in a row and N the number of carriers in a column. Hence, M and N constitute the defining parameters of the braiding set-up. Braiding of the preform is realized through the movements of the yarn carriers along the row and column tracks. There are four carrier movements in each braiding cycle, during which yarns criss-cross in space, and, after subjecting the crossing yarns to a certain 'jamming' (tightening) action, a finite braided length is then realized known as a 'pitch'. The yarn structure so formed during one braiding cycle will repeat itself in each successive cycle.

The topology of the yarn structure can be described geometrically by considering the yarn as a line only.[2,3] By tracing the yarn line positions in a 'control space' during one or more braiding cycles, the relative geometric positions of the yarns in space can then be determined. In this way, the yarn topology can be characterized by a set of physical parameters whose values will remain undetermined until the dimensions of the preform in question are finalized. The following gives a brief summary of the above, using two specific examples.[2,3]

2.1.1 Cartesian braids

When the row-and-column carriers on the machine bed are arranged in a Cartesian pattern, a preform of rectangular cross-section is braided. The yarn topology in the preform interior can be described by

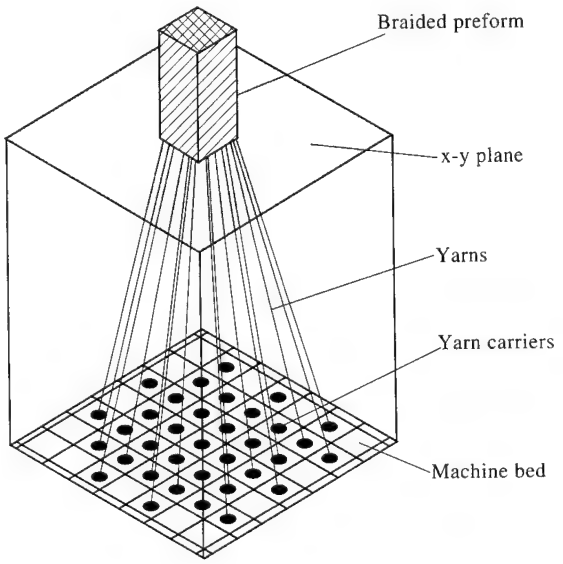

Fig. 1. Schematic representation of a 3-D braiding set-up.

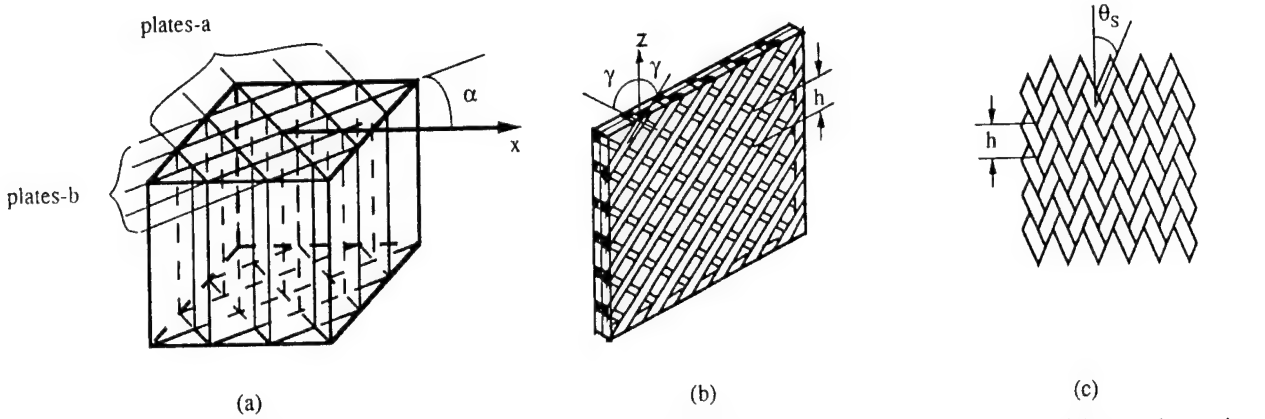

Fig. 2. Yarn topology in the preform of rectangular cross-section: (a) global view of the interior structure; (b) yarn formation in plate b; (c) view of the preform surface.

two levels, as shown in Fig. 2. Figure 2(a) shows a view where the interior is formed by two families of parallel flat plates (represented by the mid-plane of the plates), labeled plates a and plates b, respectively. These two families of plates criss-cross each other at an angle 2α, $\pm\alpha$ being the angle between the plate plane and the coordinate x axis. Thus, plates a are referred to as α-plates and plates b as $-\alpha$-plates. On a smaller scale, Fig. 2(b), the structure of each set of plates is made of two layers of parallel yarns; the yarns criss-cross at an angle 2γ, $\pm\gamma$ being the angle between the yarn and the braiding axis, z.

The length scale defining the criss-crossing pattern in the plate is denoted by h. Thus, the yarn line network (the topology) in the preform interior can now be characterized by three geometric parameters: α, γ and h; all are, so far, value-free. In practice, γ is known as the abraiding angle and h the braiding pitch. The angle α is generally 45°, but it can change when the rectangularity of the preform is changed.

On the preform surfaces, the yarn topology can be analyzed by the same procedure. Figure 2(c) shows the surface yarn topology, where two families of parallel yarn segments criss-cross at an angle of $2\theta_s$, where θ_s is the angle between the yarn segment and the braiding axis, z. Note also that the length scale of the surface pattern is characterized again by the same braiding pitch, h. If the rectangularity of the cross-section is changed (i.e. $\alpha \neq 45°$), then $\theta_s = \theta_x$ on the x surface and $\theta_s = \theta_y$ on the y surface.

Here, the surface yarn segments are the results of yarns which emerge from the preform interior at a certain step in the braiding cycle, and they then return back to the interior at another step. Hence, these appear on the surface as segments and not as continuous lines. Consequently, the surface yarn angles θ_x and θ_y are related geometrically to the yarn angles α and γ in the interior:

$$\tan\gamma = 2\sqrt{\tan^2\theta_x + \tan^2\theta_y}\,, \quad \tan\alpha = \tan\theta_x/\tan\theta_y \tag{1}$$

If the preform is braided with uniform yarn jamming, the yarn-to-yarn spacing, Δd, is considered uniform throughout the preform; the thickness of the α- or $-\alpha$-plates shown in Fig. 2(b) is $2\Delta d$. Furthermore, if $\theta_x = \theta_y = \theta_s$ then $\alpha = 45°$ and:

$$\tan\gamma = 2\sqrt{2}\tan\theta_s \tag{2}$$

Let the final preform cross-section have dimensions of $X \times W$, then the surface yarn angles θ_x and θ_y are related by the following:

$$\tan\theta_x = W/Nh\,, \quad \tan\theta_y = X/Mh \tag{3}$$

and the yarn-to-yarn spacing is:

$$\Delta d = (X\sin\alpha)/M = (W\cos\alpha)/N \tag{4}$$

Let the solid cross-sectional area of the yarn be A_f, then the fiber volume content of the preform interior is:

$$V_f = A_f/(h^2\tan\theta_x\tan\theta_y\cos\gamma) \tag{5}$$

Thus, the yarn structure in the whole preform is characterized by the parameters α, γ and h, together with the braiding set-up parameters M and N, the exterior dimensions of the preform X and W, and the specifics of the yarn used, A_f. It is noted that all parameters are constant throughout the preform in this case.

2.1.2 Tubular braids

When the yarn carriers are arranged in a circular row and radial column pattern, the resulting preform will have a tubular cross-section (usually the braiding is done over a circular mandrel). In this case, yarn lines in the preform interior as well as on the surfaces will be curved. Again, from Fig. 3(a), the interior yarn topology is composed of two families of curved plates which criss-cross each other at an angle of $2\alpha(r)$, where r is the radial position of the crossing point and $\pm\alpha$ is the local angle between the curved plates and the circle of radius r. A view on a smaller scale is

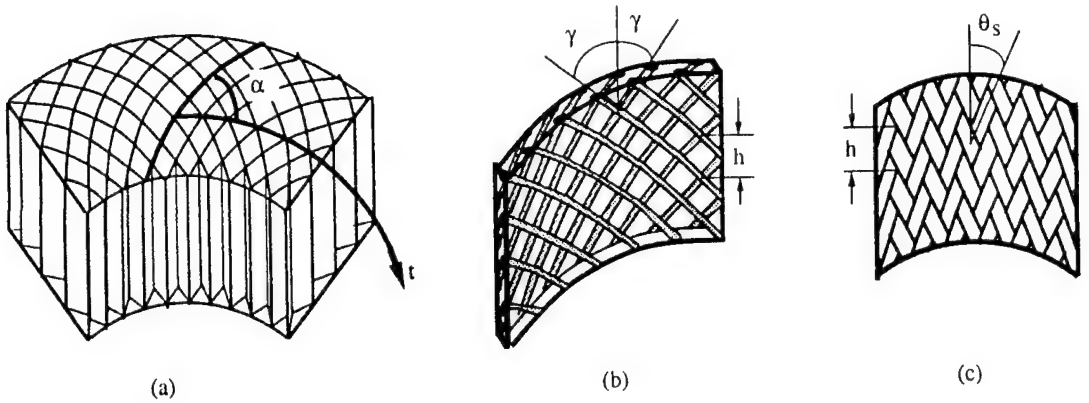

Fig. 3. Yarn topology in the preform of circular cross-section: (a) global view of the interior structure; (b) yarn formation in one of the curved plates; (c) view of the preform inner surface.

shown in Fig. 3(b), where the curved plate is composed of two families of parallel yarns which criss-cross at an angle of $2\gamma(r)$. The length scale of the criss-crossing pattern is defined by the braiding pitch, h, and the thickness of the curved plate is $2\Delta d$. As for the yarn topology on the tubular surfaces, a schematic view of the inner surface is shown in Fig. 3(c). Here, two families of parallel yarn segments form the surface, the segments criss-cross at an angle of $2\theta_{1s}$ Similarly, on the outer surface, there are two families of parallel yarn segments criss-crossing at an angle of $2\theta_2$.

Note that the yarn topology of the preform interior is geometrically similar to that in the Cartesian preforms (Fig. 2). However, the yarn angles α and γ here are functions of r due to the curvilinear nature of the geometry.

Now, given the final dimensions of the tube, the angles θ_{1s} and θ_{2s} are defined as:

$$\tan\theta_{1s} = 2\pi R_1/Mh\,,\quad \tan\theta_{2s} = 2\pi R_2/Mh \tag{6}$$

where R_1 and R_2 are the inner and outer radii of the tube, respectively.

As before, the surface yarn angles θ_{1s} and θ_{2s} are geometrically related to the interior yarn angles α and γ. These interrelations, however, are tied to the size of the yarn and the final dimensions of the tube. Omitting the algebraic details, the following is first obtained:

$$\begin{aligned}2\pi(N/M)/\lambda_1 = \sqrt{2}\{&\sqrt{(R_2/R_1)^2 - (1/\lambda^2{}_1/2)}\\ &- [(1/\lambda_1/\sqrt{2})\sec^{-1}(\sqrt{2}\lambda_1 R_2/R_1)]\\ &- \sqrt{1 - 1/(2\lambda^2{}_1)}\\ &+ (1/\sqrt{2}/\lambda_1)\sec^{-1}(\lambda_1\sqrt{2})\}\end{aligned} \tag{7}$$

where

$$\lambda_1 = (2\pi R_1)/(M\Delta d\sqrt{2}) \tag{8}$$

If M, N, R_1 and R_2 are given, λ_1 is computed from eqn (7) and Δd from eqn (8). Then, from geometry, one obtains the desired interrelationships:

$$\begin{aligned}&\sin\alpha = R_1/(\sqrt{2}\lambda_1 r)\,,\\ &\tan\gamma = 2\sqrt{2}\tan\theta_{2s}/(\lambda_2\sin 2\alpha)\end{aligned} \tag{9}$$

where

$$\lambda_2 = (2\pi R_2)/(M\Delta d\sqrt{2}) \tag{10}$$

Finally, the fiber volume fraction of the tubular preform is given by:

$$V_f = (A_f M^2)/(4\pi^2 r^2 \tan\alpha\cos\gamma) \tag{11}$$

Thus, similar to the previous case, the yarn structure in the tubular preform is completely characterized by the parameters α, γ and h, along with M, N, R_1, R_2 and A_f.

2.2 Geometric mapping between preforms of different shapes

From the two examples discussed above, it is seen that yarn topologies of rectangular and tubular cross-sectional shapes are similar because they are braided by the same braiding method. The question of whether the respective yarn topologies can be linked analytically by a proper mapping function (or functions) can now be examined, and the existence and determination of such a mapping will be developed. In order to be more specific, the discussions will be focused primarily on mappings between Cartesian and generally curvilinear preforms braided by the 4-step 1×1 method.

2.2.1 Mapping between cartesian and curvilinear braids

Let B_o be a Cartesian $[M \times N]$ rectangular preform; its yarn topology characterizing parameters are h_o, α_o, γ_o. Let the coordinates (x,y,z) describe a point in B_o and let the cross-section of B_o be spanned by a system of grids, formed by x = constant and y = constant, as shown in Fig. 4(a). The size of each grid is conveniently chosen as $\Delta x = X_o/M$ and $\Delta y = W_o/N$. Here, X_o is the total width and W_o is the total thickness of the cross-section.

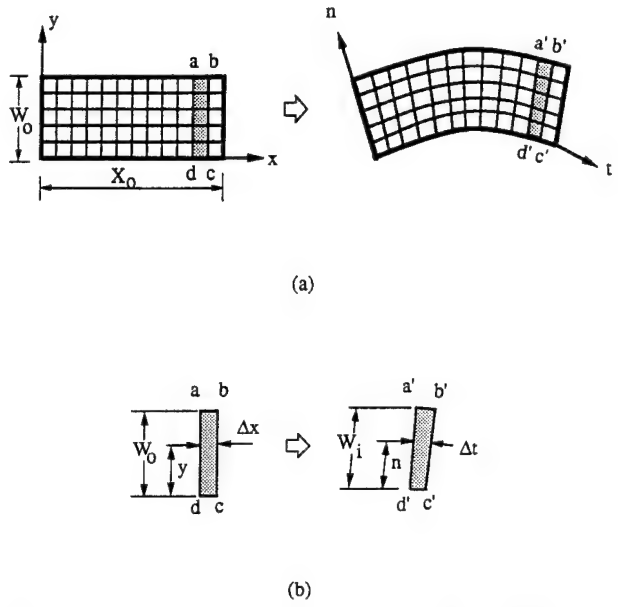

Fig. 4. Schematic representation of geometric mapping: (a) global view; (b) local view.

Now, let B_i be a curvilinear preform as shown in Fig. 4(b); its yarn topology characterizing parameters are h_i, α_i, γ_i. Assume that B_i is the image of B_o under a certain mapping function. Then, the point at (t,n,z') in B_i is the image of the point (x,y,z) in B_o; and the rectangular grid in B_o becomes the curvilinear grid in B_i. The latter grid is formed by the curvilinear coordinates t = constant and n = constant, where t and n intersect locally at the angle $\phi(t,n)$.

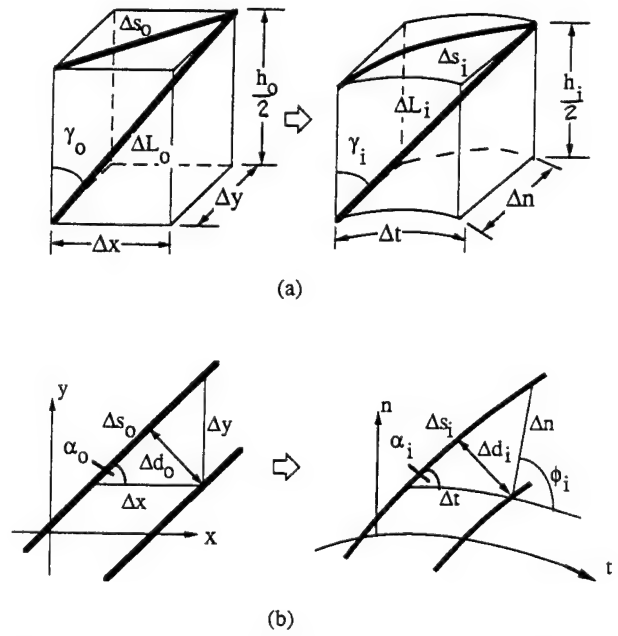

Fig. 5. Geometric relationships of yarns in rectangular and curvilinear local cells: (a) isometric view of the cells; (b) top view of the yarn-to-yarn spacing.

The mapping which takes B_o to B_i can be expressed in the general form:

$$t = g(x,y) \quad n = f(x,y) \quad z' = z/\zeta \tag{12}$$

Consider the incremental area abcd in the cross-section of B_o and the corresponding area a'b'c'd' in the cross-section of B_i, as shown in Fig. 5(a). The following local parameters are defined: $\lambda_1 = d'c'/dc$, $\lambda_2 = a'b'/ab$, W_i = the thickness of a'b'c'd'; ϕ_i = the local $\phi(t,n)$ in a'b'c'd'. It will be shown that, together with ζ, these parameters will determine the mapping functions in eqn (12) along with the appropriate yarn constraint conditions yet to be specified.

As mentioned before, yarn constraints stem from the manner in which the preform is shaped. Here, two basic shaping processes will be discussed: B_i is obtained by deforming B_o; and both B_o and B_i are braided independently. In each case, the appropriate yarn constraints will be imposed and the associated mapping will be derived.

2.2.2 Mapping due to preform deformation

If B_i is obtained by deforming B_o, it will be assumed that the yarns in the preform cannot be lengthened or buckled during deformation. Then, consider the yarn line segment of length ΔL_o in B_o as depicted in Fig. 5(a). The projections of ΔL_o onto the cross-section of B_o is Δs_o and that onto the braiding axis (z) is $h_o/2$; their respective images in B_i are ΔL_i, Δs_i and $h_i/2$. The image of the angle γ_o is γ_i. The corresponding details in the cross-sections of B_o and B_i are shown in Fig. 5(b). Here, the two solid parallel lines in B_o represent two neighboring α_o-plates, and the two solid curved lines in B_i represent the corresponding images. Note that the image of the angle α_o is α_i, and the image of the yarn-to-yarn spacing Δd_o is Δd_i, etc.

The yarn inextensibility condition requires $\Delta L_o = \Delta L_i$ This leads to:

$$\Delta s_i = m \Delta s_o \tag{13}$$

where

$$m = \sqrt{1 - (\zeta^{-2} - 1)\cot^2 \gamma_o} \tag{14}$$

From the local geometry depicted in Fig. 5(b), the following local relationships are established:

$$\Delta y = \Delta s_o \sin \alpha_o \quad \sin \alpha_i = \Delta n \sin \phi_i / \Delta s_i$$
$$\Delta n = \sqrt{\Delta s^2_i - \Delta t^2 - 2\Delta t \Delta n \cos \phi_i} \tag{15}$$

And from Fig. 4(b), the differential relationship

$$dt/dx \approx \Delta t/\Delta x = (\lambda_1 + \kappa n) \tag{16}$$

is obtained, where $\kappa = (\lambda_2 - \lambda_1)/W_i$

Thus, with eqns (13)–(16) and after some algebraic manipulations, the following differential equation is

obtained:

$$dy/dn \approx \Delta y/\Delta n = \{(\lambda_1 + \kappa n)\cot \alpha_o \cos \phi_i + \sqrt{[m^2 \mathrm{cosec}^2 \alpha_o - (\lambda_1 + \kappa n)^2 \cot^2 \alpha_o \sin^2 \phi_i]}\} \div [m^2 \mathrm{cosec}^2 \alpha_o - (\lambda_1 + \kappa n)^2 \cot \alpha_o] \quad (17)$$

Equation (17) can be integrated to obtain $y = p_1(x,n)$, which is inverted to obtain $n = f_1(x,y)$. Then, by substituting $f_1(x,y)$ for n in eqn (16) and integrating, one obtains $t = g_1(x,y)$.

Thus, if ζ and the local quantities λ_1, λ_2, W_i and ϕ_i are known, the mapping in eqn (12) is completely determined for the case of B_o deformed into B_i.

The quantities ζ, λ_1, λ_2, W_i and ϕ_i are to be determined by measurements made on the exterior surfaces of B_o and B_i; these measurements serve as 'boundary conditions'. Three measurements need to be made first, in addition to knowing $[M \times N]$; namely, the braiding pitch h_i, the yarn line angle θ_{2s} on the upper surface and θ_{1s} on the lower surface of B_i. In general, the angles θ_{1s} and θ_{2s} are not constant on the curved surfaces of B_i; hence these are to be measured at discrete points on the curved surfaces of B_i. If this is carried out, one obtains the following, using Fig. 6:

$$\zeta = h_o/h_i \quad \lambda_1 = (\tan \theta_{1s}/\tan \theta_{oy})/\zeta \quad \lambda_2 = (\tan \theta_{2s}/\tan \theta_{oy})/\zeta \quad (18)$$

where θ_{oy} is the surface angle on the y surface of B_o (assumed known).

As for the parameters W_i and ϕ_i, a relationship between the two can be obtained by means of the mapping function $n = f_1(x,y)$. Since at the location x in B_o, the thickness is W_o; the image of x in B_i is t and the image of W_o is W_i. Hence

$$W_i = f_1(x, W_o) \quad (19)$$

The expression $f_1(x,W_o)$ contains implicitly the quantities ζ, λ_1, λ_2, W_i and ϕ_i; the first three are already determined, leaving W_i and ϕ_i related by eqn (19).

In practice, preforms of complex shape are usually deformed into a preshaped mold. In such case, at least the inner surface of the preform is fixed. If the inner surface can be described by an analytical function, then W_i or ϕ_i can be determined using the inner surface function in conjunction with eqn (19). This will be further explained below.

Let the X–Y frame be used to describe globally the cross-section of B_i as shown in Fig. 7. Let the inner surface be denoted by t_1 and the outer surface by t_2. Given λ_1 and λ_2 as continuous functions of x, one can obtain $t_1 = t_1(x)$ and $t_2 = t_2(x)$ in terms of λ_1 and λ_2. Now, let the inner surface be described by the function $Y = F(X)$. Then a point on t_1 occupies the position (X_1,Y_1). It follows that:

$$dt_1 = \{\sqrt{1 + (F')^2}\}dX \quad (20)$$

where F' is the derivative of $F(X)$.

Integration of eqn (20) provides X_1 as a function of t_1; and through $t_1 = t_1(x)$, one obtains $X_1 = X_1(x)$. Since $Y_1 = F(X_1)$, one can obtain $Y_1 = Y_1(x)$.

Again, from Fig. 7, let the point (X_2,Y_2) on the outer surface be on the same n-line as the point (X_1,Y_1). Then, X_2 and Y_2 can be expressed as:

$$X_2 = X_1 + W_i \cos(\theta + \phi_i) \quad Y_2 = Y_1 + W_i \sin(\theta + \phi_i) \quad (21)$$

where

$$\cos \theta = \{\sqrt{1 + (F')^2}\}^{-1} \quad (22)$$

Since X_2 and Y_2 are now functions of x and ϕ_i, it follows that the derivatives of X_2 and Y_2 with respect to x are given by:

$$X_2' = (\partial X_2/\partial x) + (\partial X_2/\partial \phi_i)(\partial \phi_i/\partial x)$$
$$Y_2' = (\partial Y_2/\partial x) + (Y_2/\partial \phi_i)(\partial \phi_i/\partial x) \quad (23)$$

and

$$dt_2 = \{\sqrt{(X_2')^2 + (Y_2)^2}\}dx \quad (24)$$

Finally, comparing eqn (24) with $dt_2 = \lambda_2(x)dx$, one obtains:

$$\sqrt{(X_2')^2 + (Y_2')^2} = \lambda_2(x) \quad (25)$$

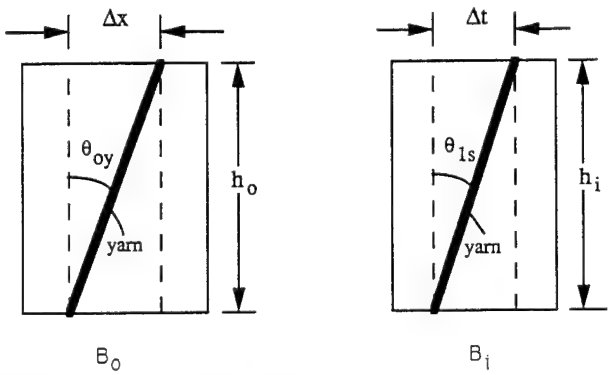

Fig. 6. Geometric relationships of a yarn on preform surface before and after mapping.

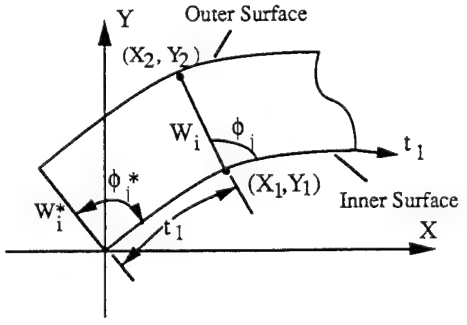

Fig. 7. The global coordinate system (X,Y) for the curvilinear preform cross-section.

Upon substitution of eqn (23) into eqn (25), a first order partial differential equation governing $\phi_i(x)$ is obtained. Integrating this for $\phi_i(x)$ requires one boundary condition which is supplied by one measurement of ϕ_i at the reference section $x = x^*$, or correspondingly at $t = t^*$. Once $\phi_i(x)$ is determined, $W_i(x)$ can be determined using eqn (19).

2.2.3 Mapping due to direct braiding

If both B_o and B_i are braided independently, yarns in both are assumed uniformly jammed. Then the condition $\Delta d_o = \Delta d_i$ is imposed. If so, $\Delta L_o \neq \Delta L_i$. This results in the following relationships, from Fig. 5(b):

$$\begin{aligned} \sin \alpha_i &= \sin \alpha_o/(\lambda_1 + \kappa n) \\ \Delta y/\Delta n &= \sin(\phi_i - \alpha_i)/\cos \alpha_o \end{aligned} \tag{26}$$

The above leads to the differential relationship:

$$\begin{aligned} dy/dn = \{&\sin \phi_i \sqrt{(\lambda_1 + \kappa n)^2 - \sin^2 \alpha_o} \\ &- \sin \alpha_o \cos \phi_i\}/[(\lambda_1 + \kappa n)\cos \alpha_o] \end{aligned} \tag{27}$$

which can be integrated to obtain $y = p_2(x,n)$, and inverting to obtain $n = f_2(x,y)$.

By substituting $f_2(x,y)$ for n in eqn (16) and integrating, the mapping function $t = g_2(x,y)$ is obtained. Thus, the mapping in eqn (12) is now completely determined for the case of both B_o and B_i braided directly; it remains to determine the five mapping parameters ζ, λ_1, λ_2, W_i, and ϕ_i as before.

In this case, the dimension of B_o need not be unique as long as it is mappable to B_i. So, let $h_o = h_i$ (then $\zeta = 1$) and $\alpha_o = 45°$ (then $\theta_{ox} = \theta_{oy} = \theta_o$) From eqn (2), $\tan \gamma_o = 2\sqrt{2} \tan \theta_o$. Since the size of B_o is not specified, θ_o will remain so far undetermined.

As before, on the exterior surfaces of B_i, the braiding pitch h_i, the yarn line angle θ_{1s} on the lower surface, θ_{2s} on the upper surface can be measured at the discrete points of x or t. Then, using eqn (18), the ratio of λ_2/λ_1 can be expressed as:

$$\lambda_2/\lambda_1 = \tan \theta_{2s}/\tan \theta_{1s} \tag{28}$$

Since in B_o, $\alpha_o = 45°$; it follows that $\Delta x = \Delta y$ and that

$$W_o = N\Delta y = N\Delta x = N(\Delta t_1/\lambda_1) \tag{29}$$

where, from Fig. 6, Δt_1 can be replaced by $(h_i \cot \theta_{1s})$.

At the same time, the thickness W_o in B_o can be expressed independently by integrating eqn (27) over the thickness at a reference section in B_o or B_i:

$$\begin{aligned} W_o = \int dn\{&\sin \phi_i \sqrt{(\lambda_1 + \kappa n)^2 - \sin^2 \alpha_o} \\ &- \sin \alpha_o \cos \phi_i\}/[(\lambda_1 + \kappa n)\cos \alpha_o] \end{aligned} \tag{30}$$

where $\kappa = (\lambda_1 - \lambda_2)/W_i$ from eqn (16), and (λ_1/λ_2) is defined in eqn (28).

Note that in eqn (30) the integration interval in B_i is from $n = 0$ to W_i. Thus, the expression for W_o contains the unknowns W_i, ϕ_i and λ_1.

Now, at the reference section, say $x = 0$ in B_o or the corresponding section $t = 0$ in B_i, the quantities $\phi_i(0)$ and $W_i(0)$ can be measured. Then, from eqns (29) and (30), the quantity $\lambda_1(0)$ can be determined. It follows from eqn (18) that:

$$\tan \theta_o = \tan \theta_{1s}(0)/\lambda_1(0) \tag{31}$$

With eqn (31), $\lambda_1(x)$ and $\lambda_2(x)$ are determined using eqn (18) along with W_o from eqns (29) or (30).

Finally, the parameters W_i and ϕ_i are related from integrating the mapping function $n = f_2(x,y)$:

$$W_i = f_2(x, W_o) \tag{32}$$

where $f_2(x,W_o)$ contains the unknown parameter, $\phi_i(x)$.

Hence, either $W_i(x)$ or $\phi_i(x)$ has to be determined. As in the case considered earlier, $\phi_i(x)$ can be determined if the inner surface of B_i is described analytically. The procedure is similar to that discussed before and is not repeated here.

Before proceeding, it should be noted that determination of the desired mapping functions is rather problem-specific. It would become easier and clearer if the exact shape and/or dimensions of both B_o and B_i are specifically given. This will be demonstrated in relatively simple examples to be presented in Section 2.4.

2.3 Mapping of the topological parameters

With the mapping functions in eqn (12) fully described, not only can B_o or any sub-volume in B_o (e.g. a unit cell) be mapped to the corresponding images in B_i, but also the yarn topologies in respective preforms can be mapped from one to the other. Consequently, the parameters h_i, α_i, and γ_i characterizing the yarn topology in B_i can be related to that in B_o via the mapping functions. Similarly, the local yarn-to-yarn spacings and fiber volume contents in the respective bodies can also be linked by the same mapping.

2.3.1 Parameters in deformed preforms

If B_i is deformed from B_o, the yarn topology parameters h_o, α_o and γ_o in B_o are assumed known; the corresponding parameters h_i, α_i and γ_i in B_i are derivable from the mapping in eqn (12). From the local geometry between B_o and B_i shown in Fig. 5 and Fig. 6, one obtains readily:

$$\begin{aligned} h_i = h_o/\zeta \quad \sin \alpha_i &= (\sin \phi_i/m)(dn/dy)\sin \alpha_o \\ \cos \gamma_i &= \cos \gamma_o/\zeta \end{aligned} \tag{33}$$

where ζ and ϕ_i are previously determined mapping

parameters; m is given in eqn (14) and dn/dy in eqn (17).

2.3.2 Parameters in independently braided preforms

If both B_o and B_i are braided independently, and if the yarn topology parameters in B_o are set as $h_o = h_i$ and $\alpha_o = 45°$, the associated parameters in B_i are given by:

$$h_i(\text{measured})$$

$$\sin\alpha_i = \sqrt{2}/[2(\lambda_1 + \kappa n)]$$

$$\tan\gamma_i = \sqrt{2}\sin\phi_i/(2\sin\alpha_i)(\partial n/\partial y)\tan\gamma_o \quad (34)$$

where θ_o, λ_1 and ϕ_i are determined from eqns (31), (18) and (32), respectively, κ is given in eqn (16) and $\partial n/\partial y$ is given in eqn (27).

2.3.3 Fiber volume content

The relationships between the local fiber volume contents in B_o and B_i can be defined from Fig. 5(a). The local sub-volumes are:

$$\Delta V_o = h_o(\Delta x\Delta y)/2$$

$$\Delta V_i = h_i(\Delta t)(\Delta n)\sin\phi_i/2 \quad (35)$$

If the length of the yarn in the sub-volume in B_o is ΔL_o and that in B_i is ΔL_i, then the ratio between the fiber volume fractions V_{fo} and V_{fi} can be expressed as:

$$V_{fi}/V_{fo} = (\Delta V_o\Delta L_i)/(\Delta V_i\Delta L_o)$$

$$= [(\Delta x\Delta y)/(\Delta t\Delta n)][(\cos\gamma_o)/(\cos\gamma_i\sin\phi_i)] \quad (36)$$

Hence, if B_i is deformed from B_o, $\Delta L_i = \Delta L_o$, it follows that:

$$V_{fi}/V_{fo} = \zeta(dy/dn)/[\sin\phi_i(\lambda_1 + \kappa n)] \quad (37)$$

where dy/dn is given in eqn (17).

If B_i is braided directly, $\Delta d_i = \Delta d_o$, then

$$V_{fi}/V_{fo} = (dy/dn)/[\sin\phi_i(\lambda_1 + \kappa n)] \quad (38)$$

where dy/dn is given in eqn (27).

In either case, if V_{fo} in B_o is known, V_{fi} in B_i can be determined. Generally, V_{fi} can vary spatially in B_i; and, of course, V_{fo} is constant in B_o.

2.4 Examples: mapping from rectangular to tubular preforms

In the above, the exact exterior dimensions of the preform B_i are not explicitly specified; expression for the mapping parameters λ_1, λ_2, W_i and ϕ_i cannot be explicitly determined. If, however, the geometry of B_i is given and is relatively simple, closed form expressions for all the parameters may be obtained. The following examples involve mapping from a rectangular cross-section (B_o) to a full tubular cross-section (B_i); both of the basic shaping processes are considered.

2.4.1 Tubular preform by deformation

If B_i is of tubular shape and is deformed from B_o, which is of rectangular shape, then for B_i the coordinate n is the radial variable r and the coordinate t is the family of concentric rings where r is constant. Let the braiding pitch h_i, the inner and the outer radii R_1 and R_2 of B_i be measured. Then, the five local mapping parameters are found as:

$$\zeta = h_o/h_i \quad \lambda_1 = 2\pi R_1/X_o$$
$$\lambda_2 = 2\pi R_2/X_o \quad W_i = R_2 - R_1 \quad \phi_i = \pi/2 \quad (39)$$

which are all are constant-valued.

It follows that the desired mapping functions are:

$$t = (\lambda_1 r/R_1)x$$

$$r = (R_1 m/\lambda_1/\cos\alpha_o)\sin[\lambda_1 y/(R_1\tan\alpha_o) + \sin^{-1}(\lambda_1\cos\alpha_o/m)] \quad (40)$$

Consequently, the yarn topology parameters in B_o and B_i are linked by:

$$h_i = h_o/\zeta \quad \cos\alpha_i = (\lambda_1 r\zeta/R_1)\cos\alpha_o \quad \cos\gamma_i = \cos\gamma_o/\zeta \quad (41)$$

and, on the inner and outer surfaces, the respective yarn angles are linked by:

$$\tan\theta_{1s} = (\lambda_1\zeta)\tan\theta_{oy} \quad \tan\theta_{2s} = (\lambda_2\zeta)\tan\theta_{oy} \quad (42)$$

where θ_{oy} is the yarn line angle on the y surface in B_o.

Finally, the respective fiber volume contents in B_o and B_i are linked by:

$$V_{fi} = V_{fo}[(\zeta/m^2)\sin(2\alpha_o)/\sin(2\alpha_i)] \quad (43)$$

2.4.2 Tubular preform by direct braiding

In this case, the quantities R_1, R_2 and h_i in B_i are measured. With these measurements, two of the five mapping parameters are defined as: $W_i = (R_2 - R_1)$ and $\phi_i = \pi/2$. In the reference preform B_o, the following are assumed: $h_o = h_i$ and $\alpha_o = 45°$. It then follows that $\zeta = 1$ and $\gamma_o = \tan^{-1}(2\sqrt{2}\tan\theta_o)$, where θ_o ($= \theta_{ox} = \theta_{oy}$) is still unknown. The latter is related to the surface stretch ratios λ_1 and λ_2, and the surface yarn angles θ_{1s} and θ_{2s} in B_i through eqn (42). But, the surface yarn angles can be determined independently from B_i. Namely:

$$\tan\theta_{1s} = (2\pi R_1/M)/h_i \quad \tan\theta_{2s} = (2\pi R_2/M)/h_i \quad (44)$$

Then from eqn (29), one obtains:

$$W_o = N\lambda_1\Delta t_1 = 2\pi NR_1\lambda_1/M \quad (45)$$

But, integration of eqn (27) through the thickness of the preform in B_o and in B_i gives W_o as:

$$W_o = \int\{\sqrt{(\lambda_1 + \kappa r)^2 - 1/2}/[\sqrt{2}(\lambda_1 + \kappa r)/2]\}dr \quad (46)$$

where the integral is carried over R_1 to R_2. This is in fact obtainable also from the general expression in eqn (30). Combining eqns (45) and (46) leads to:

$$\begin{aligned}2\pi(N/M)/\lambda_1 = \sqrt{2}\{&\sqrt{(R_2/R_1)^2 - (1/\lambda^2{}_1/2)} \\ &- [(1/\lambda_1/\sqrt{2})\sec^{-1}(\sqrt{2}\lambda_1 R_2/R_1)] \\ &- \sqrt{1 - 1/(2\lambda^2{}_1)} \\ &+ (1/\sqrt{2}/\lambda_1)\sec^{-1}(\lambda_1\sqrt{2})\}\end{aligned} \tag{47}$$

which is in fact the same relationship as in eqn (7).

From eqn (47), one determines the mapping parameter λ_1, given M, N, R_1 and R_2. Consequently, the value for W_o is obtained from eqn (45); X_o and λ_2 are determined from eqn (39).

With all the five mapping parameters determined, the mapping function for $t(x,y)$ is the same as the first in eqn (40). As for r, one can obtain it either from eqn (40) or by integrating eqn (27); the latter will lead to:

$$\begin{aligned}y = \sqrt{2}R_1\{&\sqrt{r^2/R^2{}_1 - 1/\lambda^2{}_1/2} \\ &- (1/\sqrt{2}/\lambda_1)\sec^{-1}(\sqrt{2}\lambda_1 r/R_1) \\ &- \sqrt{1 - 1/(2\lambda^2{}_1)} + 1/(\sqrt{2}\lambda_1)\sec^{-1}(\lambda_1\sqrt{2})\}\end{aligned} \tag{48}$$

which can be inverted to obtain the function $r = f_2(y)$. This then completes the determination of the desired mapping functions in eqn (12).

Accordingly, the corresponding characterizing parameters for the yarn topology in B_i are found thus:

$$\begin{aligned}&h_i(\text{measured}) \\ &\sin\alpha_i = (R_1/\lambda_1/\sqrt{2})/r \\ &\tan\gamma_i = \tan\gamma_o/\sin(2\alpha_i)\end{aligned} \tag{49}$$

and the fiber volume fraction is given by:

$$V_{fi} = V_{fo}(\sin\gamma_o/\sin\gamma_i) \tag{50}$$

It is noted that, between a tubular preform which is directly braided and the one that is deformed from a rectangular preform, the respective yarn topology characterizing parameters are quite different, even though the overall dimensions of both preforms are exactly the same and braided by the same method. Clearly, the difference is due to the different internal yarn constraints stemming from the difference in the respective shaping processes.

2.5 Preform formability and braidability

As mentioned previously, one way to manufacture a preform of a certain shape is to braid first a suitable preform of one shape and then deform it into the final shape during the matrix consolidation process. Another way is to braid the preform in the final shape directly (e.g. onto a preshaped mandrel); and the same shape is preserved during matrix consolidation.

In the former, yarn stretching and compressing are not generally allowed. Hence, the question of deformability arises. The term 'deformability' refers to the permissible deformation that a preform can sustain without yarn stretching or buckling. This issue should be examined analytically, requiring considerations in the initial design of the braiding set-up (e.g. M and N), yarn selection (A_f), condition of yarn jamming (Δd), selection of the braiding pitch h, etc., in a closed design-analysis environment.

Similarly, to braid directly a preform of a certain shape, the same set of parameters must also be considered in similar design-analysis environment. Hence, the term 'braidability' refers to the permissible preform shapes that are possible without violating the interrelations linking all these parameters.

Thus, within the context of the geometric mapping discussed above, further exploration of preform deformability and braidability will be briefly discussed below.

2.5.1 Deformability

When B_o is deformed into B_i, the yarn-to-yarn spacing Δd_i cannot be always uniform throughout B_i. But, the following condition must be satisfied:

$$\Delta d_{max} \geq \Delta d_i \geq \Delta d_{min} \tag{51}$$

where Δd_{max} is the maximum yarn spacing for which the preform can maintain a solid form, while Δd_{min} is associated with the maximum yarn jamming. As such, the meaning of Δd_{max} and Δd_{min} are not very precise. However, an empirical value for each may be established given the yarn selected.

From the sketch in Fig. 5(b), a relationship between the yarn spacings in B_o and B_i is obtained:

$$\Delta d_i/\Delta d_o = (\lambda_1 + \kappa n)\sin\alpha_i/\sin\alpha_o \tag{52}$$

Owing to the inequality in eqn (51), one obtains from the above:

$$\begin{aligned}(\lambda_1 + \kappa n)\sin\alpha_i &\leq (\Delta d_{max}/\Delta d_o)\sin\alpha_o \\ (\lambda_1 + \kappa n)\sin\alpha_i &\geq (\Delta d_{min}/\Delta d_o)\sin\alpha_o\end{aligned} \tag{53}$$

The left-hand side of eqn (53) is a convex function of n; the maximum occurs inside the range of n, while the minima occur on the surfaces of B_i, $n = 0$ and $n = W_i$. Hence, the inequalities in eqn (53) can be rewritten as:

$$\begin{aligned}\max\{(\lambda_1 + \kappa n)\sin\alpha_i/\sin\alpha_o\} &\leq \Delta d_{max}/\Delta d_o \\ \min\{(\lambda_1\sin\alpha_1), (\lambda_2\sin\alpha_2)\} &\geq (\Delta d_{min}/\Delta d_o)\sin\alpha_o\end{aligned} \tag{54}$$

where α_1 and α_2 are values of α_i near the lower and the upper surfaces, respectively.

Since the mapping parameters are determined by physical measurements on the exterior of B_i, the inequality in eqn (54) thus sets the limiting window for the permissible dimensions of B_i. The exact limits can be established when the exact shapes of B_o and B_i are specified.

2.5.2 Braidability

When B_i is braided directly, the question arises as how to construct the proper braiding set-up in order to achieve the desired preform shape and dimensions. From the development in Section 2.2, it is possible to find a Cartesian preform B_o which serves as the image of B_i. Since both preforms are braided directly with the same yarn and are subjected to the same yarn jamming, the condition of $\Delta d_i = \Delta d_o$ is imposed. The idea here is to investigate the conditions that govern the braidability of B_o; if B_o is braidable under the imposed condition, the braidability of B_i is assured.

Now, let the cross-sectional dimension of B_o be $X_o \times W_o$ (see Fig. 4(a)). From Fig. 5(b), one can write:

$$\begin{aligned} \Delta d_o &= \Delta x \sin\alpha_o = 2(X_o/M)\sin\alpha_o \\ \Delta d_o &= \Delta y \cos\alpha_o = 2(W_o/N)\cos\alpha_o \end{aligned} \tag{55}$$

Substituting eqn (55) into the inequality of eqn (51) yields:

$$\Delta d_{max} \geq 2X_o W_o \sqrt{M^2 W^2{}_o + N^2 X^2{}_o} \geq \Delta d_{min} \tag{56}$$

The above inequality governs the choice of M and N in relation to the overall size of B_o, such that B_o would be braidable with uniform yarn jamming. Furthermore, since the mapping parameters λ_1, λ_2, W_i and ϕ_i as well as the yarn topology characterizing parameters α_i and γ_i of preform B_i are related to X_o and W_o, the inequality of eqn (56) can provide limiting windows for the choice of M, N, X_o and W_o. Again, this will be seen more clearly in the examples discussed below.

2.5.3 Specific examples

Take the examples considered earlier in Section 2.4, where B_o is a rectangular preform and B_i is a tubular preform. If B_i is deformed from B_o, measurements of R_1, R_2 and h_i in B_i can define all the mapping parameters (as well as yarn topology characterizing parameters). In particular, λ_1 and λ_2 are defined in eqn (39) and $\sin\alpha_1$ and $\sin\alpha_2$ can be computed from eqn (41). In order to ensure deformability, it follows from eqn (54) that restrictions must be imposed on R_1, R_2 and h_i. Namely:

$$\begin{aligned} &[2\pi R_1/(X_o \sin\alpha_o)]\sqrt{1 - (2\pi R_1 h_o \cos\alpha_o / X_o h_i)^2} \geq (\Delta d_{min}/\Delta d_o) \\ &[2\pi R_2/(X_o \sin\alpha_o)]\sqrt{1 - (2\pi R_2 h_o \cos\alpha_o / X_o h_i)^2} \geq (\Delta d_{min}/\Delta d_o) \end{aligned} \tag{57}$$

On the other hand, if B_i is braided directly, the condition in eqn (56) reduces to:

$$\Delta d_{max} \geq 2\sqrt{2}\pi R_1/(M\lambda_1) \geq \Delta d_{min} \tag{58}$$

where λ_1 is determined from eqn (47) as a function of R_1, R_2, M and N. Thus, eqn (58) provides the window for choice of R_1, R_2, M and N to ensure the braidability of B_i.

The inequality in eqn (57) or (58) also restricts the range of the yarn topology characterizing parameters α_i and γ_i as well as the geometry-related quantities such as V_{fi} and Δd_i. This can be seen from the numerical results displayed in Fig. 8, where the parameters α_i, γ_i, V_{fi} and Δd_i are plotted against the non-dimensional parameter $\lambda_1 r/R_1$ (for the purpose of definiteness, $\zeta = 1$, $\alpha_o = 45°$ and $\gamma_o = 30°$ are assumed in the numerical calculation).

Figure 8(a) shows the interaction between α_i and $\lambda_1 r/R_1$ for the deformed and the directly braided cases. In the deformed case, α_i can vary from 0° to 90° in the range $0 < \lambda_1 r/R_1 < \sqrt{2}$ as a convex function. To insure deformability, the outer surface stretch ratio λ_2 ($= \lambda_1 R_2/R_1$) must be less than $\sqrt{2}$. In the directly braided case, however, α_i can vary from 0° to 90° for all $\lambda_1 r/R_1 > 1/\sqrt{2}$ as a concave function. Here, to ensure braidability, the inner surface stretch ratio λ_1 must be greater than $1/\sqrt{2}$. At the limiting value of λ_1 in each case, B_i becomes physically impossible to make.

Figure 8(b) shows the interaction between Δd_i (normalized by Δd_o) and $(\lambda_1 r/R_1)$. In the case of B_i being directly braided, $\Delta d_i/\Delta d_o = 1$ holds for all values of $\lambda_1 r/R_1$ (note that the limit of λ_1 $1/\sqrt{2}$ remains in effect). If B_i is deformed from B_o the interaction between $\Delta d_i/\Delta d_o$ and $\lambda_1 r/R_1$ furnishes a convex function with the maximum at $\Delta d_i/\Delta d_o = \lambda_1 r/R_1 = 1$. This curve can further restrict the range of λ_1. Owing to eqn (41), $\Delta d_{min}/\Delta d_o < 1$. For instance, if in B_i the condition $1\ \Delta d_{min}/\Delta d_o$ 0·72 is desired, then from Fig. 8(b), the line $\Delta d_{min}/\Delta d_o = 0{\cdot}72$ intersects the curve at two points; these two points limit the permissible values of λ_1 and λ_2 in the interval (0·55, 1·35).

The interactions between V_{fi} (non-dimensionalized by V_{fo}) and $\lambda_1 r/R_1$ is shown in Fig. 8(c). In this case, the interaction curve is convex for the directly braided case, while concave for the deformed case, and the extremes in both cases occur at the same point. This point corresponds to $\lambda_1 = 1$ and $V_{fi} = V_{fo}$. In particular, for the directly braided case, V_{fi} approaches zero when λ_1 approaches $1/\sqrt{2}$. Hence, to ensure braidability, the restriction of $1/\sqrt{2} < \lambda_1$ must be imposed.

Finally, Fig. 8(d) shows the interaction between γ_i and $\lambda_1 r/R_1$ for the two cases. In the deformed case, γ_i is constant ($= \gamma_o = 30°$) throughout the range of $\lambda_1 r/R_1$ (note that λ_1 has already been bounded as discussed before). In the directly braided case, however, the interaction furnishes a concave curve with the minimum at $\lambda_1 r/R_1 = 1$, $\gamma_i = 30°$ and $\alpha = 45°$. If, for instance, a constant γ_i is desired throughout the tubular braid, then λ_1 should be greater than 0·9. In that case, α_i can only be about 45° or smaller as can be seen from Fig. 8(a).

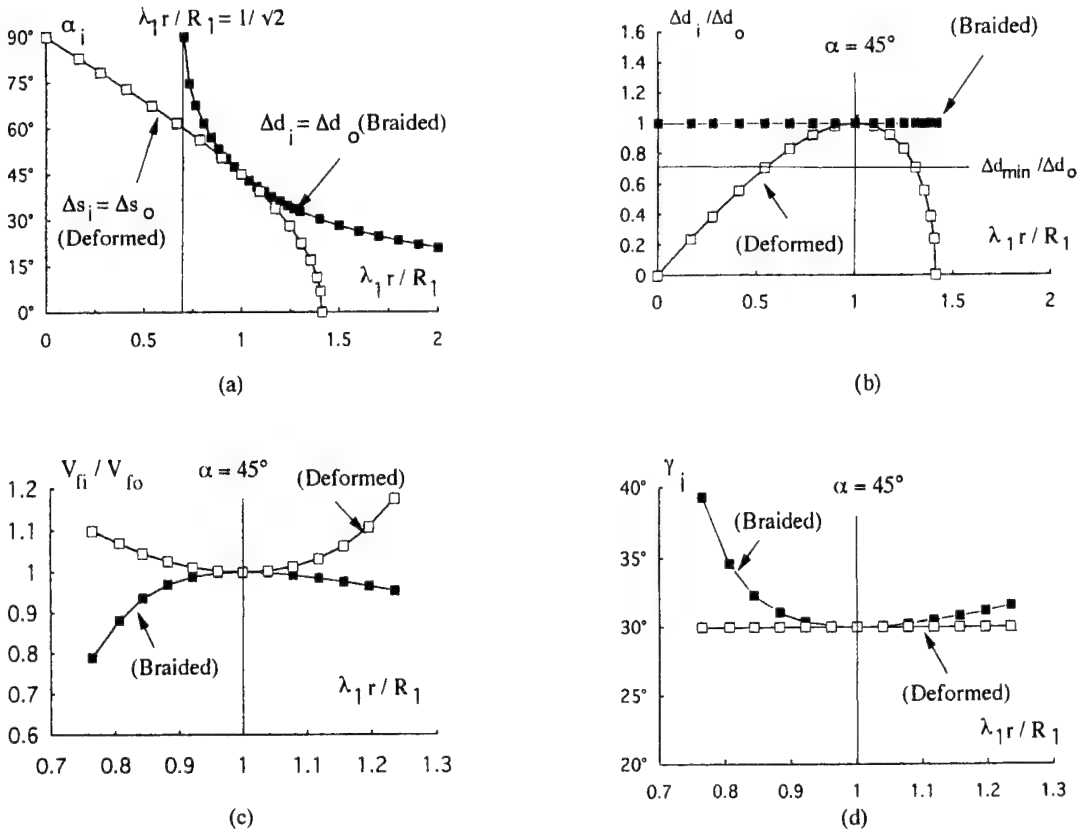

Fig. 8. Radial variation of the topological parameters in directly braided and deformed tubular preforms.

The above examples demonstrate how the mapping functions are used to address deformability and braidability of preforms having tubular cross-sections. Here, limits or windows for all the parameters may be established analytically, along with design-related limitations. Hence, an optimization may be performed when a real case of preform design is considered. Some basic elements in such an optimization setting have been discussed in more detail elsewhere.[4]

3 CONCLUDING REMARKS

In this paper, a geometric mapping method has been developed for determining the yarn structure in 3-D braided preforms of complex shapes. Specifically, the mapping can take the yarn structure in a preform of one shape to that in another shape. This is possible because the topological characteristics of the yarn structure in preforms of different shapes are similar, if the preforms are produced by the same braiding procedure. In general, the desired mapping functions must satisfy yarn constraints associated with the shaping process.

The 4-step 1×1 braiding procedure is used throughout the paper to demonstrate the topological character of the yarn structure in preforms of different shapes, and to outline the logical steps for determining the appropriate mapping functions. Two practical cases are examined in specific details: mapping due to preform deformation and mapping between two preforms by direct braiding. In each case, the yarn-constraint condition is specified and explicit mapping functions are obtained.

The developed mapping method is intended for preforms having complex shapes and is therefore extremely problem-specific. Generally, a numerical procedure may be required to obtain the desired mapping functions for complex shapes. However, the examples cited here have relatively simple shapes; the intent is to demonstrate the steps for determining the mapping functions in explicit terms without resort to numerical calculations. However, with the mapping functions obtained for each example, the issues of preform deformability and/or braidability are explored with numerical results.

Finally, it is noted that the mechanical properties of the matrix-consolidated composites may now be extracted based on the details of the yarn structure in the preforms. For this, some suitable micromechanics models are needed.[3,4] This and other related developments will be addressed in separate papers.

On the subject of the mechanical properties, it is noted that yarn structure is not the only important element in determining the properties of braided

composites. Other intangible factors, such as the loss of fibers during braiding, voids introduced during matrix consolidation, residual stresses trapped during fabrication, and other manufacture-related anomalies, may all play a vital role. These topics are outside the scope of the present paper.

ACKNOWLEDGEMENT

This work was supported by a grant from the Air Force Office of Scientific Research.

REFERENCES

1. *Textile Structural Composites*, ed. T. W. Chou & F. K. Ko. Elsevier Science Publishers, 1989.
2. Wang, Y. Q. & Wang, A. S. D., On the topological yarn structure in 3-D rectangular and tubular braided preforms. *Comp. Sci. Technol.*, **51** (1994) 575–86.
3. Wang, Y. Q. & Wang, A. S. D., Microstructure/property relationships in three-dimensionally braided fiber composites. *Comp. Sci. Technol.*, **53** (1995) 213–22.
4. Wang, Y. Q. & Wang, A. S. D., Spatial distribution and thermomechanical properties in 3-D braided tubular composites. *Proc. ICCM-10*, Vol. IV, pp. 285–94. Whistler, Canada, August 1995.

Applied Composite Materials **00:** 1–12, 1996.
© 1996 *Kluwer Academic Publishers. Printed in the Netherlands.*

FIRST PROOFS

AUTHOR PROOFS

Spatial Distribution of Yarns and Mechanical Properties in 3D Braided Tubular Composites

Y. Q. WANG
Kansas State University, Manhattan, KS 66502, U.S.A.

A. S. D. WANG
Drexel University, Philadelphia, PA 19104, U.S.A.

(Received 25 July 1996; accepted 16 September 1996)

Abstract. This paper outlines a method which links the following analytically simulated events in sequence: (1) braiding of a 3D preform of tubular cross-section – characterized by a set of braiding parameters defining the braiding setup and braiding steps; (2) geometric description of the yarn topology in the braided preform – in explicit terms of a set of topological parameters defined by the preform shape and the braiding parameters; (3) description of the exact yarn distribution after preform consolidation with a binding matrix – the values of the topological parameters are related to the exterior dimensions and surface features of the consolidated preform; and (4) forecasting the mechanical properties in the final composite – via a suitable micromechanics model that takes into account the spatial yarn distribution in the composite and properties of the constituents.

It is shown that these sequential events form a closed-loop linkage which connects the properties of the final composite all the way to the initial preform braiding setup design; the analytically derived interrelationships in each link can provide for design simulations of three dimensionally braided, complex-shaped and property-specific composite articles.

In order to obtain explicit interrelationships, the 4-step 1×1 braiding procedure is utilized in the analytical development. For the same reason, a graphite yarn and an epoxy resin with known properties are used in illustrative examples. There can be more than one braiding setup design for a preform to have the same shape and overall dimensions; but the yarn structure and properties in the final composite can differ widely if different braiding setups are used. Hence an optimization for a composite shape to meet the prescribed requirements may be conducted using the developed closed-loop.

Key words: textile composites, design of 3D braided preforms, yarn structures, composite properties, close-loop design optimization.

1. Introduction

In recent years, various textile technologies have been utilized to manufacture fibrous composite articles directly in their near-net-shapes. Three-dimensional (3D) braiding with continuous yarns is one such emerging technology which finds itself in increased industrial applications [1]. Basically, 3D braiding involves the braiding of a fabric preform of certain initial shape, impregnating it with a binding matrix material and consolidating the green composite to its final and solid shape. To the extent that the functional performance of the final product may depend largely on the manners in which the preform is braided, shaped and

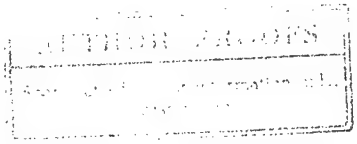

VTEX(P) PIPS No.: 121406 MATHKAP
ACMA115.tex; 16/10/1996; 18:12; v.5; p.1

consolidated, a rational design/analysis of the fabrication process in each stage is needed.

In a series of recent studies [2–5], it has been shown that the topological structure of the yarns in a 3D preform is uniquely determined by the braiding procedure adopted, and the topology can be characterized geometrically in terms of some physical parameters [2]. When the preform is consolidated in its final solid shape, the exterior dimensions and some braiding features on the solid surfaces will provide the necessary condition for determining the exact yarn distribution inside the shape [2, 3]. The knowledge of yarn distribution in the composite provides input to models that forecast mechanical properties [4]. Thus, an analytical design loop is complete which takes into account all the key parameters from preform fabrication to forecasting the functional performance of the final composite.

In this paper, the above close-loop design/analysis concept will be explored using a class of 3D preforms braided with a tubular cross-sections. We begin with the characterization of the initial braiding setup design, in conjunction with the 4-step 1×1 braiding procedure. Based on the braiding setup and braiding steps, the topology of the yarns in the braided preform is obtained in terms of three free-valued parameters. When the preform is matrix-consolidated to its final solid shape and dimensions, the values of the topological parameters are then fixed; and the spatial distribution of the yarn in the solid fully described. Finally, the mechanical properties of the composite are forecasted via a suitable micromechanics model with inputs from the spatial yarn distribution and properties of the constituents. In each link of the loop, the connecting relationships are expressed in explicit terms of the characterizing parameters.

Two specifically designed tubular preforms are simulated through the close loop as illustrations. Here, a graphite yarn of 12K fibers and an epoxy resin with known properties are used as the constituent materials. The two preforms are designed with differing braiding setups but are braidable to have the same inner and outer radii. Their respective yarn structures and mechanical properties are obtained and compared. The results show that tubes of the same exterior shape and dimensions can be fabricated from differing braiding setups; but the spatial yarn distributions and mechanical properties can vary significantly with braiding setup.

The issue of preform design optimization is raised; a brief discussion on the subject is presented at the end.

2. Braiding, Yarn Structure and Property Relations

2.1. Characterization of Braiding Setup and Braiding Steps

Figure 1 shows a schematic illustration of the braiding setup for a tubular preform. The preform being braided is hung above the machine bed, on which yarn carriers are arranged in a pattern consisting of circumferential rows and radial columns.

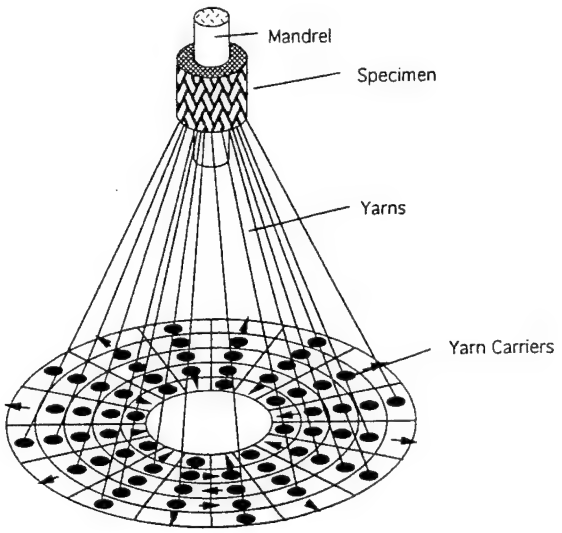

Figure 1. Schematics of the braiding setup for a tubular preform.

The preform is braided through movements of the yarn carriers along the row and column tracks. Here, we consider only the 4-step 1×1 method for purpose of definiteness. This particular method has four row-and-column movements in a braiding cycle, during which the yarns are made to crisscross in space; a certain yarn jamming (tightening) action is applied upon each cycle of braiding and a finite length of the preform is thus braided. The yarn structure formed will repeat itself in successive cycles. A full description of this braiding procedure is detailed in [2].

The size of the braiding setup is characterized as follows: let M be the number of yarn carriers in each circular row and N, be the number of yarn carriers in each radial column; the braiding setup is expressed as $[M \times N]$. If a mandrel of radius R_1 is used in the braiding (as shown in Figure 1), the outer radius of the braided preform will depend on the yarn size, yarn jamming and other braiding characteristics. At this point, the parameters M, N and R_1 will define the size of the braiding setup.

2.2. Characterization of Yarn Topology

Given the parameters M, N and R_1, the topology of the yarn structure formed during each braiding cycle can be described without regard to yarn size and yarn jamming. This is done by considering the yarn as a line which traces inside a control space during one braiding cycle. The resulting topology is characterized by a set of three geometric parameters whose values would remain free. For

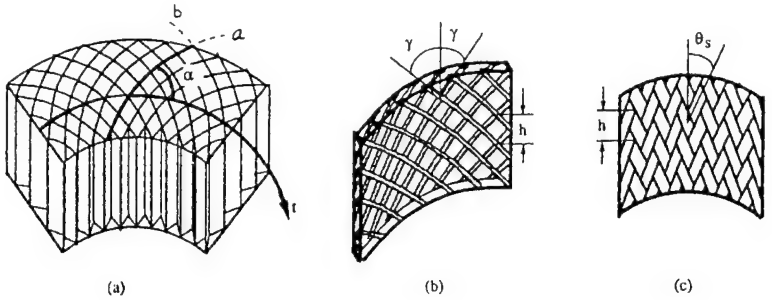

Figure 2. Anatomy of the yarn topology in tubular braids by the 4-step 1 × 1 method: (a) the interior structure of 2-families (a and b) of crisscrossing curved plates; (b) the angle-plied structure of an enlarged curved plate from family-*a*; and (c) the weave-like pattern of yarn segments on the tube's inner surface.

reason of brevity, only the key elements in the topology characterization will be discussed here since most of the details have been fully described in [2].

The yarn structure in the tubular preform so braided is schematically shown in Figure 2. A wedge section of the interior structure is shown in Figure 2a: the preform core is composed of two families of curved plates crisscrossing each other at the angle 2α. Note that α is the angle between the curved plate and the circle of radius r; hence, α is a function of r. Each of the curved plates is formed by two layers of parallel yarns crisscrossing at the angle of 2γ, resembling that of an angle-plied laminate as shown in Figure 2b. Here, γ is the off-axis angle referred to the braiding axis of the preform; γ is also a function of r.

The length scale defining the crisscrossing pattern in each plate is the braiding pitch h, the braided length during each cycle. At this stage, the preform is still not consolidated; none of the above parameters could be precisely defined. Nonetheless, α, γ and h fully define the topology of the preform's interior structure.

The yarn structure on the preform's inner surface is formed by a family of crisscrossing yarn segments; the pattern is characterized by the braiding pitch h and the angle θ_{1s} as shown in Figure 2c. Similarly, the preform's outer surface is characterized by h and the angle θ_{2s}. Generally, $\theta_{1s} \neq \theta_{2s}$.

The angles θ_{1s} and θ_{2s} are geometrically related to h, M and the exterior dimensions of the preform: the inner radius R_1 and the outer radius R_2:

$$\tan\theta_{1s} = 2\pi R_1/Mh \qquad \tan\theta_{2s} = 2\pi R_2/Mh. \tag{1}$$

Note that R_2 remains unspecified at this stage, although R_1 is specified at the outset. In summary, the tubular braid is composed of three cylindrical layers: the core, the inner and outer surface layers. Each is endowed with a distinctive yarn structure as described above.

2.3. Determination of the Topological Parameters

Let the yarn used be now selected and assume yarn jamming during braiding is uniformly applied. Then the yarn-to-yarn spacing, denoted by d, will be a finite-valued constant throughout the braid. The value of d defines both the braiding pitch h and the outer radius R_2 if the inner radius R_1 is prescribed. The geometric relationship linking all these parameters is (see detailed derivation in the Appendix):

$$2\pi(N/M)/\lambda = \sqrt{2}\Big\{\sqrt{[R_2/R_1)^2 - [(1/\lambda/\sqrt{2})\sec^{-1}(\sqrt{2}\lambda R_2/R_1) - \\ -\sqrt{[1-1/(2\lambda^2)]} + (1/\sqrt{2}/\lambda)\sec^{-1}(\lambda\sqrt{2})\Big\}, \tag{2}$$

where

$$\lambda = (2\pi R_1)/(Md\sqrt{2}). \tag{3}$$

Using the above, the interior yarn angles α and γ are determined as:

$$\sin\alpha = R_1/(r\lambda\sqrt{2}), \tag{4}$$

$$\tan\gamma = 2\sqrt{2}\tan\theta_{1s}/(\lambda\sin 2\alpha). \tag{5}$$

And, if the solid cross-section A_f of the braiding yarn is also known, the fiber volume content in the composite tube is given by:

$$V_f = (A_f M^2)/(4\pi^2 r^2 \tan\alpha\cos\gamma) \tag{6}$$

which is a function of r as well.

Suppose that h and R_2 are measured physically from an actually braided tube; then d can be determined from (2). Consequently, the parameters α, γ are determined from (4), (5) and (3), as functions of r and V_f is defined by (6).

2.4. Preform Design Considerations

If ~~the circular preform is~~ in the design stage ~~and~~ the values of R_1 and R_2 are prescribed, it is necessary to select the yarn size along with the would-be values of h, M and N. Generally, the values of h may be estimated given the yarn selection and the expected yarn structure characteristics (e.g. γ and V_f are prescribed in advance); ~~it is then followed by~~ selecting the values for M and N. The value for d is provided by (2). Clearly, d must have values that are compatible with the selected yarn; or it may become physically unacceptable, raising the issue of preform braidability.

If the circularly braided preform is deformed from being circular during matrix consolidation, the surface features will not be axisymmetric as before. In that case, the topological parameters can still be determined by a geometric mapping

scheme [3]. The resulting yarn-to-yarn spacing d inside the braid may vary from position to position. This raises the issue of preform deformability [5].

Generally speaking, different $[M \times N]$ combinations may be used to produce tubular preforms that have the same prescribed dimensions; but the yarn structures endowed in the preforms may differ widely depending on the particular braiding setup, which in turn causes differences in the mechanical properties of the consolidated tubes. The latter will be discussed below.

3. Mechanics Modeling and Mechanical Properties

With the yarn structure in the composite tube fully described, its mechanical properties may be extracted by using a suitable mechanics model. In what follows, a simple volume-averaging approach is adopted to determine the "effective" composite properties for the tubes.

As described earlier, the composite tube may be viewed as a cylindrically layered structure with the core, the inner and outer surface layers. Each layer has its own distinctive yarn structure. In general, it is necessary to model the core and the surface layers separately. But if the tube is braided with large value of N, the surface layers will be thin relative to the core; then the effect of the surface layers may be disregarded and the characterization of the core alone would be sufficient.

3.1. THERMOELASTIC MODELING

As shown in Figure 2a, the yarn structure in the tube's core consists of two families of crisscrossing curved plates; and each plate is composed of two layers of parallel yarns, see Figure 2b. Here, the curved plates will be modeled as a curved $[\pm\gamma]$ angle-plied laminate of thickness $2d$, while the γ-ply will be modeled as an off-axis unidirectional (UD) lamina of thickness d. The fiber volume content of the UD ply is V_f computed from (6).

The UD lamina will be treated as a linearly elastic and transversely isotropic material in its principal coordinates (L, T, z); its five independent elastic constants are determined following the micromechanics model outlined by Chamis [6]:

$$\begin{aligned} &E_L = V_f E_f + (1 - V_f) E_m, \quad E_T (= E_z) = E_m / [1 - (1 - E_m / E_f) \sqrt{V_f}], \\ &G_{LT} = G_m / [1 - (1 - G_m / G_f) \sqrt{V_f}], \\ &\nu_{LT} = V_f \nu_f + (1 + \nu_f) \nu_m, \qquad \nu_{Tz} = [E_T / (2 G_{LT}) - 1]. \end{aligned} \tag{7}$$

Similarly, the thermal expansion coefficients of the UD lamina are found via the micromechanics model by Schapery [7]:

$$\begin{aligned} \beta_L &= [\beta_f E_f V_f + \beta_m E_m (1 - V_f)] / [E_f V_f + E_m (1 - V)], \\ \beta_T = \beta_z &= \beta_f V_f (1 + \nu_f) + \beta_m (1 - V_f)(1 + \nu_m) - \\ &\quad - \beta_L [\nu_f V_f + \nu_m (1 - V_f)]. \end{aligned} \tag{8}$$

The thermoelastic constants are then subjected to rotations about the z-axis locally by the angles $+\gamma$ and $-\gamma$, respectively; and the angle-plied $[\pm\gamma]$ plate can be modeled according a volume-average procedure outlined by Pagano [8]. Specifically, the in-series model is used to derive the in-plane laminate properties by volume-averaging the associated lamina stiffness constants, and the out-of-plane properties by volume-averaging the associated lamina compliance constants. The expressions for the thermoelastic constants of the off-axis lamina as well as the $[\pm\gamma]$ laminates will be omitted here for reasons of brevity; details are found in [4].

As the core of the tube is composed of 2 families of curved $[\pm\gamma]$ laminates; these palates intersect each other with the angle $\alpha(r)$ and $-\alpha(r)$, respectively, at the concentric circle of radius r (see Figure 2a). Hence, the properties of the overall tube can be obtained by an additional round of coordinate transformation and volume-averaging procedure.

Let the coordinates $(1,2,3)$ be the spatial directions of the overall tube: axis-1 is in the tube's longitudinal direction, axis-2 in the circumferential direction and axis-3 in the radial direction. The elastic constants of the $[\pm\gamma]$ laminates are first transformed to the global coordinates $(1,2,3)$; and the elastic constants of the overall tube are found by volume-averaging the compliance as outlined in [6]. This results in a set of "effective" elastic properties for the tube's core, being orthotropic in the coordinates $(1,2,3)$. The effective thermal expansion coefficients of the tube are obtained similarly following the outlines in [7]. For brevity, expressions for these properties are omitted here (see [4] for details).

3.2. Illustrative Examples

Two tubular preforms will be considered as illustrative examples. These tubes are to be braided using a graphite yarn with 12K fibers, and to be consolidated with an epoxy resin; both constituents come with known properties. Namely, for the yarn, the solid cross-sectional area is $A_f = 0.477\,\text{mm}^2$; for the fiber in the yarn, the elastic modulus is $E_f = 234.4\,\text{GPa}$, the Poisson ratio $\nu_f = 0.22$, and the thermal expansion coefficient $\beta_f = 0$; for the resin, the elastic modulus is $E_m = 34.5\,\text{GPa}$, the Poisson ratio $\nu_m = 0.34$ and the thermal expansion coefficient $\beta_m = 70\,\mu\varepsilon/^\circ\text{C}$. In addition, the minimum yarn-to-yarn spacing of the 12K graphite yarn under maximum yarn jamming condition is empirically determined as $d_{\text{min}} = 0.6\,\text{mm}$.

Now, let the tubular preform be braided under uniform yarn jamming and the final dimensions of the tube be $R_1 = 60\,\text{mm}$ and $R_2 = 100\,\text{mm}$. Then, the initial design will be as follows:

Given the yarn size ($A_f = 0.477\,\text{mm}^2$), the braiding pitch h and the yarn-to-yarn spacing d may be empirically estimated: say $h = 4\,\text{mm}$ and $d = 0.7\,\text{mm}$ ($d > d_{\text{min}}$ ensures braidability). With these preliminary selections, at least two braiding setup combinations: $[M \times N] = [380 \times 47]$ and $[M \times N] = [532 \times 35]$

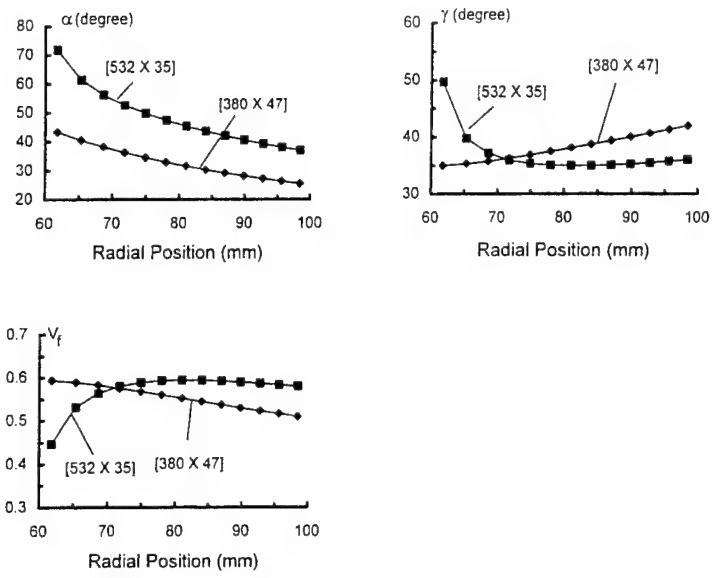

Figure 3. Comparison of the parameters $\alpha(r)$, $\gamma(r)$ and the property $V_f(r)$ in the tubular braids of 380 × 47] and 5342 × 35].

will satisfy (2). This ensures that these two $[M \times N]$ setup designs can each yield a tube with the same exterior size R_1 and R_2 with expected $h = 4\,\text{mm}$ and $d = 0.7\,\text{mm}$. However, difference between the two tubes can be seen in the yarn imprints on the tubes' surfaces as the yarn angle θ_{1s} on the inner surface and θ_{2s} on the outer surface depend on the number M. Internally, the values for the parameters α, γ and V_f in the two tubes also differ; so are the respective mechanical properties.

Figure 3 shows a comparison of the parameters α, γ and V_f (all plotted as functions of radial position r) for the two cases. For the tube of $[M \times N] = [380 \times 47]$, the angle α is about 45° at the inner surface and it gradually decreases radially to about 25° at the outer surface; the angle γ increases from 35° to about 40°; and the fiber volume fraction V_f decreases from 0.6 to about 0.5 in the same radial range. In contrast, in the tube of $[532 \times 35]$, the angle α in the latter case decreases sharply from 75° to about 40° radially. The behavior of γ is also erratic in that it decreases from 50° to about 35° within the first-third of tube thickness; it remains at about 35° for the next two-thirds of tube thickness. The behavior of V_f is similar, as is seen in Figure 3.

The mechanical properties of the tubes reflect the characteristics of their yarn structures. The effective elastic moduli and thermal expansion coefficients of the tube $[380 \times 47]$ are shown in Figure 4, where all quantities are plotted as functions of r. A display of the same for the tube $[532 \times 35]$ is shown in Figure 5.

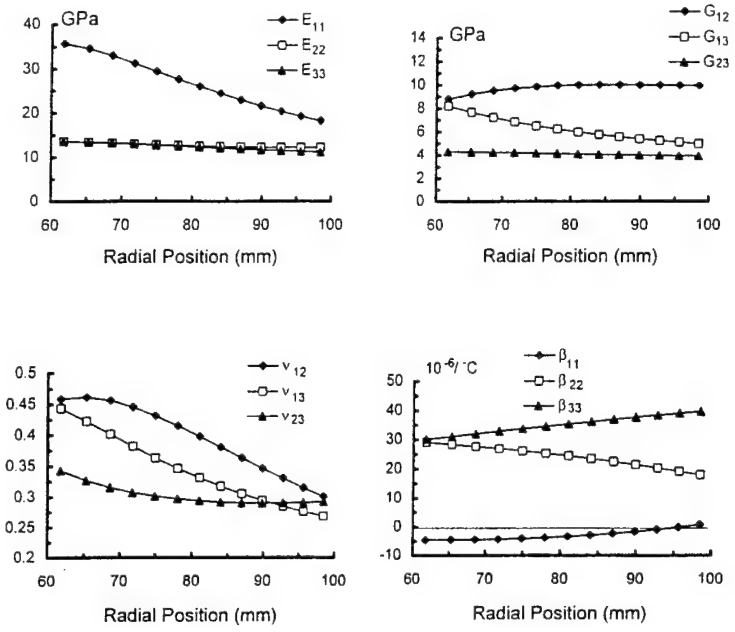

Figure 4. Radial behaviors of the predicted elastic orthotropic constants in the [380 × 47] composite tube.

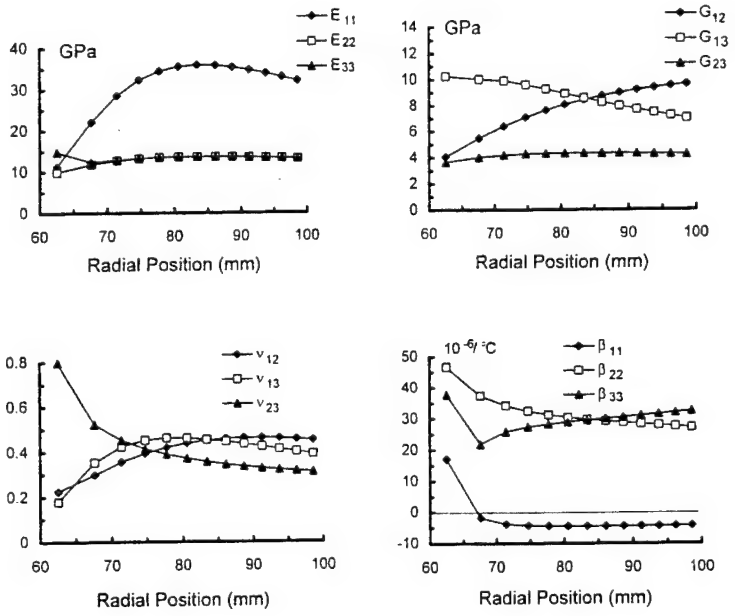

Figure 5. Radial behaviors of the predicted elastic orthotropic constants in the [532 × 35] composite tube.

A comparison of the corresponding properties between these two tubes shows that the radial variation of all the constants is relatively gradual in the first case, while rather erratic in the second case. In may be said that the second tube represents a bad design compared to the first, although both are braidable and meet the same shape and dimensional requirements.

3.3. A Brief Discussion on Optimal Design

Clearly, there can be more than one braidable preform design to meet the same tube size requirement. But the yarn structure and the properties in the final product can differ widely. It is possible that an optimal preform design may be found which meets most if not all of the preset property requirements through selections of the M, N, h and d combinations. The extent to which this can be done is provided by the analytical interrelationships outlined in this paper, as these form a closed loop linking not only the variables defining the successive stages in fabrication but also the properties of the final product. This optimal design concept can be potentially useful for complex-shaped and property-specific composite articles. It's full development requires the specifics in the design constraints; that is beyond the scope of the present paper.

Appendix: Derivation on Equation (2) of the Text

Figure A is a wedge of the tube's cross-section in which the geometric details of the yarn lines (projections on cross-section) are delineated. The thickness of the tube is defined by its inner radius R_1 and outer radius R_2; curve-a and curve-a' are two adjacent yarn lines from family-a which intersect two adjacent yarn lines, curve-b and curve-b' from family-b; curve-a and curve-b intersect at point A which is located at (r, θ); the intersecting angle between curve-a (or b) with the circle of radius r is α. The local grid, denoted as $ABCD$ in the figure, is formed by these four yarn lines; the grid represents the smallest unit-cell in the braided tube.

With uniform yarn-jamming, the yarn-to-yarn spacing d is a constant throughout the tube; this is represented by the line DE of the grid. From the local geometry, the following relations are obtained:

$$\tan\alpha = DF/AF = \Delta r/(r\Delta\theta), \tag{A.1}$$

$$\sin\alpha \approx DE/DB = d/(2r\Delta\theta). \tag{A.2}$$

Note that, for the entire tube, there are M yarn lines in family-a or family-b; hence

$$2\Delta\theta = 2\pi/M. \tag{A.3}$$

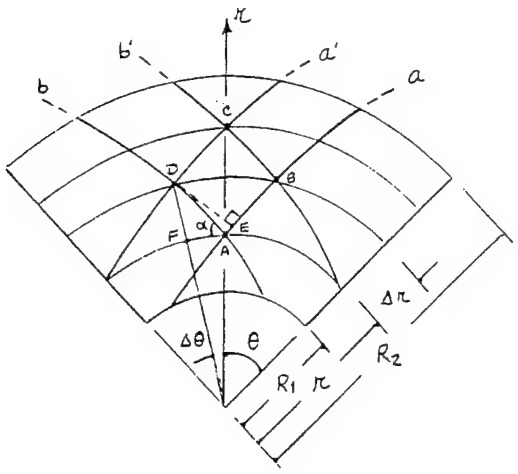

Figure A. Local geometry of yarn lines in the braided tube cross-section.

With the above, it is straight forward to obtain:

$$\Delta\theta/\Delta r = \left[\sqrt{(4\pi^2 r^2 - d^2M^2)}\right]/(dMr). \tag{A.4}$$

Integration of (A.4) along, say, curve-b from the inner radius to the outer radius yields

$$\theta_2 - \theta_1 = \sqrt{[(4\pi^2 R_2^2)/(d^2M^2) - 1]} - \sqrt{[(4\pi^2 R_1^2)/(d^2M^2) - 1]} + \\ + \sec^{-1}[2\pi R_2/(dM)] - \sec^{-1}[2\pi R_1(dM)]. \tag{A.5}$$

Since there are N rows of yarn carriers radially, the left-hand-side of (A.5) is easily

$$\theta_2 - \theta_1 = 2N\pi/M. \tag{A.6}$$

Introducing the non-dimensional variable (Equation 3 of text):

$$\lambda = (2\pi R_1)/(Md\sqrt{2}) \tag{A.7}$$

together with (A.6), (A.5) becomes:

$$2\pi(N/M)/\lambda = \sqrt{2}\Big\{\sqrt{[(R_2/R_1)^2 - 1/(2\lambda^2)]} - \\ - (1/\lambda/\sqrt{2})\sec^{-1}(\sqrt{2}\lambda R_2/R_1) - \\ - \sqrt{[1 - 1/(2\lambda^2)]} + (1/\sqrt{2}/\lambda)\sec^{-1}(\lambda\sqrt{2})\Big\}, \tag{A.8}$$

which is Equation (2) in the text.

Acknowledgements

The results reported here are obtained during the course of a research supported by a grant from the Air Force Office of Scientific Research.

References

1. Chou, T. W. and Ko, F. K. (eds.), *Textile Structural Composites*, Elsevier Science Pub., 1989.
2. Wang, Y. Q. and Wang, A. S. D., 'On the Topological Yarn Structure in 3D Rectangular and Tubular Braided Preforms', *J. Composites Science and Technology* **51**, 1994, 575–586.
3. Wang, Y. Q. and Wang, A. S. D., 'Geometric Mapping of Yarn Structures Due to Shape Change in 3D Braided Composites, *J. Composites Science and Technology* **54**, 1995, 359–370.
4. Wang, Y. Q. and Wang, A. S. D., 'Microstructure-property Relationships in 3D Braided Composites, *J. Composite Science and Technology* **53**, 1995, 213–222.
5. Wang, Y. Q. and Wang, A. S. D., 'Formability of 3D Braided Composites', *Proceedings, ICAM '96*, Beijing, China, 1996.
6. Chamis, C. C., 'Simplified Composite Micromechanics Equations for Hygral, Thermal and Mechanical Properties', *SAMPLE Quart.*, April 1984, 14.
7. Schapery, R. A., 'Thermal Expansion Coefficients of Composites Based on Energy Principles', *J. Composite Materials* **2**(3), 1968, 380.
8. Pagano, N. J., 'Exact Moduli of Anisotropic Laminates', in *Mechanics of Composite Materials*, G. P. Sendeckyj (ed.), Academic Press, New York, 1974, 23.

Add: City? New York

Peking Univ. Press PP. 160-167

ELSEVIER

Composites Science and Technology **53** (1995) 213–222
Elsevier Science Limited
Printed in Northern Ireland

0266-3538(95)00021-6

MICROSTRUCTURE/PROPERTY RELATIONSHIPS IN THREE-DIMENSIONALLY BRAIDED FIBER COMPOSITES

You-Qi Wang* & A. S. D. Wang

Department of Mechanical Engineering, Drexel University, Philadelphia, Pennsylvania 19104, USA

(Received 25 October 1993; revised version received 24 March 1994; accepted 15 December 1994)

Abstract

Three-dimensional braiding is a unique way of manufacturing composite structures directly in their final shapes. In the process, the fibers (yarns) are braided first into a structural preform which is then impregnated with a matrix material and consolidated into the final shape. The purpose of this paper is to demonstrate the analytical link between manufacturing and microstructure, and to properties of braided composites. A descriptive methodology for the yarn skeletal structure in the preform is presented based on the braiding procedure. The yarn skeletal structure so identified preserves the topological character in preforms of any permissible shape. This feature allows the determination of the yarn structure in the consolidated composites whose shape may be distorted during consolidation. From the final yarn structure, local and global properties of the composite can be obtained through a modeling procedure. Structural shapes braided by the four-step 1×1 procedure are used as examples; numerical results of thermomechanical properties in variously braided preforms are presented in explicit terms of the braiding parameters.

Keywords: three-dimensional braiding, yarn structure, thermoelastic properties

1 INTRODUCTION

Textile composites technology by preforming is an application of textile processes to produce structured fabrics, known as preforms. The preform is then impregnated with a selected matrix material and consolidated into a permanent shape. Braiding with continuous fibers or yarns can place three-dimensional (3D) reinforcements in monocoque structural composites. Since the braiding procedure dictates the yarn structure in the preform and the yarn structure dictates the properties of the composite, designing the braiding procedure so as to yield the desired structural shape that is endowed with the desired properties is an important element in textile composites technology.

This paper presents an analysis method which attempts to bridge the relationships between the braiding procedure and the properties for 3D braided structural shapes. The method contains two related developments, with the first concerning the determination of the yarn structure and the second concerning the extraction of mechanical properties from a mechanics model.

With the method presented, general yarn topology in preforms braided by a given textile procedure is established first. From the general topology, basic unit cells are then identified. It will be shown that preforms of different cross-sectional shapes but braided by the same procedure are all composed of the same basic unit cells. Furthermore, if the cross-sectional shape of a preform is distorted during matrix consolidation, the general yarn topology in the preform is unchanged; only the values of the characterizing parameters are covariant with the shape change. This feature provides the ease in determining the yarn structure in the final shape from that in the initial shape by a proper topological mapping.

With the yarn structure fully described, both local and global properties in the structural shape are then estimated by a suitable mechanics modeling procedure.

The popular four-step 1×1 braiding procedure is used to demonstrate the successive developments. Determination of yarn structures in various preforming states is contained in Section 2. An illustrative property modeling approach is described in Section 3, where the thermomechanical properties in the basic unit cells and in preforms of different cell compositions are derived. All results are expressed in explicit terms of the braiding parameters to demonstrate the direct link between the braiding parameters and the resulting properties.

A set of summarizing remarks is contained in Section 4.

* Present address: Kansas State University, Manhattan, Kansas 66502, USA.

2 BRAIDING, YARN TOPOLOGY AND BASIC UNIT CELLS

Several braiding methods are used to fabricate preforms.[1–5] These are often classified by the kind of fabric they produce: 2D or 3D. The former is suitable for plate or thin-walled shapes, while the later is suitable for solid or thick-walled shapes. Many differing procedures exist for 3D braiding, such as the two-step,[4] four-step,[3] the interlock process,[5] etc. Within each procedure, there are also variations: the 'four-step 1×1', the 'four-step 1×2', for instance. The four-step 1×1 method will be adopted in this paper for the purpose of illustration only.

2.1 The 'four-step 1×1' procedure

A schematic set-up for the four-step 1×1 braiding procedure is shown in Fig. 1. The preform being braided is hung above the machine bed, on which yarn carriers are arranged in a prescribed pattern. Braiding is realized through the movements of yarn carriers on the machine bed. Figure 2 illustrates the carrier pattern and movement steps in one braiding cycle. Here, the initial yarn carrier pattern is designed for a solid preform of square cross-section. In each carrier movement step, the carriers only move one position either along the column or the row directions. Specifically, step-1 involves carrier motions in alternate rows and step-2 involves carrier motions in alternate columns, as indicated by the arrows in each step; step-3 involves row motions which reverse those in step-1 and step-4 involves column motions which reverse those in step-2. Note that the yarn carrier pattern after step-4 returns to the initial pattern, thus completing a cycle. After each cycle of braiding, the yarns are generally subjected to a jamming action so

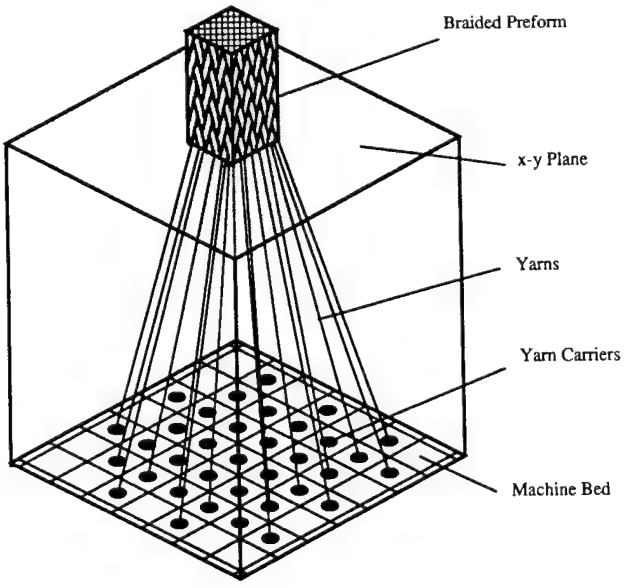

Fig. 1. Schematic diagram of a 3D braiding set-up.

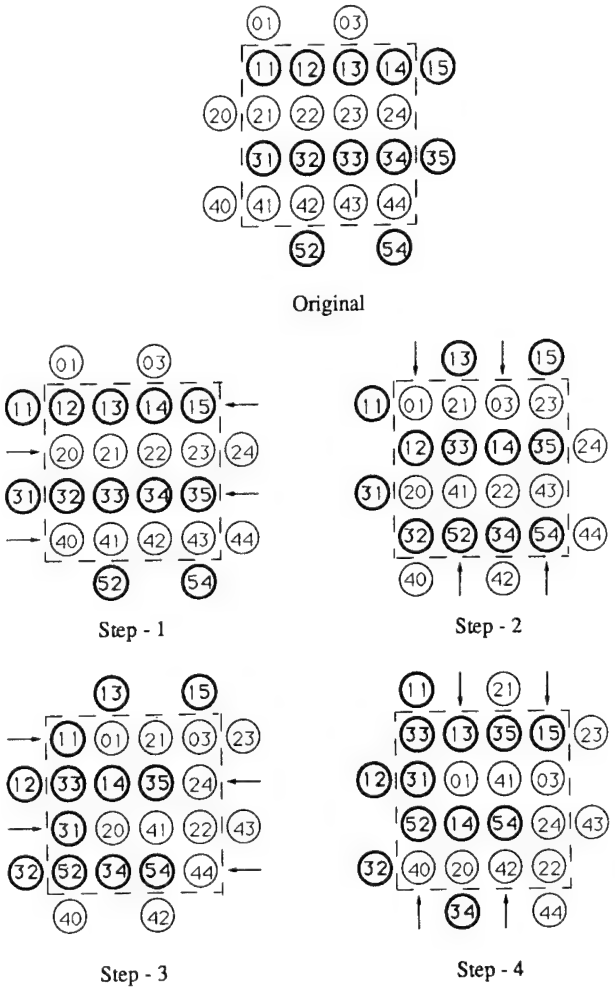

Fig. 2. Yarn carrier movement in one braiding cycle of the four-step 1×1 procedure.

the yarns are closely packed; and a finite length of the preform is realized, known as a pitch. Uniform jamming after each braiding cycle will result in a constant pitch along the length of the preform.

Clearly, the exact yarn carrier pattern dictates the cross-sectional shape of the preform. A rectangular pattern is commonly denoted by $[M \times N]$, M being the number of rows and N the number of columns of the yarn carriers on the machine bed. The set-up shown in Fig. 2 would furnish a (4×4) square cross-section. The actual size of the preform cross-section (also the pitch) depends on the yarn used and the condition of yarn jamming. It should also be noted that both the size and the shape of the preform may be changed during the matrix consolidation process.

2.2 A control-volume method for yarn topology

There have been studies devoted to describing the yarn network in 3D braids.[6–9] The general approach is to follow the braiding procedure and identify the yarn network in space. For the preform interior, a single repetitive unit cell is usually identified which is

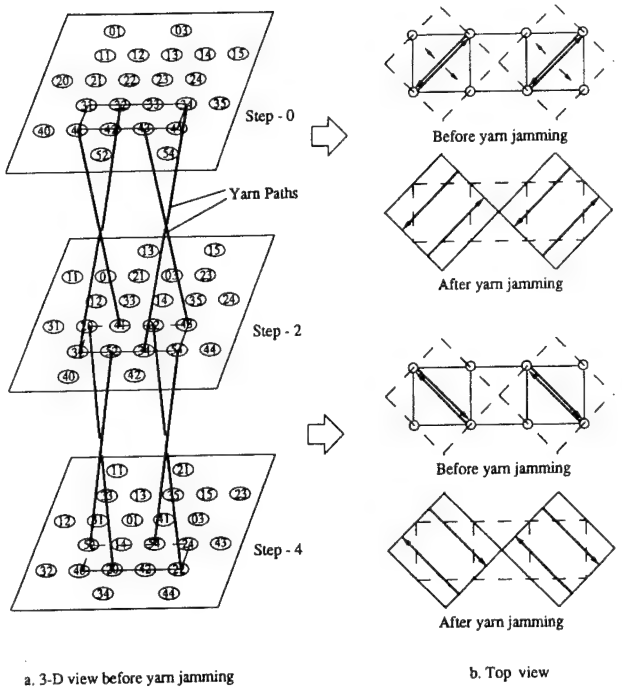

Fig. 3. Yarn trace in the control volume before and after yarn jamming.

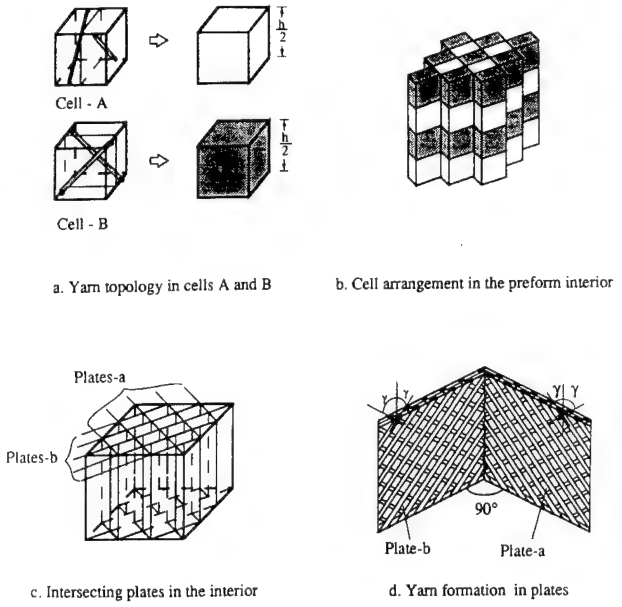

Fig. 4. Yarn topology in the preform interior.

considered to represent the basic character of the preform yarn structure (see, for example, Ref. 6). On the boundary (i.e. the surfaces) of the preform, unique yarn structures exist (see Refs 7–9); this then necessitates separate yarn representation on the preform boundary. Most of the studies, however, were aimed primarily at describing the yarn structures post mortem; the topological nature of the yarn structures and the associated characteristics were not emphasized.

In this section, a control volume method is outlined to describe the general topology in preforms braided by the four-step 1×1 procedure. The purpose is to demonstrate the association between the braiding procedure and the resulting yarn topology.

Follow the yarn carrier movements shown in Fig. 2 for one braiding cycle and trace the yarn paths in space. Instead of following all the carriers, a set of representative carriers will be selected. Figure 3(a) shows the selected carriers (numbered 31–34 and 41–44 at the step-0); the subsequent movements of these carriers form a control space, or a control volume (CV). Thus, during the first two steps, carriers (41, 32) and (43, 34) exchange their respective positions inside the CV; at the same time, carriers (31, 33, 42, 44) move to positions outside the CV. This then forms four crisscrossing yarns inside the upper half of the CV. Similarly, during the next two steps, four crisscrossing yarns are formed in the lower half of the CV.

Essentially, the yarn trace in the CV discussed above characterizes the general topological character of the yarn structure in the preform interior. Specific characterization of the yarn topology will be explained in more detail below.

2.3 Basic unit cells of the interior

Assume that a uniform yarn jamming is applied after the braiding steps; the action will then straighten and reposition the yarns in the CV, as shown in Fig. 3(b). Specifically, the yarns in the top half of the CV form a pair of identical cells, denoted as cell-*A*; and the yarns in the lower half of the CV form a pair of identical cells, denoted as cell-*B*. Yarn lines in cell-*A* and cell-*B* are shown in Fig. 4(a). Note that the jamming action defines yarn inclination angle γ in the unit cells and the pitch of the braid for one cycle, denoted by h.

The preform interior may be treated as a composition of the basic cells, as shown in Fig. 4(b). It can be readily seen that the yarns in the interior unit cells form two families of flat plates which span the entire preform interior, as shown in Fig. 4(c). These plates intersect each other at right angles, and are orientated $\pm 45°$ with respect to the preform surfaces. Each of the flat plates is formed by two groups of crisscrossing yarns (Fig. 4(d)). These are, of course, the same crisscrossing yarns found in the unit cells.

The individual unit cells and the general topology of the interior as a whole are now fully characterized by two free parameters: the braiding angle γ and the braiding pitch h. These two parameters remain free until the preform is consolidated into its final shape.

2.4 Yarn topology on surface and the surface cell

To trace the yarns on the surface, it is convenient to select a 'control surface'. Referring to Fig. 2 at step-0,

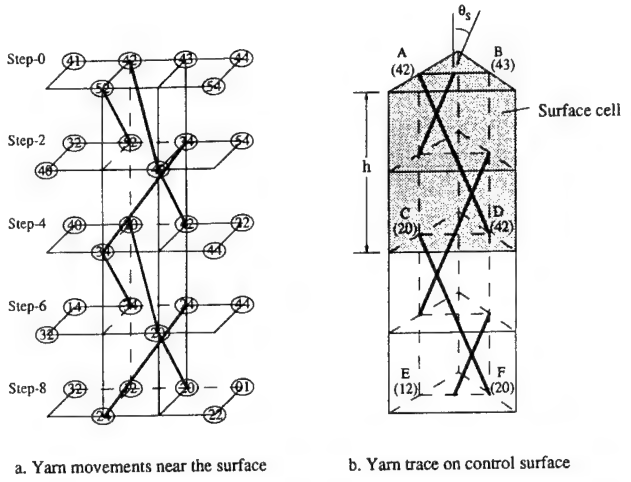

a. Yarn movements near the surface

b. Yarn trace on control surface

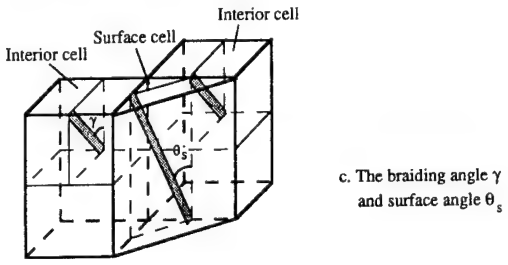

c. The braiding angle γ and surface angle θ_s

Fig. 5. Yarn trace on the surface and surface cell.

the vertical plane containing carriers (41–44) will be selected. Yarn carrier movements across the control surface during eight steps are shown in Fig. 5(a). Follow the carrier 42 for example; it exits the control surface from the interior at step-2 and re-enters at step-4. Similarly, carrier 34 exists the control surface after step-4 and re-enters at step-6. Upon yarn jamming, the yarns will be straightened (with a slight bend which is omitted here) and re-position themselves on the surface defined by *ABCD* in Fig. 5(b). The yarns lying in the surface incline with the braiding axis at the angle $\pm\theta_s$.

A basic cell on the surface may be defined. This is shown by the darkened triangular prism in Fig. 5(b). The yarn topology in the cell is characterized by the angle θ_s and the pitch h. But, from the geometry shown in Fig. 5(c), the surface yarn inclination angle θ_s is readily related to the braiding angle γ of the interior. Thus,

$$\tan\gamma = 2\sqrt{2}(\tan\theta_s) \qquad (1)$$

Hence, the yarn topology on the preform surface is fully characterized by the same γ and h which characterize the preform interior.

Finally, it is possible to mimic the physical look of the preform surface based on the yarn topology. The first frame in Fig. 6 shows the theoretical yarn lines on the surface (thick lines) and the theoretical yarn lines behind the surface (thin lines), or in the preform

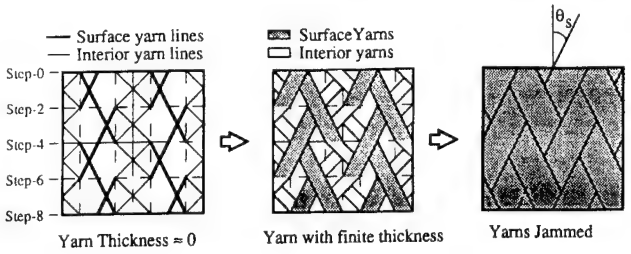

Fig. 6. Yarn structure on the surface before and after yarn jamming.

interior. In the second frame, the yarn lines are replaced by yarns of a finite thickness. In the last frame, the yarns on the surface close up and cover over the interior yarns upon yarn jamming, thus revealing the physical look of the surface. The surface look is relevant for the fact that only the surface yarn angle θ_s and the braiding pitch h can be readily measured with precision. Since it is generally difficult to measure the interior braiding angle γ, eqn (1) can be used to calculate γ by knowing θ_s.

2.5 Yarn topology at corners and the corner cell

The actual preform corner is a rounded surface on which inclining yarns distribute. In the following, only an approximate description for the yarn topology at the corner is presented. Using Fig. 2, a control surface at the corner is defined which contains carrier 44 and 35 at step-0. Yarn carrier movements across the control surface for six steps are shown in Fig. 7(a) (the control surface is JKLM). Here, carrier 44 comes onto the control surface from the interior at step-0. It moves outside the surface at step-2 and shifts a position at step-4; it then returns to the surface again at step-6. Upon yarn jamming, the yarn segment brought by carrier 44 becomes straightened; and it adjusts to a new position as shown in Fig. 7(b). The straightened yarn inclines with braiding axis by the angle θ_c.

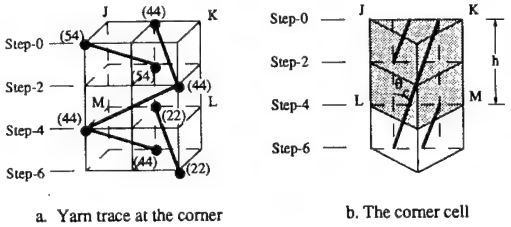

a. Yarn trace at the corner

b. The corner cell

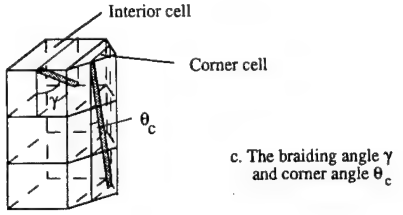

c. The braiding angle γ and corner angle θ_c

Fig. 7. Yarn trace near the corner and the corner cell.

A unit cell at the corner is defined as shown in the darkened triangular prism in Fig. 7(b). When the corner cell is pitted against an interior cell (Fig. 7(c)), the following geometric relationship is then obtained:

$$\tan \theta_c = (\tan \gamma)/6 \qquad (2)$$

Consequently, the yarn topology at the preform corners are also fully characterized by the braiding angle γ and the pitch h.

2.6 Cell composition of preform

At this point, the general yarn topology in rectangular preforms braided by the 4-step 1×1 method has been fully described in terms of two free parameters: γ and h. Specifically, any such preform may be regarded as a composition of the basic cells (interior, surface and/or corner), though the exact manner of composition depends on the initial yarn carrier pattern of the braiding set-up.

Figure 8 shows a few braided cross-sections by the 4-step 1×1 procedure. Note that one of the $[6 \times 6]$ cross-sections (Fig. 8(a)) has corner cells at all four corners; the corresponding yarn carrier pattern is similar to that shown in Fig. 2. However, a slight modification of the carrier pattern can yield a $[6 \times 6]$ cross-section without any corner cell (Fig. 8(b)). Figure 8(c) is a $[5 \times 5]$ cross-section with only two corner cells at opposing corners, while Fig. 8(d) is a $[5 \times 6]$ cross-section with two corner cells on adjacent sides.

The point to be made here is that cell composition can be changed by altering the yarn carrier pattern,

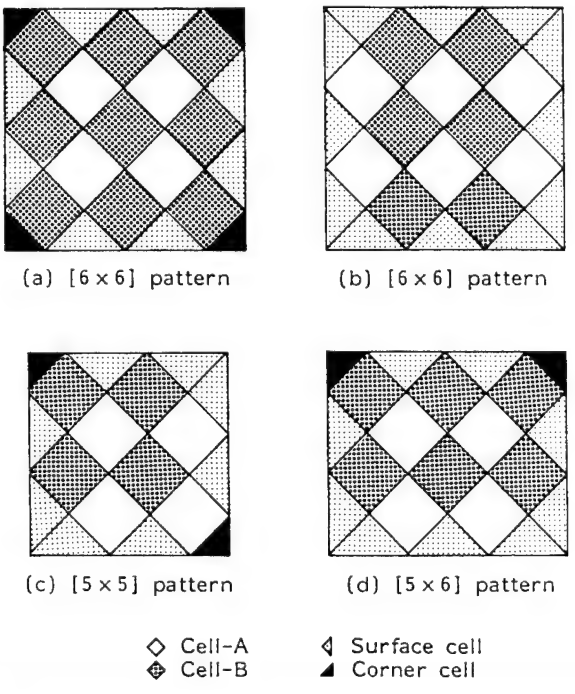

Fig. 8. Braided cross-sections by the 4-step 1×1 procedure.

but the general topology in the basic unit cells is covariant with the braiding procedure alone.

2.7 Topological mapping

Finally, a brief discussion on the subject of topological mapping is in order. As is seen in the above, the general yarn topology in a preform is defined solely by the braiding procedure followed; yarn carrier pattern can only change the cell composition in the preform. In the case of the 4-step 1×1 rectangular braids, the general topology is fully described by two free parameters (γ and h) whose values can be fixed only after the preform is finally consolidated. While the overall shape of a preform is generally determined by the yarn carrier pattern on the machine bed, the final shape of the preform is determined after matrix consolidation. In particular, the initial preform shape may be radically distorted during matrix consolidation, either intentionally or unintentionally. In that case, the yarn structure in the final shape may be inferred from the yarn structure in the initial shape.

This can be readily achieved by utilizing the unique properties of topological mapping. By treating the yarns as convected lines in the solid, it is possible that the yarn topology in the initial preform shape be mappable to that in the final consolidated shape, or vice versa. Determination of the exact mapping function requires the complete knowledge of the two shapes and how one shape is physically deformed to the other shape. As different physical processes impose different constraints on the mapping function, considerable analysis details need to be deployed for this topic. To elaborate these details, however, are outside the scope of the present paper. Interested readers are referred to a separate paper published elsewhere.[10]

3 EVALUATION OF MECHANICAL PROPERTIES

In principle, both the local and global properties of the consolidated preform should be predictable once its internal yarn structure is given in full detail; and this should be achieved with a realistic micromechanics modeling approach. For 3D braided composites, several modeling methods which derive the so-called 'effective properties' have appeared in the open literature.[6,9,11] Due to the 3D nature of the yarn structure, however, a considerable simplification is made in the presentation of the true microstructure in the braids. Generally, these methods follow either the volume-averaging of stiffness[12] or the volume-averaging of compliance technique[13] and treat only the unit cells in the interior. Both of these techniques are akin to the 'rule-of-mixture'; and they provide only first-order bounds for the desired effective properties.[14] Some numerical approaches have also

been explored in recent years, by treating the unit cells as truss-like structures via a finite element procedure.[15–17]

In this section, a simple but analytical modeling approach is followed to extract both the local and the global 'effective properties' of the consolidated preforms. The purpose is to link the manufacturing parameters explicitly to the properties of the braided composites. To this end, a mixed volume-averaging of stiffness and compliance procedure is employed.[10–20] For reason of simplicity but without the loss of generality, a class of preforms which are braided by the 4-step 1×1 procedure and have a square cross-section before and after consolidation will be used as examples. Furthermore, the preform cross-sections have corner cells at all four corners.

3.1 Property evaluation procedures

Each of the basic cells—the interior, surface and corner cell—will be modeled first in order to extract the 'local' properties. The global properties of the overall consolidated preform will then be evaluated based on the cell-composition structure of the preform. A brief discussion of these developments is given below.

3.1.1 The interior cells

The interior of the preform is composed of alternating unit cells *A*s and *B*s; each is endowed with a distinct yarn structure (see Fig 4(a) (b)). Assume that the characterizing braiding parameters h and γ are given, and the required input information concerning the thermoelastic properties of the fiber (of the yarn), the matrix and the fiber–matrix volume contents are also known (see Ref. 21 for the estimation of V_f).

Then, each yarn in cell-*A* or cell-*B* is treated as an off-axis unidirectional ply so that the cell itself is an angle-ply laminate, $[\pm\gamma]$. The ply is considered as an elastic, transversely isotropic solid with the effective engineering constants, E_{LL}, E_{TT}, G_{LT}, ν_{LT} and ν_{TT}, the coefficients of thermal expansion α_L, α_T and the coefficients of moisture expansion β_L, β_T (L refers to the fiber direction; T, transverse to the fiber direction). The effective elastic constants of the ply are evaluated based on a rule-of-mixture model;[18] the effective thermal and moisture expansion coefficients of the ply are evaluated by a similar model;[19] the corresponding properties of the $[\pm\gamma]$ angle-ply laminate are derived based on a lamination model.[20]

For completeness, key derivations in the above are contained in the Appendix.

3.1.2 The surface and corner cells

Based on the yarn structure shown in Fig. 5(b), the surface cell is treated as an assemblage of two unidirectional plies with the fiber orientations of $+\theta_s$ and $-\theta_s$ with respect to the braiding axis. Let $[\mathbf{S}]$, $\{\boldsymbol{\alpha}\}$, $\{\boldsymbol{\beta}\}$ and $[\mathbf{S}]'$, $\{\boldsymbol{\alpha}\}'$, $\{\boldsymbol{\beta}\}'$ be the compliance, the thermal and moisture expansion coefficients for the $+\theta_s$-ply and the $-\theta_s$-ply, respectively; the corresponding compliance properties of the surface cell are obtained by volume-averaging the compliance:

$$[S_s] = ([\mathbf{S}] + [\mathbf{S}]')/2$$
$$\{\alpha_s\} = (\{\boldsymbol{\alpha}\} + \{\boldsymbol{\alpha}\}')/2 \qquad (3)$$
$$\{\beta_s\} = (\{\boldsymbol{\beta}\} + \{\boldsymbol{\beta}\}')/2$$

As for the corner cell, yarn segments are aligned at the angle θ_c with the braiding axis (see Fig. 7(c)). Hence, the corner cell will be considered just as an off-axis unidirectional ply. The compliance, the thermal and moisture expansion coefficients referred to the braiding-axis are derived similarly using the angle θ_c instead of θ_s.

Finally, it should be noted that, depending on the location and orientation of the interior, surface or corner cell, the properties of the cell must be transformed to the preform's global coordinates.

3.1.3 The overall preform

Given the local properties of the interior, the surface and the corner cells, the global properties of the overall consolidated preform are determined by the exact cell composition structure of the preform. Here, again, the volume-averaging technique is used to evaluate the various properties. However, cell composition can be different from one preform to another, even though the basic cells are all the same. For instance, preforms of $[6 \times 6]$ and $[12 \times 12]$ patterns are composed by the same basic cells but have different cell compositions; hence, they will have different global properties. This and other peculiar characteristics of braided composites are further illustrated by the following numerical results.

3.2 Numerical illustrations

As mentioned, preforms braided by the 4-step 1×1 procedure are considered; each preform has a square cross-section before and after consolitation with corner cells at the four corners. The fiber in the yarn and binding matrix used in the consolidation have the following thermoelastic properties:

$E_f = 234$ GPa $\quad \nu_f = 0{\cdot}22 \quad \alpha_f = 0{\cdot}18 \times 10^{-6}$ per °C

$E_m = 3{\cdot}45$ GPa $\quad \nu_m = 0{\cdot}34 \quad \alpha_m = 72 \times 10^{-6}$ per °C

The fiber volume fraction of the consolidated preform is assumed to be $V_f = 0{\cdot}5$; the braiding angle γ is a running variable, ranging from 5° to 60°; the braiding pitch h is set at unity. Three cross-sectional patterns are considered: $[4 \times 4]$, $[8 \times 8]$, and $[12 \times 12]$.

To show the connection between braiding and property, all properties are expressed as functions of the braiding angle γ. All properties are referred to the

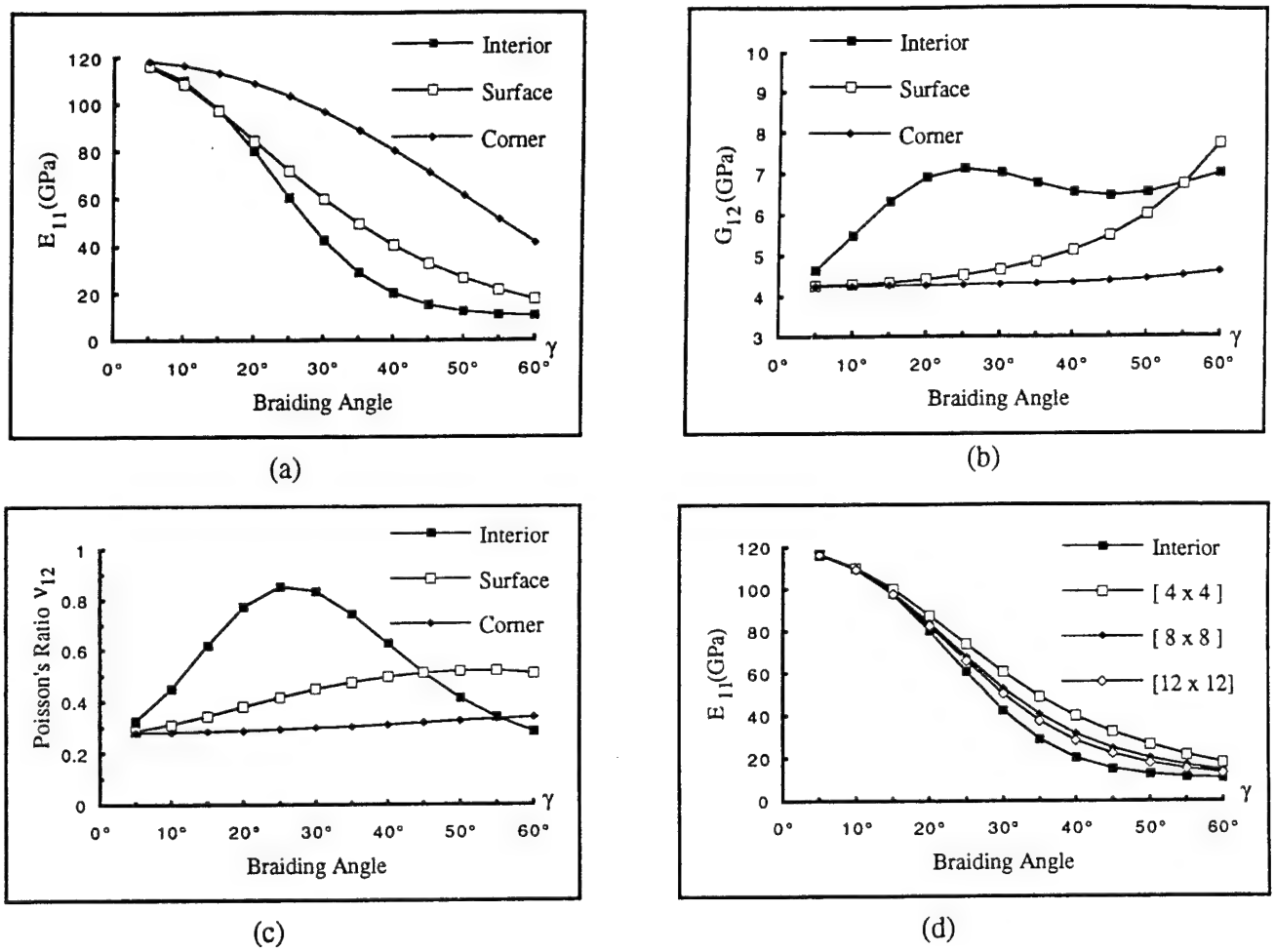

Fig. 9. Elastic moduli of the interior, surface, and corner cells, and in specimens of different sizes.

global coordinates (1, 2, 3) of the preform, 1 being the direction of the braiding axis; 2–3 defines the preform cross-sectional plane. For purposes of illustration, only a few key and revealing properties are shown graphically in Figs 9 and 10.

Figure 9(a) shows the calculated axial elastic moduli E_{11} for the interior, surface and corner cells individually. It is seen that the corner cell has the highest E_{11} value as it should; the interior cell has the lowest E_{11} and the surface cell has a value in between. The influence of γ is considerable in the range of 25° to 55°.

Figure 9(b) shows the calculated shear moduli G_{12} of the various cells as functions of γ. Note that G_{12} of the interior is high in the γ range of 15° to 50° while G_{12} of the surface is high in the γ range of 55° or greater. The corner cell provides negligible shear resistance and it is not affected by γ.

Figure 9(c) shows the variation of ν_{12} as a function of γ. Here, the effect of γ on ν_{12} of the interior cell is most significant.

Now, given the cell composition structure of a preform, it is possible to evaluate its global properties of the preform such as the axial stiffness, bending rigidity, torsional rigidity, etc. And these properties are affected by the preform's cell composition.

Figure 9(d) shows global axial stiffness E_{11} of three preforms: $[4 \times 4]$, $[8 \times 8]$ and $[12 \times 12]$. It is seen that the smaller the size the higher the value of E_{11} or the larger the size the lower the values of E_{11}. This is due to proportionally higher boundary area to interior area ratio in the smaller preform (the boundary areas are stiffer axially than the interior). Hence, for preforms of very large sizes, the effects of the boundary areas become negligible; and the global E_{11} approaches that of the interior area.

Other global properties of the preforms are evaluated similarly; interested readers are referred to Ref. 17.

Lastly, some results for the thermal expansion coefficients α_1 and α_2 $(=\alpha_3)$ are shown in Fig. 10. Here, again, the effect of γ on the thermal properties of the basic cells are considerable, Fig. 10(a). Consequently, the global thermal response will vary with the cell composition structure as well, Fig. 10(b).

Note the peculiar behavior of α_1 of the interior; it

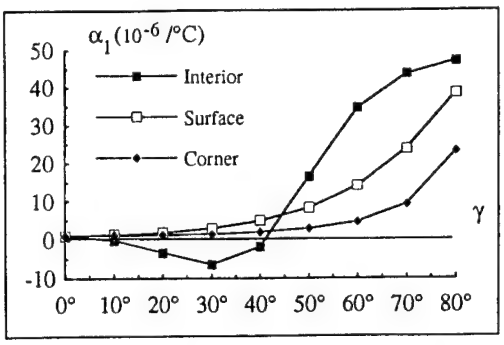

a. Thermal Expansion Coefficients of the Interior, the Surface and the Corner

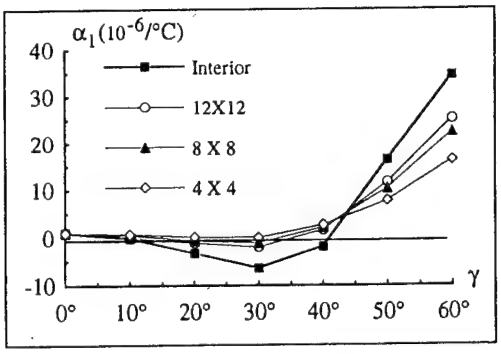

b. Thermal Expansion Coefficients in preforms of different sizes

Fig. 10. Thermal expansion coefficients.

becomes negative in the γ-range of 10° to 40°. The negative thermal expansion of α_1 develops owing to the interlaminar and intralaminar shear deformation in the interior cell structure.

The above results demonstrate clearly that both local and global properties are sensitive to the braiding angle γ in certain γ-ranges. In particular, properties of the interior, surface and corners can be significantly different; and the preform as a whole has properties profoundly influenced by the cell composition structure. The latter is controlled by the yarn carrier pattern at the out set of the braiding process.

4 CONCLUSIONS

In this paper, an analysis method is presented which describes the yarn structures in 3D braided preforms. By tracing the yarn lines in space during the braiding cycle, the general topology of the yarn structure can be analytically established, which depends solely on the braiding method. From the general topology, basic unit cells in the interior and on the boundary are identified and the preform as a whole is treated as a structural composition of the basic cells. The general topology thus provides a geometric description for the individual basic cells as well as for the preform as a whole.

It is then shown that preforms of different cross-sectional shapes but braided by the same procedure have the same topological characteristics; i.e. they are characterized by the same set of parameters. In such cases, a geometric mapping may exist between two preforms of different shapes; and the yarn topology in one shape may be found from that of the other, or vice versa. This mapping concept may be applied to cases where the two different shapes are braided individually, or where the shape of one preform is deform into another shape during matrix consolidation.

Modeling of the basic cells is carried out by a simple micromechanics procedure. It reveals that it is generally possible to analytically relate the preform properties to the braiding parameters. It also shows that the preform as a whole is one without homogeneous properties, since the cells in the preform interior are different from those on the boundary.

Finally, it is mentioned that the method presented in this paper can be applied to preforms of complex shapes, such as a tubular cross-section; or it can be applied to other braiding methods, such as the 4-step 1×2.

REFERENCES

1. Bluck, B. M., High speed bias weaving and braiding. US Patent No. 3,426,804, Feb. 1969.
2. Maistre, M. A., Construction of a three dimensional structure. German Patent No. P2301696.8, 1973.
3. Florentine, R., Apparatus for weaving a three-dimensional article. US Patent No. 4,312,261, January, 1982.
4. McConnell, R. F. & Popper, P., Complex shaped braided structures. US Patent No. 4,719,837, January, 1988.
5. Cole, P. M., Three dimensional structures of interlocked strands. US Patent No. 4,737,399, April, 1988.
6. Ko, F. K., Three dimensional fabrics for composites—an introduction to the Magnaweave structure. *Proc. ICCM-4*, Japan Society for Composite Materials, Tokyo, 1982, p. 1609.
7. Li, W., On the structural mechanics of 3-D braided preforms for composites. PhD thesis, North Carolina State University, NC, USA, 1990.
8. Lei, C., Cai, Y. J. & Ko, F. K., Finite element analysis of 3-D braided composites. In *Adv. in Eng. Software and Workstations*, Elsevier Science, 1992, p. 187.
9. Kostar, T. D. & Chou, T. W., Design and automated fabrication of 3-D braided preforms for advanced structural composites. In *Composite Materials Technology III*, Elsevier Science, 1992, p. 63.
10. Wang, Y. Q. & Wang, A. S. D., On topological mapping of yarn structures in 3-D braided preforms. *Proc. 9th Tech. Conf.*, Amer. Soc. Composites. Technomic, Lancaster, PA, 1994.
11. Yang, J. M., Ma, C. L. & Chou, T. W., Fiber inclination model of three-dimensional textile structural composites. *J. Comp. Mater.*, **20** (1986) 472.

12. Voigt, W., Ueber die beziehung zwischen den beiden elastizitats-constanten isotroper Korper. *Ann. der Phys. und Chemie* (Leipzig), **38** (1889) 537.
13. Reuss, A., Berechnung der fliessgrenze von mischkristallen auf grund der plastizitatsbedin-gung fuer einkristalle. *ZAMM*, **9**, (1929) 49.
14. Hill, R., The elastic behavior of a crystalline aggregate. *Proc., Phys. Soc.* (London), **A185** (50) (1952) 349.
15. Ma, C. L., Yang, J. M. & Chou, T. W., Elastic stiffness of three-dimensional braided textile structural composites. In *Composite Materials: Testing and Design* (ASTM STP 893), ed. J. M. Whitney. American Society for Testing and Materials, Philadelphia, PA, USA, 1986, p. 404.
16. Let, C., Wang, A. S. D. & Ko, F., A finite cell model for 3-D braided composites. In *Adv. Composites Processing Technology*, eds T. H. Chiang & R. A. Taylor. ASME MD-5, New York, USA, 1988, p. 45.
17. Moharjerjasbi, S., Structure and mechanical properties of 3-D braided composites. PhD thesis, Drexel University, 1993.
18. Chamis, C. C., Simplified composite micromechanics equations for hygral, thermal and mechanical properties. *SAMPE Quart.*, **April** (1984) 14.
19. Schapery, R. A. Thermal expansion coefficients of composites based on energy principles. *J. Comp. Mater.*, **2**(3) (1968) 380.
20. Pagano, N. J., Exact moduli of anisotropic laminates. In *Mechanics of Composite Materials*, ed. G. P. Sendeckyj. Academic Press, New York, USA, 1974, p. 23.
21. Wang, Y. Q. & Wang, A. S. D., On topological yarn structure of 3-D rectangular and tubular braided preforms. *Comp. Sci. Technol.*, **51** (1994) 575.

APPENDIX: MODELING THE PROPERTIES OF THE INTERIOR

The unidirectional lamina

Consider the interior unit cell A or B. Each half of the cell contains a single fiber strand (or yarn), which is now treated as a unidirectional composite lamina. Assume that the volume fraction of fiber V_f and the properties of the fiber and matrix are given. Following the methods in Refs 18 and 19, the thermoelastic constants of the lamina are calculated. Thus, the constitutive law for the unidirectional lamina, expressed in the (L, T, Z) coordinates, is given by

$$\{\varepsilon\} = [S]\{\sigma\} + \Delta T\{\alpha\} + \Delta W\{\beta\} \tag{A1}$$

where ΔT and ΔW are the change of temperature and moisture content, respectively; and

$$[S] = \begin{bmatrix} S_{11} & S_{12} & S_{12} & 0 & 0 & 0 \\ S_{12} & S_{22} & S_{23} & 0 & 0 & 0 \\ S_{12} & S_{23} & S_{22} & 0 & 0 & 0 \\ 0 & 0 & 0 & 2(S_{22}-S_{23}) & 0 & 0 \\ 0 & 0 & 0 & 0 & S_{66} & 0 \\ 0 & 0 & 0 & 0 & 0 & S_{66} \end{bmatrix} \tag{A2}$$

$$\{\alpha\} = \{\alpha_L, \alpha_T, \alpha_T, 0, 0, 0\}^T$$

$$\{\beta\} = \{\beta_L, \beta_T, \beta_T, 0, 0, 0\}^T$$

The non-zero elements in $[S]$ are given by

$$S_{11} = 1/E_{LL}; \quad S_{12} = -\nu_{LT}/E_{LL}; \quad S_{22} = 1/E_{TT};$$
$$S_{23} = -\nu_{TT}/E_{TT}; \quad S_{66} = 1/G_{LT}$$

A rotation about Z-axis

The fiber direction of the lamina in the unit cell orients with the preform braiding axis (X_1) at the angle γ or $-\gamma$. The compliance $[S]$ and the hygrothermal coefficients $\{\alpha\}$ and $\{\beta\}$ of the lamina will now be referred to the braiding axis, by a coordinate transformation involving a rotation about the Z-axis through the angle γ or $-\gamma$. Accordingly, the compliance matrix $\mathbf{[S]}$, the hygrothermal expansion coefficients $\{\boldsymbol{\alpha}\}$ and $\{\boldsymbol{\beta}\}$ of the lamina after the transformation are:

$$\begin{aligned} \mathbf{[S]} &= [T]_\varepsilon [S][T]_\sigma^{-1} \\ \{\boldsymbol{\alpha}\} &= [T]_\varepsilon \{\alpha\} \\ \{\boldsymbol{\beta}\} &= [T]_\varepsilon \{\beta\} \end{aligned} \tag{A3}$$

where

$$[T]_\sigma = \begin{bmatrix} m^2 & n^2 & 0 & 0 & 0 & 2mn \\ n^2 & m^2 & 0 & 0 & 0 & -2mn \\ 0 & 0 & 1 & 0 & 0 & 0 \\ 0 & 0 & 0 & m & -n & 0 \\ 0 & 0 & 0 & n & m & 0 \\ -mn & mn & 0 & 0 & 0 & m^2-n^2 \end{bmatrix} \tag{A4}$$

$$[T]_\varepsilon = \begin{bmatrix} m^2 & n^2 & 0 & 0 & 0 & mn \\ n^2 & m^2 & 0 & 0 & 0 & -mn \\ 0 & 0 & 1 & 0 & 0 & 0 \\ 0 & 0 & 0 & m & -n & 0 \\ 0 & 0 & 0 & n & m & 0 \\ -2mn & 2mn & 0 & 0 & 0 & m^2-n^2 \end{bmatrix} \tag{A5}$$

In the above, $m = \cos(\pm\gamma)$ and $n = \sin(\pm\gamma)$, the sign of γ being appropriate with the particular lamina in the cell.

The properties of the cell

The properties of the cell are derived by treating the cell as a $[\pm\gamma]$ laminate. A model similar to that developed in Ref. 20 is used here; it is essentially a mixed volume averaging technique. Specifically, the in-plane laminate moduli are derived by volume-average of stiffness, while the out-of-plane moduli are derived by volume-average of compliance. The procedure amounts to the following physical assumptions:

(1) the in-plane strains, $\boldsymbol{\varepsilon}_{11}$, $\boldsymbol{\varepsilon}_{22}$, $\boldsymbol{\varepsilon}_{12}$, are constant throughout the thickness of the laminate under the in-plane loading; and

(2) the out-of-plane stresses, $\boldsymbol{\sigma}_{33}$, $\boldsymbol{\sigma}_{23}$, $\boldsymbol{\sigma}_{31}$, are constant throughout the thickness of the laminate under the out-of-plane load.

It then follows that the non-zero elements in the compliance matrix $[S_c]$ for the cell in its own natural coordinates are given by

$$
\begin{aligned}
S_{c11} &= \mathbf{S}_{11} - \mathbf{S}_{16}^2/\mathbf{S}_{66} \\
S_{c12} &= \mathbf{S}_{12} - \mathbf{S}_{16}\mathbf{S}_{26}/\mathbf{S}_{66} \\
S_{c22} &= \mathbf{S}_{22} - \mathbf{S}_{26}^2/\mathbf{S}_{66} \\
S_{c66} &= \mathbf{S}_{66} - (\mathbf{S}_{11}\mathbf{S}_{26}^2 + \mathbf{S}_{22}\mathbf{S}_{16}^2 \\
&\quad + 2\mathbf{S}_{12}\mathbf{S}_{16}\mathbf{S}_{26})/(\mathbf{S}_{11}\mathbf{S}_{22} - \mathbf{S}_{12}^2) \\
S_{cij} &= \mathbf{S}_{ij} \quad \text{when } i = 1, 2, 3 \text{ and } j = 3 \\
S_{cii} &= \mathbf{S}_{ii} \quad \text{when } i = 4, 5
\end{aligned}
\tag{A6}
$$

The thermal expansion coefficients are given by:

$$
\begin{Bmatrix} \alpha_{c1} \\ \alpha_{c2} \\ \alpha_{c3} \end{Bmatrix} = \begin{bmatrix} S_{c11} & S_{c12} & 0 & \cos^2\gamma & \sin^2\gamma \\ S_{c21} & S_{c22} & 0 & \sin^2\gamma & \cos^2\gamma \\ 0 & 0 & 1 & 0 & 0 \end{bmatrix} \begin{bmatrix} 0 & S_{11} & S_{12} & 0 \\ 0 & S_{21} & S_{22} & 0 \\ 1 & 0 & 0 & 1 \end{bmatrix}^{-1} \begin{Bmatrix} \alpha_L \\ \alpha_T \\ \alpha_T \end{Bmatrix} \tag{A7}
$$

and the moisture expansion coefficients $\{\beta_c\}$ can be similarly found as in eqn (A7).

Properties of the preform interior

The preform interior is composed of cells A and B arranged alternately. Also, cells A and B are oriented at $\pm 45°$ with the reference frame of the preform. Hence, to obtain the properties of the interior in the preform reference frame, a coordinate transformation must be performed for cells A and B. The transformations involve a rotation of cell-A about the X_1-axis by 45° and a rotation of cell-B by $-45°$. Both transformations can be readily obtained using the formula in eqns (A4) and (A5). Thus, omitting the details in the algebra, six engineering constants of the interior are obtained:

$$
\begin{aligned}
E_{11} &= 1/S_{c11} \\
E_{22} &= E_{33} = 4/(S_{c22} + 2S_{c23} + S_{c44} + S_{c33}) \\
G_{12} &= G_{13} = 2/(S_{c55} + S_{c66}) \\
G_{23} &= 1/(S_{c22} + S_{c33} - 2S_{c23}) \\
\nu_{12} &= \nu_{13} = -E_{11}(S_{c21} + S_{c31})/2 \\
\nu_{23} &= E_{22}S_{c44}/2 - 1
\end{aligned}
\tag{A8}
$$

The thermal and moisture expansion coefficients in the interior are obtained as:

$$
\alpha_1 = \alpha_{c1} \qquad \beta_1 = \beta_{c1}
$$

$$
\alpha_2 = \alpha_3 = (\alpha_{c2} + \alpha_{c3})/1 \qquad \beta_2 = \beta_3 = (\beta_{c2} + \beta_{c3})/2
$$

PROGRESS IN ADVANCED MATERIALS AND MECHANICS

Proceedings of the International
Conference on Advanced Materials

August 12-15, 1996, Beijing, China

Chief Editors

Wang Tzuchiang *Tsu-Wei Chou*

Peking University Press, Beijing, China

1996

Proceeding of ICAM'96

FORMABILITY OF 3-D BRAIDED COMPOSITES

Youqi Wang
Kansas State University
Manhattan, KS 66506

and

Albert S.D. Wang
Drexel University
Philadelphia, PA 19104

ABSTRACT: A 3-D braided preform is a construction of yarns nestled in a unique 3-dimensional network. The topology of that network depends on the particular braiding procedures followed. When the preform is deformed later from one shape to another shape, the topological characteristics of the yarn network will be preserved if certain physical constraints are obeyed. Specifically, for a permissible deformation, the yarns will be inextensible and their spacings will be finite. The latter is bounded by a minimum spacing due to actual yarn size and a maximum spacing for avoidance of yarn buckling. These constraints will limit the extent to which the preform can be deformed, thus raising the issues of preform formability or deformability.

This paper discusses a class of 3-D preforms braided by the 4-step 1x1 procedure, which undergo deformation from one shape to another shape. It is shown that the topology of the yarn network in one shape may be mapped to the another shape by a proper mapping function. And, the mapping obeys the geometric constraints mentioned above. Consequently, limiting windows can be established within which the mapping will result only in permissible preform deformations. Two examples are worked out in detail to illustrate the developed procedures.

KEY WORDS: 3-D braiding, formability, deformability, textile composites

I. INTRODUCTION

Fiber-reinforced composites have been fabricated by 3-D braiding by using continuous yarns and following a certain procedure in order to form a near-net-shape. However, preforms are often braided in one shape and deformed into another shape during the matrix consolidation stage. From a design view point, it may become necessary to analyze priori the preform's ability to deform as desired, given the initial and the desired shapes. Since the preform is a uniquely constructed network of yarns, shape change is invariably constrained by the geometric interactions of the nestled yarns. Specifically, throughout the deformed preform, the yarns should not be stretched or compressed axially; the yarn may press against but not cut into each other; and the yarn spacings may not be too loose as to cause preform wrinkling. Clearly, these constraints will limit the extent to which the preform can be deformed, raising the issues of preform formability.

In a series of recent papers [1-3], it was shown that the topology of the yarn network in 3-D braids is geometrically describable based on the braiding procedure alone. The topology is described geometrically by a set of dimensional parameters; their actual values are determined by measurements made on the preform surfaces [1,2]. Hence, when a preform is deformed from one shape to another shape, only the values of the characterizing parameters will change

provided that the the topological character of the yarn network is unchanged. As it turned out, such deformation processes can be described by properly determined geometric mapping functions [3].

In this paper, we discuss briefly the topological characteristics in preforms braided by the 4-step 1x1 procedure; this is followed by an outline for determining the mapping functions between prescribed initial and final preform shapes. Discussions are then focussed on conditions of preform formability; limiting windows for permissible preform deformations are established by identifying the mapping functions that satisfy the imposed deformation constraints. Two examples are worked out in detail to illustrate the complete procedure.

II.FORMABILITY OF 3-D BRAIDED PREFORMS

Topological Structure in Initially Braided Preforms.

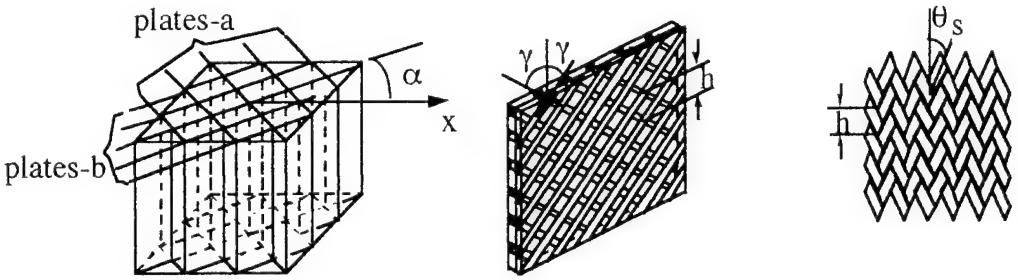

Fig.1. Yarn topology in the rectangular preform: (a) global view of the interior structure; (b) Yarn formation in plate b; (c) view of the preform surface

A "control volume" approach has been detailed in [1] which describes the topological structure in 3-D braided preforms, given the starting-up braiding pattern and the ensuing braiding steps. Fig. 1 shows the key features in the yarn topology for preforms of solid square or rectangular cross-sections braided by the 4-step 1x1 method: the yarn structure in the preform interior consists of 2 families of crisscrossing plates where the angle α characterizes how the plates intersect, see Fig.1a; each of the plates is formed by 2 families of parallel yarns crisscrossing with the intersecting angle γ, see Fig 1b; on the bounding surfaces of the preform, the braiding pattern is shown in Fig. 1c, where the yarns display a weaved pattern characterized by the parameters h and θ_s.

Assuming that the yarns are uniformly jammed during braiding, they will then maintain a uniform yarn-to-yarn spacing Δd_o throughout ; the surface angle θ_s can be geometrically related to α and γ. Thus, only the values of α, γ and h

are needed to defined the entire yarn structure in the preform. And, their values are determined by measurements made on the preform surfaces. When this is done, properties such as the unit-cells, distribution of fiber volume content, the yarn-to-yarn spacing Δd_o etc. can be determined accordingly [1,2].

Permissible Preform Deformation.

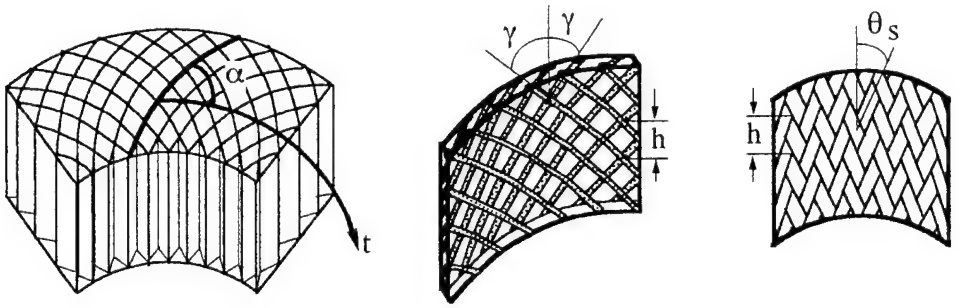

(a) (b) (c)

Fig.2 Yarn formation in a deformed preform

Now, consider the preform of rectangular cross-section and let it be deformed into a curved cross-section as shown in Fig. 2. If the deformation is "permissible", the topological characteristics in the yarn network will be preserved. Namely, the preform interior still consists of 2 families of crisscrossing plates, only that they are now curved (see Fig. 2a) resulting in the characterizing angle α being a function of position. Similarly, the yarns which form the plates continue to have the same crisscrossing topology but the characterizing angle γ also become a function of position, see Fig. 2b. The topology of the surface is shown in Fig. 2c where the parameter h and the parameter θ_s on the preform surfaces may be spatially dependent as well. The yarn-to-yarn spacing Δd in the deformed preform is no longer uniform.

Geometric Mapping.

In order to determine the spatial functions α, γ and h and other related properties in the deformed preform, a geometric mapping method has been detailed in [3]. The essence of that development is that given the initial and the final shapes of the preform, a one-to-one mapping can be found if the deformation is "permissible". With the mapping function, then, the spatial distribution of α, γ and h in the final shape can be obtained from those in the initial shape. The term "permissible" deformation specifically requires that: (1) the yarns will remain inextensible; and (2) the yarn-to-yarn spacing Δd is bounded by a minimum Δd_{min} and a maximum Δd_{max}. These bounds stem from the fact that the yarn size is finite and the yarns cannot become too loose as to cause preform wrinkling due to deformation.

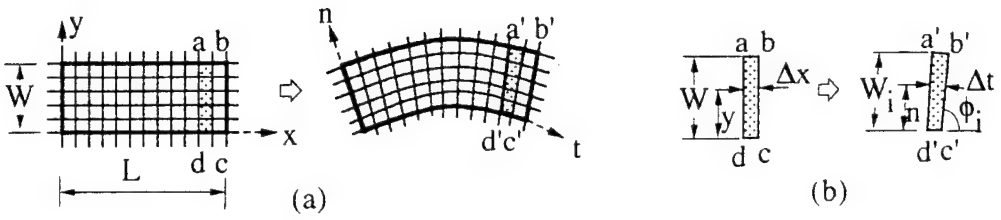

Fig.3 Transformation of coordinate systems and mapping relations

As it was shown in [3] that only the yarn inextensible condition is needed to obtain a class of functions that will fulfill the intended mapping; the bounds imposed on the yarn-to-yarn spacing Δd, in fact, provide allowable windows for those functions that will result in "permissible" deformations.

In this section, we refer to [3] for the key results in the mapping functions. In the interest of clarity, consider Fig. 3, where the preform of initial cross-section LxW is deformed into the curved wedge-like cross-section (Fig. 3a); the associated deformation of a local cross-sectional area (shaded) is shown in Fig. 3b; the preform also deforms axially by a uniform stretch $1/\zeta$. The initial and final shapes themselves and the yarn network embedded therein are linked by the mapping functions of the general form

$$t = t(x,y) \qquad n = n(x,y) \qquad z' = z/\zeta \tag{1}$$

where (x,y,z) are Cartesian coordinates describing a point in the initial shape, and (t,n,z') are curvilinear coordinates describing the corresponding point in the final shape.

Imposition of the yarn inextensibility condition yields the first order, point-wise differential relationships for $\Delta t/\Delta x$ and $\Delta n/\Delta y$ (see Eqs. 16 and 17 in ref. [3]):

$$\Delta t/\Delta x = (\lambda_1 + kn) \tag{2}$$

$$\Delta n/\Delta y = \{(\lambda_1+kn)\cot\alpha_o\cos\phi_i + \sqrt{[m^2\csc^2\alpha_o-(\lambda_1+kn)^2\cot^2\alpha_o\sin^2\phi_i]}\} \div [m^2\csc^2\alpha_o-(\lambda_1+kn)^2\cot\alpha_o] \tag{3}$$

where

$$k = (\lambda_2 - \lambda_1)/W_i \qquad m = \sqrt{[1-(\zeta^{-2}-1)\cot^2\gamma_o]} \tag{4}$$

and the subscripts o and i refer to quantities in the initial and the final shapes, respectively. Point-wise integration of $\Delta t/\Delta x$ and $\Delta n/\Delta y$ and satisfaction of point-wise surface conditions then yield the mapping functions in (1).

The surface conditions include local measurements of a'b', d'c', h_i, W_i and the local n-t intersect angle ϕ_i; see Fig. 3b. Generally, these measurements are possible after the initial shape is actually deformed into the final shape. If the final shape is prescribed, then the bounding surfaces and the surface features of the final shape must either be analytically or point-wise described so that the

differential relations for $\Delta t/\Delta x$ and $\Delta n/\Delta y$ can be fully integrated; see [3].

After the mapping functions in (1) are fully integrated, they can then be used to obtain the spatially dependent values of α_i and γ_i and other related properties in the final shape. In particular, the local yarn-to-yarn spacing is given by

$$\Delta d_i = (\lambda\mu \sin\phi_i/m)\Delta d_o \qquad (5)$$

where

$$\lambda = \Delta t/\Delta x; \qquad \mu = \Delta n/\Delta y \qquad (6)$$

Preform Formability.

For "permissible" deformation, then the following constraint is imposed:

$$\Delta d_{max} \geq \Delta d_i \geq \Delta d_{min} \qquad (7)$$

or

$$(\Delta d_{max}/\Delta d_o) \geq (\lambda\mu\sin\phi_i)/m \geq (\Delta d_{min}/\Delta d_o) \qquad (8)$$

In (8), the quantities λ, μ, m and ϕ_i are related geometrically by the following equation [3]:

$$\lambda^2 + \mu^2 + 2\lambda\mu \cos\phi_i - 2m^2 = 0 \qquad (9)$$

The inequality in (8) together with (9) provide the formability control conditions.

Illustrative Examples.

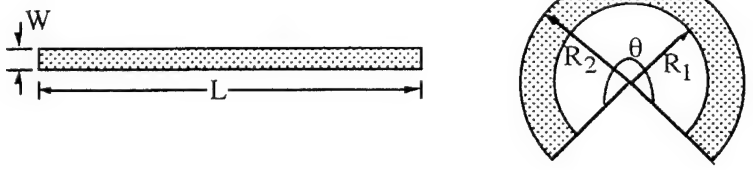

Fig.4 Forming of a tubular preform

Two examples of preform deformation will be examined as to their formability. The first is a narrow rectangular cross-section of size LxW, which is to be deformed into a circular arc section defined by the inner radius R_1, outer radius R_2 and the containing angle θ as shown in Fig.4. Let the preform be uniformly stretched length-wise as defined by ζ in (1). The following are obtained from the resulting mapping functions [3]:

$$\phi_i = 90^o \qquad \lambda = \theta r/L \qquad \lambda_1 = \theta R_1/L \qquad \lambda_2 = \theta R_2/L \qquad (10)$$

$$R_2 = (\sqrt{2}\, mL/\theta) \sin [(\theta W/L) + \sin^{-1}\{\theta R_1/(\sqrt{2}\, mL)\}] \qquad (11)$$

Furthermore, the formability control condition in (9) reduces to

$$\lambda^2 + \mu^2 - 2m^2 = 0; \tag{12}$$

and the control inequality in (8) becomes:

$$(\Delta d_{max}/\Delta d_o) \geq (\lambda\mu)/m \geq (\Delta d_{min}/\Delta d_o) \tag{13}$$

Eliminate μ from (13) by using (12) and we obtain

$$[\Delta d_{max}/(m\Delta d_o)] \geq (\lambda/m)\sqrt{[2-(\lambda/m)^2]} \geq [\Delta d_{min}/(m\Delta d_o)] \tag{14}$$

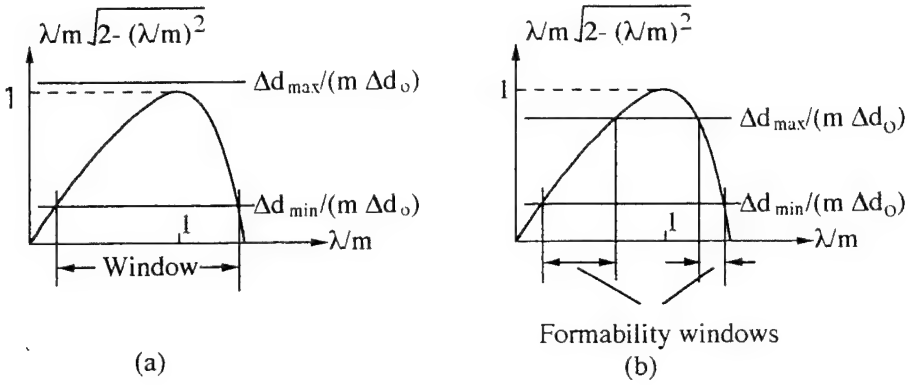

Fig.5 Formability windows

The inequality in (14) represents the extent to which the radius r of the deformed body is allowed to be; variation of r is seen through the term λ define in (10). A graphic display of the middle term in the inequality (14) as a function of λ/m indicates that it is a convex function in the range of $(0, \sqrt{2})$, with the maximum value of 1 occurring at $\lambda/m = 1$; see Fig. 5. Note that while the lower bound $\Delta d_{min}/(m\Delta d_o)$ should always be less than 1, the upper bound $\Delta d_{max}/(m\Delta d_o)$ may be greater or smaller than 1 depending on the the value of m.

If $\Delta d_{max}/(m\Delta d_o)$ is greater than 1, only one permitting window for λ/m is available as shown in Fig. 5a. Specifically, (14) reduces to:

$$(mL/\theta)\sqrt{[1+\sqrt{(1-\kappa_1^2)}]} \geq R_2 \geq R_1 \geq (mL/\theta)\sqrt{[1-\sqrt{(1-\kappa_1^2)}]} \tag{15}$$

where $\kappa_1 = \Delta d_{min}/(m\Delta d_o)$.

If $\Delta d_{max}/(m\Delta d_o)$ is less than 1, then two permitting windows are defined:

$$(mL/\theta)\sqrt{[1-\sqrt{(1-\kappa_2^2)}]} \geq R_2 \geq R_1 \geq (mL/\theta)\sqrt{[1-\sqrt{(1-\kappa_1^2)}]} \tag{16}$$

$$(mL/\theta)\sqrt{[1+\sqrt{(1-\kappa_1^2)}]} \geq R_2 \geq R_1 \geq (mL/\theta)\sqrt{[1+\sqrt{(1-\kappa_2^2)}]} \tag{17}$$

where $\kappa_2 = \Delta d_{max}/(m\Delta d_o)$.

Since R_1 and R_2 are geometrically governed by (11), the above inequalities can be rewritten to bound the inner (smaller) radius R_1 alone.

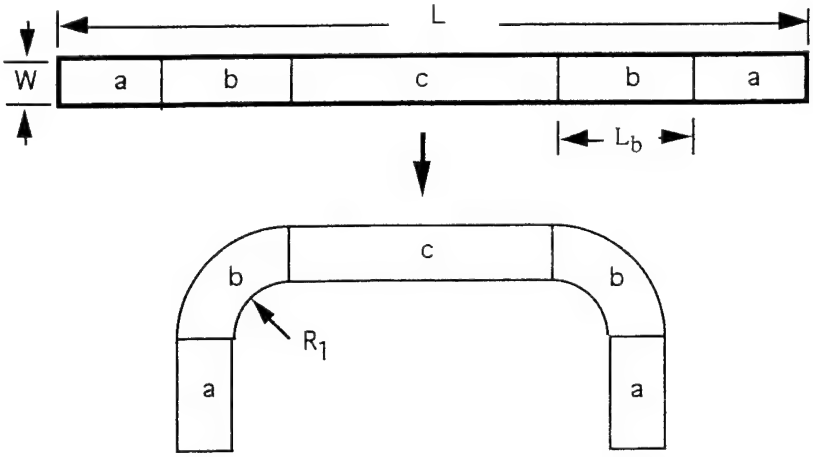

Fig.6 Forming of a U-section

In the second example, let the initial preform of the rectangular cross-section LxW be deformed into a U section as shown in Fig. 6. The interest here is to determine the smallest radius R_1 at the 90° bend that can be achieved through permissible deformation. Clearly, the results in the first example can be used readily; thus, from (15) the lower bound of the radius should be

$$R_1 = (2mL_b/\pi)\sqrt{[1-\sqrt{(1-\kappa_1^2)}]} \qquad (18)$$

where L_b is the undeformed length of the bend, and $\theta = \pi/2$.

Since the minimum value of R_1 is directly proportional to L_b, it is possible to make L_b the smallest value so that the outer radius R_2, computed from (11), will also satisfy the upper bound in (15):

$$(2mL_b/\pi)\sqrt{[1+\sqrt{(1-\kappa_1^2)}]} = R_2 \qquad (19)$$

Combining Eqs.(18) and (19), the smallest possible radius R_1 at 90° bend is:

$$(R_1)_{min} = \frac{W_i\sqrt{[1-\sqrt{(1-\kappa_1^2)}]}}{\sqrt{[1+\sqrt{(1-\kappa_1^2)}]} - \sqrt{[1-\sqrt{(1-\kappa_1^2)}]}} \qquad (20)$$

where $W_i = R_2 - R_1$ is the thickness. If the design thickness of the U section is given, the smallest possible radius can be derived from Eq.(20). Then , the length

L_b and the thickness W of the original rectangular cross section can be determined by Eqs.(18) and (11).

If R_1 is smaller than $(R_1)_{min}$, part b of the rectangular cross section can not be deformed into a perfect partial circular arc. Shear strain will occur. Thus, the n-t intersection angle ϕ_1 (see Fig.3.b) is no longer 90°. This problem is outside of the scope of this paper and will be discussed in a separate paper later.

III.CONCLUDING REMARKS

In this paper, we demonstrated that deformability of 3-D braided preform from one shape to another could be determined analytically for a class of braids. This can be a useful tool for the design and fabrication of braided composites. The premise of the formability analysis is based on the requirement that the yarn network topology in the braided preform remains unchanged characteristically during the prescribed shape change. In this context, a family of geometric mapping functions satisfying certain geometric constraints may be obtained. The mapping functions not only can map the shape change but also the yarn network embedded in the shape.

With the mapping, the prescribed preform deformation can be described by a chosen physical parameter which is then bounded by some physical limits. In this paper, we impose the limits Δd_{max} and Δd_{min} on the yarn-to-yarn spacings in the deformed shape, assuming that these limits come empirically from actual braiding experience.

Acknowledgments: This work was partially supported (to ASD Wang) by a grant from the Air Force Office of Scientific Research.

REFERENCES

[1] Wang, Y. Q. and Wang, A. S. D., On the topological yarn structure in 3-D rectangular and tubular braided preforms, Comp. Sci. Technol., 51 (1994) 575-586.

[2] Wang, Y. Q. and Wang, A. S. D., Microstructure/property relationships in 3-D braided fiber composites, Comp. Sci. Technol., 53 (1995) 213-222.

[3] Wang, Y. Q. and Wang, A. S. D., Geometric mapping of yarn structures due to shape change in 3-D braided composites, Comp. Sci. Technol., 54 (1995) 359-370.

THERMOELASTIC PROPERTIES OF 3-D BRAIDED COMPOSITES: EXPERIMENT AND PREDICTIONS

A. S. D. Wang
Department of Mechanical Engineering
Drexel University
Philadelphia, PA 19104

Soheil Mohajerjasbi
Boeing Defense & Space Group
Helicopters Division
Philadelphia, PA 19142

ABSTRACT.

Thermoelastic constants are obtained both analytically and experimentally for a class of 3-D braided composites. In the experiment, preforms of square and rectangular cross-sections are braided by the 4-step 1x1 method using an E-glass yarn and a high modulus graphite yarn. The preforms are then consolidated by a resin transfer molding (RTM) procedure with an epoxy resin. The consolidated composite bars of various cross-sectional sizes are cut and prepared for testing under a 4-point-bend loading condition for their elastic bending properties, and their effective thermal expansion coefficients in the temperature range of $25^{o}C$ to $100^{o}C$.

In the analysis, a brief introduction is given for the geometric description of the yarn structures in 3-D preforms braided by the 4-step 1x1 method. Based on the yarn structure, this class of preforms is shown to be composed of an interior core region and a surface layer region; in each region, a distinctive yarn structure exists. The effective thermoelastic constants in each region are extracted using a simple 3-D micromechanics model based on their respective yarn structures; and these constants are then used to forecast the various properties in conjunction with the 4-point-bending and the thermal expansion tests. A comparison between the tested and the forecasted results is made.

Acknowledgments: The results reported in this paper were obtained during the course of research supported by the Air Force Office of Scientific Research and by Boeing Defense & Space Group, Helicopters Division.

INTRODUCTION.

Textile preforming offers a great potential for cost-effective production of certain precision composites as individual parts or as whole structures. In particular, 3-D braiding can furnish multi-dimensional fiber reinforcement in one integrated structural network which may have a complex shape. Thus, cost saving is envisioned in its ability to manufacture composite structures with the desired near-net-shape and the required functional properties in one automated process. However, for such potential to be fully realized, successful developments must be made in braiding automation and matrix-consolidation technologies, along with research in preform design, analytical models for properties and methodologies for performance evaluation.

In this paper, the emphasis is placed on modeling of thermomechanical properties in a class of 3-D braided composites. Some preliminary results of experimental and analytical nature from an on-going research are presented. In the experiment, preforms of square and rectangular cross-sections are braided by the 4-step 1x1 method. Specifically, three preforms of differing square cross-sections are braided using an E-glass 12K yarn and three preforms of differing rectangular cross-sections are braided using the graphite AS-4-G2-12K yarn. These six preforms are consolidated into composite bars by a resin transfer molding (RTM) procedure with the epoxy resin PR-500. A total of 16 specimens are cut from the six consolidated bars; and these specimens are then strain-gaged and tested under 4-point-bending for the global bending properties in the elastic range, and tested again for their global thermal expansion coefficients in the temperature range of $25^{o}C$ to $100^{o}C$.

In the analysis, a method for describing the geometric structure of the 3-D yarn network in the preforms is first reviewed. This provides the necessary quantitative relationships linking the governing parameters in the braiding procedure to that in the preform yarn structure, and to the final dimensions of the matrix-consolidated composite. The detailed yarn structure in the preform also provides the necessary basis for construction of a suitable 3-D mechanics model from which the effective local and global properties of the consolidated composites can be extracted. In particular, in the considered class of preforms, each is comprised of a core region and a surface layer region; and in each region, a distinctive yarn structure exists. Consequently, the thermoelastic properties of the core and the surface layer regions are generally different.

Both the core and the surface layer regions are homogenized with their effective thermoelastic constants extracted by a simple 3-D micromechanics model. These constitutive properties are then incorporated in a simple composite beam theory to forecast the global properties that are experimentally measured in the testing program.

Finally, the analytical results are compared with the corresponding test results.

YARN STRUCTURES IN PREFORMS.

The topological structure of the yarns inside a braided preform before matrix consolidation can be determined based solely on the particular braiding setup and the braiding procedures. Yarn structure topology in preforms braided by the 4-step 1x1 method has been fully treated by Wang and Wang (1994a, 1994b, 1995) and Mohajerjasbi (1993, 1995). In this section, only the pertinent elements in the subject will be discussed.

The 4-Step 1x1 Braiding.

Fig. 1 is a schematic illustration for the braiding setup for preforms of a square or rectangular cross-section by the 4-step 1x1 method. The preform being braided is hung above the ma-

chine bed, on which yarn carriers are arranged in a row-and-column pattern. Braiding is realized through the movements of the yarn carriers along the row and column tracks. In this case, four steps of carrier movements constitute a braiding cycle; during each cycle, yarn lines are made to crisscross in space and a finite braided length is realized known as a "pitch". The yarn structure so formed during one braiding cycle will repeat itself in successive cycles. If M is the number of carriers in a column and N is the number in a row, then the resulting preform cross-section is a rectangle known as an [MxN] braid.

Yarn Structure Topology.

The topology of the yarn structure formed during one braiding cycle can be geometrically described by considering the braiding yarns as lines; then, by tracing the yarn lines in certain selected "control spaces", their relative position in space is established. For preforms of rectangular cross-sections, a distinct yarn network in the core and a distinct yarn network on the bounding surfaces are identified. In the interior, two groups of parallel planes crisscross each other at the angle 2α (α is the angle between the plane and the x-axis) as shown in Fig. 2a. Each of these planes is actually formed by two groups of parallel yarns crisscrossing with the angle 2γ (γ is the angle between the yarn line and the braiding axis-z) as shown in Fig. 2b. During each braiding cycle, the preform advances a finite braiding pitch which is denoted by h in Fig. 2b.

Similarly, on the surfaces of the preform, the yarn structure is formed by two groups of parallel yarn segments as shown in Fig. 2c. These crisscrossing segments are oriented at the angle $\pm\theta_s$ with the braiding axis-z. The surface yarn angle $\theta_s = \theta_x$ on the preform surface parallel to the x-axis; $\theta_s = \theta_y$ on the surface parallel to the y-axis. In general, these surfaces yarn angles are not equal; however, if the interior planes crisscross at $2\alpha = 90^o$, then $\theta_x = \theta_y$.

Basic Unit Cells in the Interior.

From the above, the yarn structure in the preform is seen to be repetitive for each braiding pitch h. Thus, it is convenient to define the representative unit cells which comprise the preform of length h. Specifically, in the interior, two basic unit cells are identified shown as cell-A and cell-B in Fig. 3. Each cell is a cuboid with the height h; the cross-section is a square if $\alpha = 45^o$ or a parallelogram if $\alpha \neq 45^o$. The orientation of the cross-section is such that the diagonal BC in cell-A or DE in cell-B is parallel to the x-axis. Each basic unit cell is composed of a top-half and a bottom-half, each half containing two crisscrossing yarns. Note that the yarns in the top-half are topologically different from those in the bottom-half; the top-half of cell-A is, however, identical to the bottom-half of cell-B, and vice versa.

Basic Unit Cells on the Surface.

On the preform surfaces, a basic unit cell can be identified as shown in Fig. 4. Here, the cross-section of the cell is an equilateral triangle; the yarns in the cell are surface segments, representing the portion of the yarns that emerge from the interior to the surface and then return back into the interior during one cycle of braiding. These yarn segments crisscross at the angle θ_s with the braiding axis z as shown in Fig. 4. Now, if the angle $\alpha \neq 45^o$, $\theta_s = \theta_x$ in cell situated on the surfaces parallel to x-axis, and $\theta_s = \theta_y$ for cells situated on the surface parallel to y-axis. If $\alpha = 45^o$, $\theta_s = \theta_x = \theta_y$.

The geometric relation between the interior and the surface cells are illustrated in Fig. 5. It should also be noted that, at the four corners, a corner cell which is different from the surface cell can be identified, see Mohajerjasbi (1993) and Wang and Wang (1994a); it's effect on the overall yarn structure is, however, relatively negligible.

The matrix consolidated preform can now be regarded as a composition of the variously defined unit cells, as shown in Fig. 6 where the interior cells A (blank) and B (darkened) form the "core", and the surface and corner cells (shaded) form the "boundary layer" enclosing the core. Note that a thin surface layer is added to the overall cross-sectional size, due to fact that the preform surface becomes resin-rich after matrix consolidation. The cross-section of the surface cells is now approximated as a pentagon as shown in Fig. 6.

Defining the Governing Parameters.

Now, let the actual cross-section of the matrix consolidated preform be W_x by W_y. Then, together with the braiding pitch h, the geometric parameters governing the yarn structure can be defined. First, the fundamental units of the unit cells are defined by (see Fig. 6),

$$\Delta x = W_x/(M+1) \qquad \Delta y = W_y/(N+1) \tag{1}$$

where $\Delta x/2$ and $\Delta y/2$ represent the resin-rich surface layer thicknesses mentioned above.

Then, from Fig 4, the surface yarn angles are defined by:

$$\tan\theta_x = \Delta x/h \qquad \tan\theta_y = \Delta y/h \tag{2}$$

From Figs. 5 and 6, respectively, one obtains

$$\tan\alpha = \Delta y/\Delta x \qquad \tan\gamma = (2/h)\sqrt{(\Delta x^2+\Delta y^2)} \tag{3}$$

Note that, if $W_x/W_y \approx M/N$, then $\Delta x \approx \Delta y$, $\alpha \approx 45^o$ and

$$\tan\gamma = 2\sqrt{2}\,\tan\theta_s \tag{4}$$

Fiber Volume Fractions.

From the above, one can determine the volume of each unit cell and thus also its fiber volume content. Specifically, let the solid cross-section of the braiding yarn be A_f; then the fiber volume fraction V_{fi} of the interior cells (for both A and B), V_{fsx} and V_{fsy} of the surface cells (situated along x- and y- axes) are given respectively by:

$$V_{fi}=A_f/(\Delta x\Delta y\cos\gamma) \quad V_{fsx}=[A_f\sqrt{(h^2+\Delta x^2)}]/(h\Delta x\Delta y) \quad V_{fsy}=[A_f\sqrt{(h^2+\Delta y^2)}]/(h\Delta x\Delta y) \tag{5}$$

In summary, the yarn structure in the composite is geometrically defined by the quantities h, W_x and W_y as described above. The knowledge of the solid cross-sectional area A_f of the braiding yarn provides the fiber volume fraction of each kind of the unit cells. Finally, the whole composite can be represented by a certain composition of the various unit cells, with the pattern determined by the initial preform braiding setup.

MODELING THERMOELASTIC PROPERTIES.

The approach taken to model the thermomechanical properties of the consolidated preform is to first model the basic unit cells, and then the global properties of the composite as a whole, based on its particular cell composition. The essential elements in the modeling approach are briefly described below.

Modeling the Basic Cells.

As shown in Fig. 3, the interior cells A or B have a top-half and a bottom half; the top-half of A is identical to the bottom-half of B, and vise versa. Each half contains two crossing yarns; those in the top-half resemble a $[\pm\gamma]$ angle-plied laminate and those in the bottom half resemble a $[_{+}\gamma]$ laminate. Following the practice of material homogenization, each group of parallel yarns is modeled as a unidirectional (UD) ply with the fiber volume fraction V_{fi}. Further, the UD ply is treated as composite of collimated fibers and a binding matrix, whose properties are known (both are assumed here as linearly elastic and isotropic materials). Then, by a model such as that given by Chamis (1984), the UD ply is homogenized as a transversely isotropic material. In its principal coordinates (L,T, z), the five elastic constants are determined as:

$$E_L=V_fE_f+(1-V_f)E_m \qquad E_T(=E_z)=E_m/[1-(1-E_m/E_f)\sqrt{V_f}] \qquad G_{LT}=G_m/[1-(1-G_m/G_f)\sqrt{V_f}$$

$$\nu_{LT} = V_f\nu_f + (1-V_f)\nu_m \qquad \nu_{Tz} = [E_T/(2G_{LT}) -1] \tag{7}$$

The three thermal expansion coefficients are determined by the model of Schapery (1968):

$$\beta_L = [\beta_fE_fV_f + \beta_mE_m(1-V_f)]/[E_fV_f + E_m(1-V_f)]$$

$$\beta_T = \beta_z = \beta_fV_f(1+\nu_f) + \beta_m(1-V_f)(1+\nu_m) - \beta_L[\nu_fV_f + \nu_m(1-V_f)] \tag{8}$$

The next step is to extract the thermoelastic constants of the $[\pm\gamma]$ laminates as a homogenized 3-D solid. This is done by using a volume-average procedure similar to that suggested by Pagano (1974) in conjunction with the classical lamination theory. Briefly, an in-series model is used to derive the in-plane laminate properties by volume-averaging the associated ply stiffness, while an in-parallel model is followed for the out-of-plane properties by volume-averaging the associated ply compliance. The derivation for the thermoelastic constants is rather lengthy; details are found in Wang and Wang (1994b).

Similarly, the surface cell is regarded as cross-plied $[\pm\theta_s]$ laminate; its thermoelastic constants can be found accordingly.

Modeling the Consolidated Preform As A Whole.

The consolidated preform as a whole has a homogenized core and a bounding surface layer. In each region, the thermoelastic constants are referred to the global coordinates (x,y,z) by a proper coordinate rotation about the z-axis. Then, the global response of the composite under certain applied loading conditions can be forecasted by treating the preform as a composite member. For instance, the total fiber volume content V_{fc} and the axial tensile modulus E_t of the composite member may be estimated respectively as

$$V_{fc}=(V_{fi}A_i+V_{fs}A_s)/A \qquad E_t = (E_iA_i + E_sA_s)/A \tag{9}$$

where A_i is the cross-section area of the core region, A_s is that of the surface layer region; and A is the total cross-section area of the bar (= $A_i + A_s$).

Similarly, if the bar is under pure bending, the effective flexural modulus E_{fl} of the bar can be estimated by the simple beam theory as:

$$E_{fl} = (E_iI_i + E_sI_s)/I \tag{10}$$

where I (= $I_i + I_s$) is the area moment of inertia with respect to the bending axis of the bar. And, the effective thermal expansion coefficient β_z in the axial direction of the bar can also be estimated:

$$\beta_z = (\beta_iE_iA_i + \beta_sE_sA_s)/(E_iA_i + E_sA_s) \tag{11}$$

Clearly, global response properties pertinent to other loading conditions, such as torsion, can be similarly estimated.

EXPERIMENT AND RESULTS.

In this section, the various phases of the experiment are described. It begins with the braiding of the preforms, followed by a description of the RTM matrix consolidation procedure, the test specimen preparation and loading conditions for bending properties and for thermal expansion coefficients. The global composite responses measured under these loading conditions are also presented along with their counterparts forecasted using the model described in the previous section.

Braiding the Preforms.

Six preforms of length 0.61 m (24 inch) were braided by the 4-step 1x1 method on a semi-automated braiding track at Drexel's Fibrous Composites Laboratory. Effort was made during the braiding process to achieve uniform yarn jamming. However, as braiding progressed, some fiber loss was observed (the leading part of the preform may contain more fibers than the trailing part). Three preforms of [11x11], [11x7] and [11x3] were braided using the AS4-G2 12K graphite yarn, and three preforms of [11x11], [8x8] and [4x4] were braided using a 12K E-glass yarn. The pertinent thermomechanical properties of the yarns are:

Yarn	E_f (axial)	ν_f	β_f (axial)	A_f
Graphite	235.0 GPa	0.22	-1.0 $\mu/^oC$	0.48 mm^2
E-glass	72.4 GPa	0.20	5.0 $\mu/^oC$	2.12 mm^2

where μ denotes a micro (10^{-6}) strain.

RTM Processing.

The braided preforms were RTM-processed at Boeing Defense & Space Group, Helicopter

Division. Efforts were made in tooling preparation in order not to distort the original rectangularity of the preforms during RTM processing. However, as can be seen in Table 1, the cross-section of each preform was still somewhat distorted (i.e. W_x:$W_y \neq$ M:N).

The resin of choice is the 3M PR-500 epoxy. Two epoxy bars in bulk and cured form were tested in uniaxial tension and pure bending; the following pertinent thermomechanical properties were obtained: E_m= 4.5 GPa, ν_m= 0.38 and β_m= 55 $\mu/^oC$.

The resin injection apparatus used was the Venus Gusmer Ram System. This is a constant injection rate, computer-controlled processing unit with staged resin preheating from the storage cylinder at 82°C (180°F) to the feed hose at 132°C (270°F). The three graphite preforms were processed at 30 cc/m injection rate with a stall pressure of 1 MPa (150 psi); the total process time was 14.5 minutes and the process and cure temperature was maintained at 177°C (350°F). The three glass preforms were processed also at the 30 cc/m injection rate, but with a stall pressure of 1.24 MPa (180 psi) and a total process time of 18.7 minutes; the same process and cure temperature of 177°C (350°F) as the graphite preforms was applied.

Test Specimen Preparation.

The matrix consolidated preforms were cut into test specimens suitable for 4-point bending. The [11x11] and [8x8] glass bars each yielded two specimens of 305 mm (12 inch) in length; the rest of the braids each yielded three specimens of 203 mm (8 inch) in length. Thus, a total of 16 test specimens were obtained. Pertinent external measurements of W_x, W_y and h for these 16 specimens are listed in Table 1.

Each specimen was strain-gaged prior to testing. A pair of 90°-rosettes were mounted at the center portion of the specimen; one rosette was mounted on the tensile side of of the specimen, and one on the compressive side. The gages and the mounting adhesive used were rated over 100°C.

4-Point-Bend Tests and Results.

The 4-point bending test fixture used can be adjusted to accommodate a pure bending section between 100 mm to 200 mm (4 to 8 inch). The pure bending span for the [11x11] and [8x8] glass specimens was set at 200 mm (8 inch), while for the rest of the specimens it was set at 125 mm (5 inch). Loading was applied at room temperature, using an Instron tester with the stroke control rate of 0.25 mm/min for the longer span and 0.125 mm/min for the shorter span. Loading was terminated when the longitudinal strains reached 0.35%; unloading at the same rate then followed.

Thus, for each test, 4 loading-unloading strain gage recordings were obtained as functions of the applied load. In the longitudinal strain range (0.35%), loading and unloading essentially followed the same path. Concurrent transverse strain gage readings provided the Poisson ratio ν_{zx} for each specimen tested. These measurements are listed in Table 1. The label ε_{fl} denotes the measured longitudinal strain per unit of bending moment applied; and the (+) sign refers to the measurement made on the tensile side, (-) refers to the compression side. Similar labels are also used for the measured Poisson ratio ν_{zx}.

From these data, there is an indication that the measured axial strain on the compressive side is higher than on the tensile side in most of the cases. In addition, the values for the Poisson ratios of the three groups of graphite specimens vary considerably; the exact reason

for the rather large variation is not known.

The flexural modulus E_{fl} for each bar tested was deduced from the corresponding value of ε_{fl} based on the simple beam theory. Since the measured ε_{fl} on the tensile and compressive sides of the bar are different, the deduced E_{fl} values on the respective sides of the bars are also different. The averaged values of the flexural modulus $E_{fl}(+)$ and $E_{fl}(-)$ so computed are listed in Table 3. Note that the values of E_{fl} obtained from test are decreasing with decreasing size of the specimen. For instance, the average $E_{fl}(+)$ is 43 GPa for the graphite [11x11] specimen, 36.9 GPa for the [11x7] specimen, and 31.9 GPa for the [11x3] specimen. However, such trend is not evident in the glass specimens of different cross-sectional sizes.

Note also that there is a disparity in the measured ν_{zx} between the GR11x7 and GR11x3 specimens. The disparity is possibly due to the stronger surface effect in the thinner GR11x3 specimens.

Thermal Expansion Tests and Results.

The thermal expansion tests were conducted in the temperature range from 25°C to 100°C, using the specimens that were already strain-gaged for testing under 4-point bending. The specific test procedures followed that described in Whitney, et. al. (1982) and Dally and Riley (1965), where electrical strain gages are used to measure the expansional strains. With two pairs of 90° rosettes mounted on each specimen, composite thermal strains longitudinal and transverse to the beam axis could be measured on both sides. Essentially, the thermal expansion coefficients $\beta_z(+)$, $\beta_z(-)$ were equal, as were the values of $\beta_x(+)$ and $\beta_x(-)$. Table 1 lists the average values of the measured β_z and β_x. Generally, β_z is much smaller compared to β_x. In fact, for all the graphite specimens, the measured β_z values are negative.

PREDICTED RESULTS AND COMPARISONS.

Predicted Results.

For each specimen, the exterior measurements of W_x, W_y and h listed in Table 1 were used to compute the values of α, γ and other pertinent yarn structure parameters as described in Section II, including the cross-sectional core area A_i, surface area A_s, the respective fiber volume fractions V_{fi} and V_{fs} etc. Table 2 lists the computed values for α, γ, V_{fi} and V_{fs} for each specimen tested. It is noted that the calculated fiber volume content of the the core region is higher than in the surface layer region.

With the properties of the yarn and matrix given, the thermoelastic properties of the unit cells in the interior and on the surfaces were characterized according to the micromechanics procedures described earlier. Table 2 lists the computed values of E_z, ν_{zx}, and β_z for the interior and the surface cells. Note that the corresponding properties in the core and the surface regions are not the same.

Comparison Between Predicted and Test Results.

The composite flexural modulus E_{fl}, Poisson ration ν_{zx}, thermal expansion coefficients β_z

and β_x for each specimen were computed based on its particular cell composition as discussed before. These four computed global properties are compared to their (averaged) experimental counterparts in Table 3. In general, the predicted flexural properties are within the norms of the experimental range. The predicted results for the thermal expansion coefficients, however, indicate an over-estimation for β_z and an under-estimation of β_x; some suspected reasons for the disagreement are discussed below.

DISCUSSIONS.

Yarn Structure Representation.

It is the authors' assessment that the geometrical description of the yarn structure in 3-D braided composites as outlined in this paper is reasonably sound. In particular, the unit-cell representation allows extraction of the thermomechanical properties at the local level; the cells in the core and surface regions have different yarn structures and hence different properties. Hence, the consolidated preform as a whole is treated as a composite member with distinct core and surface regions. Consequently, the global response of a specimen under specific loading is in fact a structural property unique to that particular physical setting; only the properties of the basic unit cells may be considered as "basic and common" without regard to the overall dimensions of the composite and the applied loading.

Modeling.

The micromechanics models adopted to extract the thermoelastic properties of the various basic unit cells were rather simple. Nevertheless, they do provide useful predictions for a set of chosen thermomechanical properties for the braided specimens. For example, in the three graphite specimen groups, size effect on the flexural modulus (E_{fl} is decreasing with decrease of specimen cross-section, see Table 3) was recorded, and the effect is closely predicted by the model. One reason for the size effect is attributed to the fact that the specimens of larger cross-section have a higher fiber volume content than that of a smaller cross-section (see Table 2). The cause of this is not due to specimen geometry; rather, it just comes from the manner in which the specimens were braided and/or consolidated.

Another example is that the small (sometimes negative) thermal expansion coefficients in the axial direction are also predicted by the model. The agreement between the predicted and measured TECs is relatively poor, however. One reason for the poor correlation is due to the fact that the model does not account for the residual thermal stresses in the consolidated preform.

Clearly, an improved, refined and perhaps more rigorous model may provide better correlation with the experimental results.

Experiment.

Braided specimens typically have cross-sections much thicker than the conventional laminated composite by UD tapes. It is, generally speaking, more difficult to conduct characterization tests compared to the laminated tape systems. The 4-point bend test adopted here represents only the first effort in systematically characterizing the properties of braided composites. More tests are being planned for a number of other specimen geometries and/or loading conditions.

The thermal expansion test was conducted in a rather narrow temperature range. Use of the

electrical strain gages may also introduce errors in thermal strain readings. A refined test method is needed to account for thermal residual stress effects.

Finally, it is noted that the test data provided in this paper, though limited, has been presented for the first time in terms of all the key braiding variables, as all of which influence the obtained properties to some extent. This is important for future reference or for comparison of results by other researchers in the field.

REFERENCES.

Chamis, C. C., 1984, "Simplified Composite Micromechanics Equations for Hygral, Thermal and Mechanical Properties," *SAMPLE Quart.* April, p.14.

Dally, J. W. and Riley, W. F., 1965, "*Experimental Stress Analysis*," McGraw-Hill, New York. pp.377-379.

Mohajerjasbi, S., 1993, "Structure and Mechanical Properties of 3-D Braided Composites," Ph.D Thesis, Drexel University.

Mohajerjasbi, S., 1995, "Modeling and Analysis of 4-Step 3-D Cartesian Braided Composites Including Axial Yarns," Proc. 36th AIAA-ASME-ASCE-AHS-ASC Structures, Structural Dynamics & Materials Conference, April, pp. 8-16.

Pagano, N. J., 1974, "Exact Moduli of Anisotropic Laminates," in *Mechanics of Composite Materials*, ed. G. P. Sendeckyj. Academic Press, New York, p.23.

Schapery, R. A., 1968, "Thermal Expansion Coefficients of Composites Based on Energy Principles," *J. Composite Materials*, Vol 2 p.380.

Wang, Y. Q. and Wang, A. S. D., 1994a "On the Topological Yarn Structure in 3-D Rectangular and Tubular Braided Preforms", *J. Composites Science & Technology* , Vol 51, pp. 575-586.

Wang, Y. Q. and Wang, A. S. D., 1994b "Microstructure-Property Relationships in 3-D Braided Composites", *Proc. 1st International Specialists Meeting on Mesostructure and Mesomechanics in Fibre Composites*, Univ. Toronto, pp.174-196. Also *J. Composites Science & Technology* , Vol 53, 1995. pp. 213-222.

Wang, Y. Q. and Wang, A. S. D., 1995, "Geometric Mapping of Yarn Structures in 3-D Braided Composites Due to Shape Change," to appear in *J. Composites Science & Technology*.

Whitney, J. M., Daniel, I. M. and Pipes, R. B., 1982, "*Experimental Mechanics of Fiber Reinforced Composite Materials*," Prentice-Hall, New York, pp.79-80.

TABLE 1 . Experimentally Measured Quantities

Specimen	W_x mm	W_y mm	h mm	ε_{fl} (+) με/N-m	ε_{fl} (-) με/N-m	υ_{zx} (+)	υ_{zx} (-)	β_z μ/C	β_x μ/C
GR 11x11-1	12.58	11.41	3.40	83.59	91.45	0.78	0.87	-11.8	21.3
GR 11x11-2	11.94	12.75	3.43	79.65	91.45	0.67	0.61	-13.4	31.3
GR 11x11-3	12.00	12.82	3.40	66.86	68.83	0.53	0.54	-14.8	41.71
Average	**12.17**	**12.33**	**3.41**	**76.70**	**83.91**	**0.66**	**0.67**	**-13.3**	**31.46**
GR 11x7-1	13.65	7.95	3.30	168.58	153.4	0.80	0.81	-11.7	36.23
GR 11x7-2	14.87	8.00	4.00	183.56	161.27	0.80	0.77	- -	- -
GR 11x7-3	15.30	7.75	4.15	184.87	182.9	0.81	0.82	-13.5	36.00
Average	**14.61**	**7.90**	**3.81**	**179.00**	**165.86**	**0.80**	**0.80**	**-12.6**	**36.1**
GR 11x3-1	13.60	4.53	3.68	601.80	672.60	0.50	0.46	-8.40	58.36
GR 11x3-2	13.88	4.72	3.56	672.60	778.80	0.54	0.52	-6.00	48.73
GR 11x3-3	13.65	4.55	3.56	692.28	700.13	0.51	0.53	-11.7	40.82
Average	**13.70**	**4.60**	**3.61**	**655.56**	**717.24**	**0.52**	**0.50**	**-8.70**	**49.3**
GL 11x11-1	26.59	23.50	8.3	13.87	14.46	0.44	0.41	2.16	48.06
GL 11x11-2	26.67	23.52	8.3	14.75	16.23	0.41	0.40	6.03	37.90
Average	**26.63**	**23.51**	**8.3**	**14.31**	**15.35**	**0.43**	**0.40**	**4.10**	**43.00**
GL 8x8-1	18.92	17.32	7.82	40.32	37.37	0.41	0.37	2.16	46.20
GL 8x8-2	18.92	17.68	7.72	37.70	40.00	0.44	0.43	2.16	42.91
Average	**18.92**	**17.50**	**7.77**	**39.01**	**38.68**	**0.43**	**0.40**	**2.16**	**44.57**
GL 4x4-1	11.10	10.64	5.74	259.23	268.18	0.41	0.38	2.30	- -
GL 4x4-2	11.00	10.34	6.48	209.26	214.55	0.47	0.47	2.60	- -
GL 4x4-3	11.15	10.52	6.86	236.00	214.37	0.50	0.53	3.20	- -
Average	**11.07**	**10.50**	**6.36**	**234.83**	**232.37**	**0.46**	**0.46**	**2.70**	- -

TABLE 2 Computed Quantities Based on the Averaged Input for Six Specimen Classes

Specimen Class	α	γ	V_{fi}	V_{fs}	E_{zi}	E_{zs}	ν_{zxi}	ν_{zxs}	β_{zi}	β_{zs}	β_{xi}	β_{xs}
GR 11x11	45.3^{o}	40.3^{o}	60%	48%	33.3 GPa	49.0 GPa	0.6	0.5	-3.0 μ/C	2.6 μ/C	23 μ/C	38 μ/C
GR 11x7	38.5	39.8	51	41	29.9	44.9	0.6	0.5	-3.4	3.0	27	43
GR 11x3	45.2	42.0	49	38	21.8	35.0	0.6	0.5	0.6	4.7	26	46
GL 11x11	41.5	35.6	60	50	23.6	29.6	0.4	0.4	10.1	11.3	30	42
GL 8x8	42.6	36.5	64	53	25.0	29.3	0.4	0.4	10.1	11.0	27	42
GL 4x4	43.0	43.9	63	48	20.5	25.1	0.37	0.4	14.5	12.7	25	42

TABLE 3 Comparison of Predicted and Measured Global Properties (averaged)

Specimen Class	Bending Modulus. E_{fl} GPa			Poisson's Ratio ν_{zx}		TEC β_z		β_x	μ/C
	Experiment		Prediction	Experiment	Prediction	Exp.	Pred.	Exp.	Pred.
GR 11x11	43.0 (+)	39.6 (-)	38.0	0.66	0.6	-13.3	-1.8	31.5	25.4
GR 11x7	36.9 (+)	36.3 (-)	37.2	0.80	0.6	-12.6	0.3	36.1	30.8
GR 11x3	31.9 (+)	29.1 (-)	29.8	0.52	0.6	-8.7	3.5	49.3	32.3
GL 11x11	28.5 (+)	26.7 (-)	25.4	0.43	0.4	4.1	10.4	43.0	32.0
GL 8x8	26.5 (+)	26.9 (-)	27.1	0.43	0.4	2.2	10.7	44.6	31.8
GL 4x4	21.2 (+)	21.4 (-)	23.2	0.46	0.4	2.7	13.3	- -	31.1

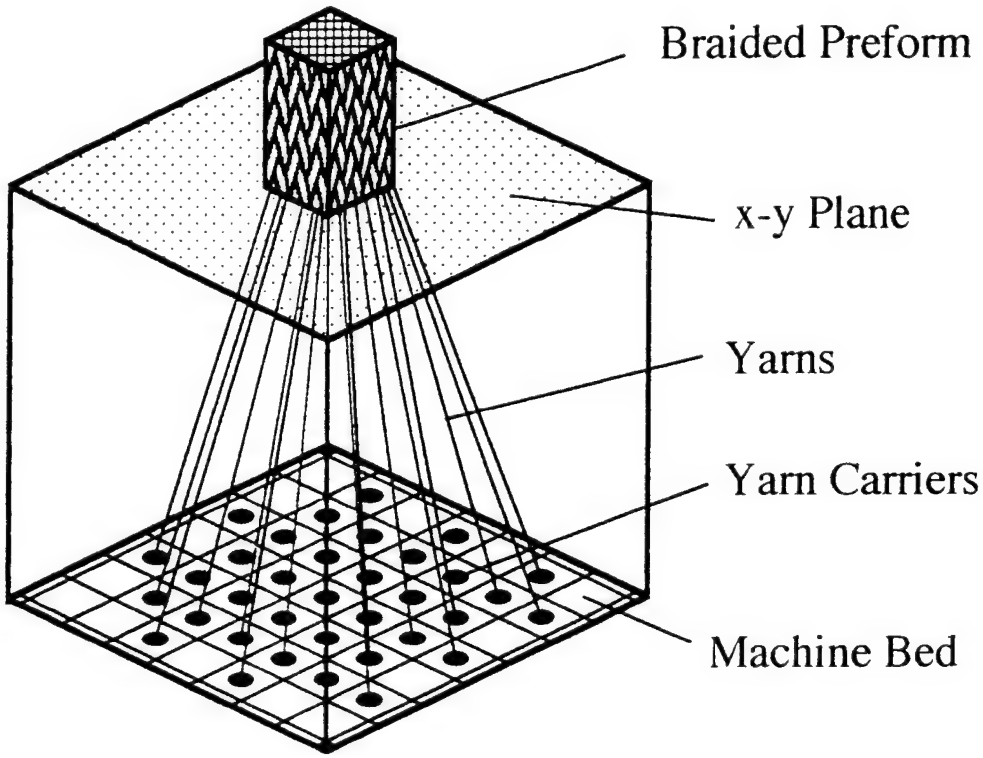

Fig. 1 Braiding setup for preforms of square or rectangular cross-sections.

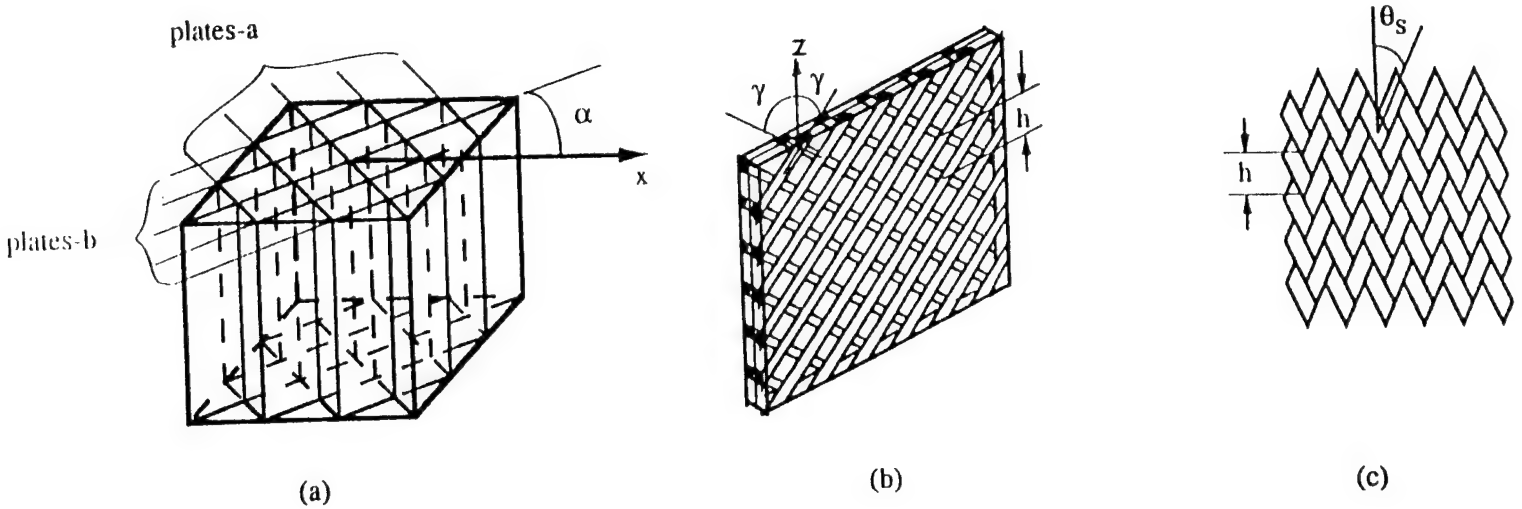

Fig. 2. Yarn topology in the preform of rectangular cross-section: (a) a global view of the interior structure; (b) yarn formation in a plate-b; and (c) a view of the preform's surface.

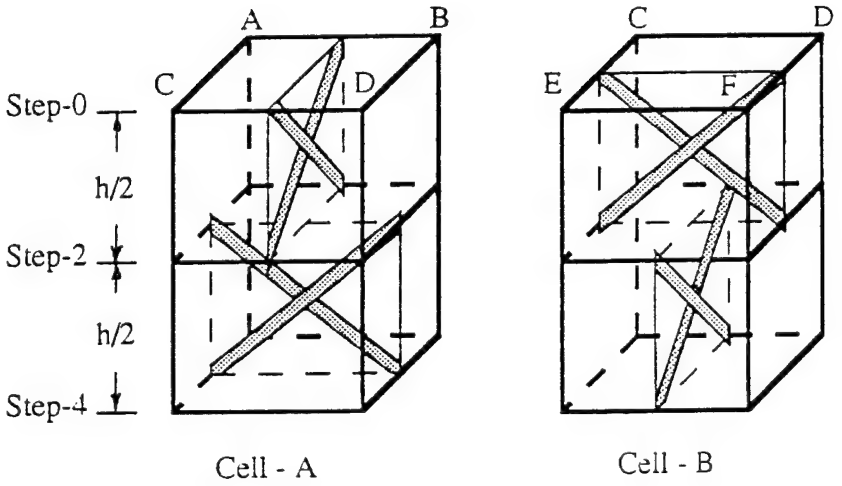

Fig. 3 Unit cells in the preform interior

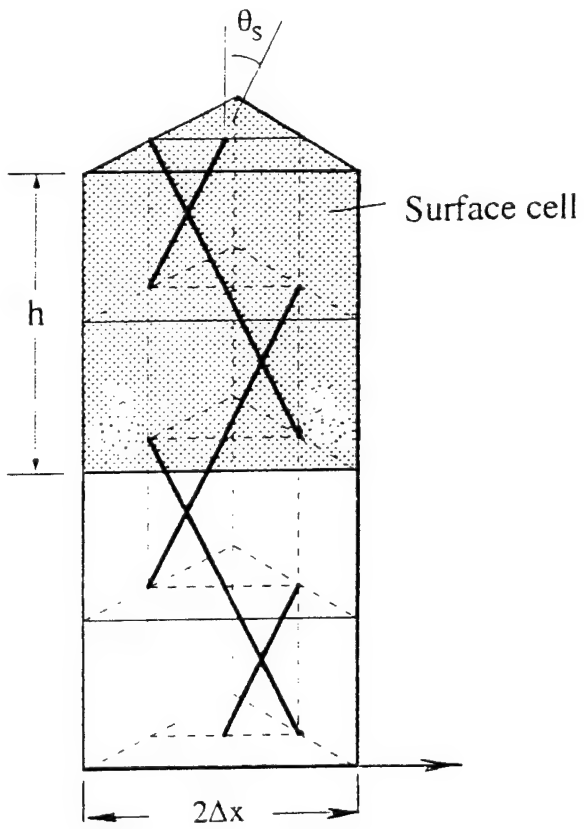

Fig. 4 Unit cell on the preform surface

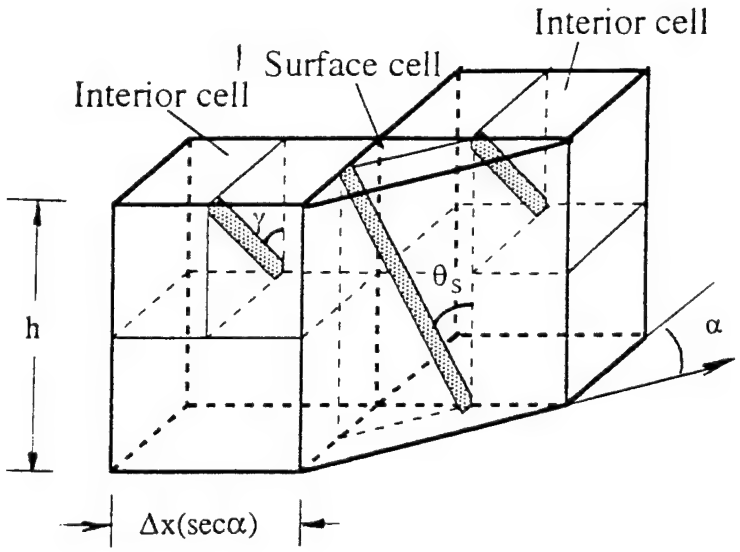

Fig. 5 Geometric relation between surface cell and interior cells

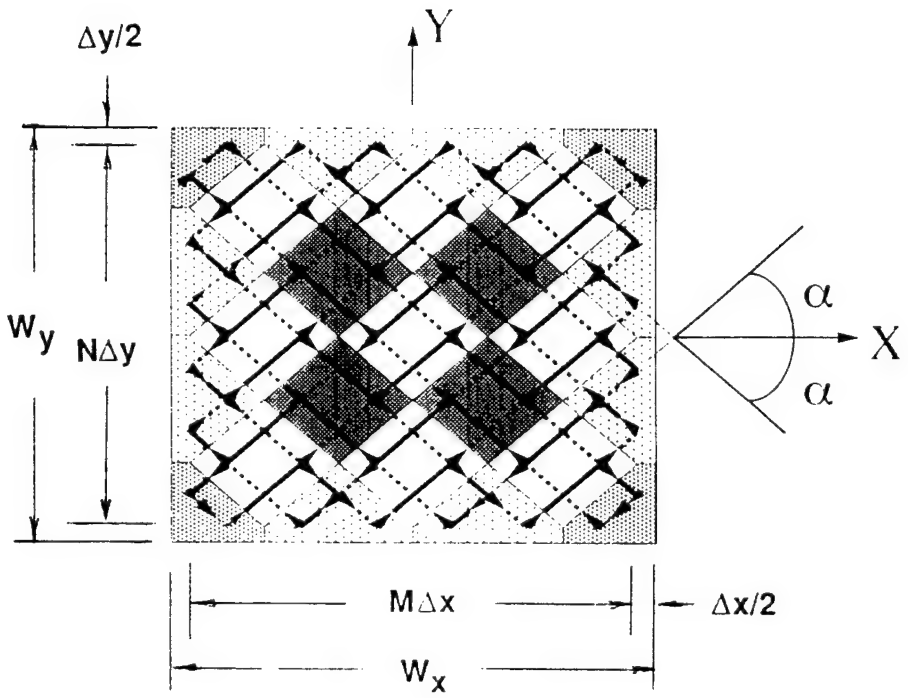

Fig. 6. Cell composition in the preform cross-section

STIFFNESS AND STRENGTH PROPERTIES IN 3D BRAIDED STRUCTURAL COMPOSITES

A. S. D. Wang and Amrita Kumar

Department of Mechanical Engineering and Mechanics
Drexel University, Philadelphia, PA 19104 USA

SUMMARY: Structural beam members of square and rectangular cross-sections are first braided three-dimensionally with continuous yarns; these are then consolidated with an epoxy matrix. The consolidated composites are tested under 4-point bending load. Local and global deformation responses, including load-induced damage initiation and progression, are studied along with established analysis models.

Under 4-point bending, the load-deflection response of the composites exhibited a linearly elastic regime until a critical load is reached. At that load, spontaneous damages in the yarn-matrix interfaces occurred due to compression in the pure-bending zone. After the critical load, a slow progression of the damages ensued, precipitating a prolonged inelastic response regime.

In this paper, we examine the bending response of the beams up to and including the critical load. In particular, we examine the pertinent mechanisms that caused the sudden and proliferate damages in the yarn-matrix interfaces in the compressive zone. Based on the observed global failure modes and the local damage mechanisms, an interface shear-induced damage initiation criterion is proposed.

KEYWORDS: 3D-braided composites; 4-point bending; damage modes and mechanisms; yarn-matrix interface; local and global analyses; shear-induced damage initiation criterion.

INTRODUCTION.

With a proper design of the yarn-carrier pattern and movements, 3D braiding can produce integrated fabric preforms that have the prescribed shape and the desired yarn architecture. After consolidation with a selected matrix material, the resulting fiber-reinforced composites can serve as load-carrying members with unusual properties. This particular fabrication technology has the potential to produce structural and other functional members in one integrated process.

In an on-going study, the authors have fabricated a series of 3D braided composites, which are intended as bending members suitable for use in helicopter structures. Specifically, preforms of solid square and rectangular cross-sections were braided using 12K E-glass yarns and 12K AS-4-G2 graphite yarns; these preforms were consolidated with the PR-500 epoxy resin following a resin-transfer-molding (RTM) procedure. The consolidated composites were tested under 4-point bending, where local and global load-response data were collected and analyzed with the aid of pertinent mechanics models. The global load-deflection response exhibited a linearly elastic regime

until a critical load is reached; at which point, spontaneous damages in the yarn-matrix interfaces occurred suddenly throughout the compression side of the pure-bending zone. The beam then underwent a slow damage progression as it continued to carry the applied load.

In what follows, we begin with a brief presentation on the pertinent yarn structures in the composites and the associated mechanics models for extracting their elastic properties; we then examine the mechanisms responsible for the observed sudden initiation of yarn-matrix interface failures at the critical load. With the aid of a series of photomicrographs taken from selected sections of the tested specimens, a shear-induced damage initiation criterion is then proposed.

YARN STRUCTURES AND PROPERTY MODELS.

The cross-sectional shape of a braided preform is dictated by the particular yarn-carrier pattern laid on the braiding machine, while the general yarn architecture in the braided preform is determined by the yarn-carrier movements in each repetitive braiding cycle. Wang, et. al. [1] developed a "control space" approach to describe geometrically the yarn structure topology based on the yarn-carrier movements alone; the exact yarn structure in the matrix-consolidated composite can then be defined by it's external dimensions.

Braiding and Yarn Architecture.

The 3D braids studied in this paper were fabricated using the popular 4-step 1x1 braiding procedure [1]. For preforms of solid square or rectangular cross-sections, a typical physical look of the preform exterior is shown in Fig.1a; note the distinct yarn patterns on the bounding surface and at the corner. From the exterior, one cannot see the yarn structure inside the preform. The latter can be determined using the "control space" method first outlined in [1]. Geometrically, the interior yarn structure is composed of two groups of parallel plates (labeled α and $-\alpha$ in Fig.1b) which crisscross at the angle 2α (α is measured from x-axis); the $\pm\alpha$-plates are formed by two groups of parallel yarns which crisscross with the angle 2γ (γ is measured from z-axis), as shown in Fig.1c. Normally, the $\pm\alpha$-plates are 90^{o} from each other; but this orthogonality could be slightly distorted during to matrix consolidation. A linear scale, known as the braiding pitch h, represents the preform length braided during each cycle. Thus, the interior yarn structure is geometrically characterized by three free parameters: α, γ and h.

Fig.1d is a section of a matrix-consolidated [11x11] E-glass specimen, cut along the α-plane. Compare this actual interior yarn structure with that described by the "control space" method.

The yarn structure on the bounding surface of the preform is a thin layer which is composed of two groups of parallel yarn segments as shown in Fig.1e; the crisscrossing yarn segments orient at the angle $\pm\theta_S$ with the braiding axis-z. Since there are two pairs of surfaces, so $\theta_S = \theta_X$ on surfaces in the x-axis and $\theta_S = \theta_y$ on surfaces in the y-axis. These are related to the interior angles α

and γ [1]:

$$\tan\theta_x = (1/2)\tan\gamma\sin\alpha \quad \tan\theta_y = (1/2)\tan\gamma\cos\alpha \tag{1}$$

Similarly, at each of the four corners, a group of parallel yarn segments exists with the angle θ_c, see Fig.1f. Again, θ_c is related to the interior angles by:

$$\tan\theta_c \approx (1/6)\tan\alpha\tan\gamma \tag{2}$$

Therefore, the cross-section of the preform is an area composition of the interior core, the four bounding surface layers and the four corner areas; each has its own unique yarn structure; and all can be characterized by the three free parameters α, γ and h.

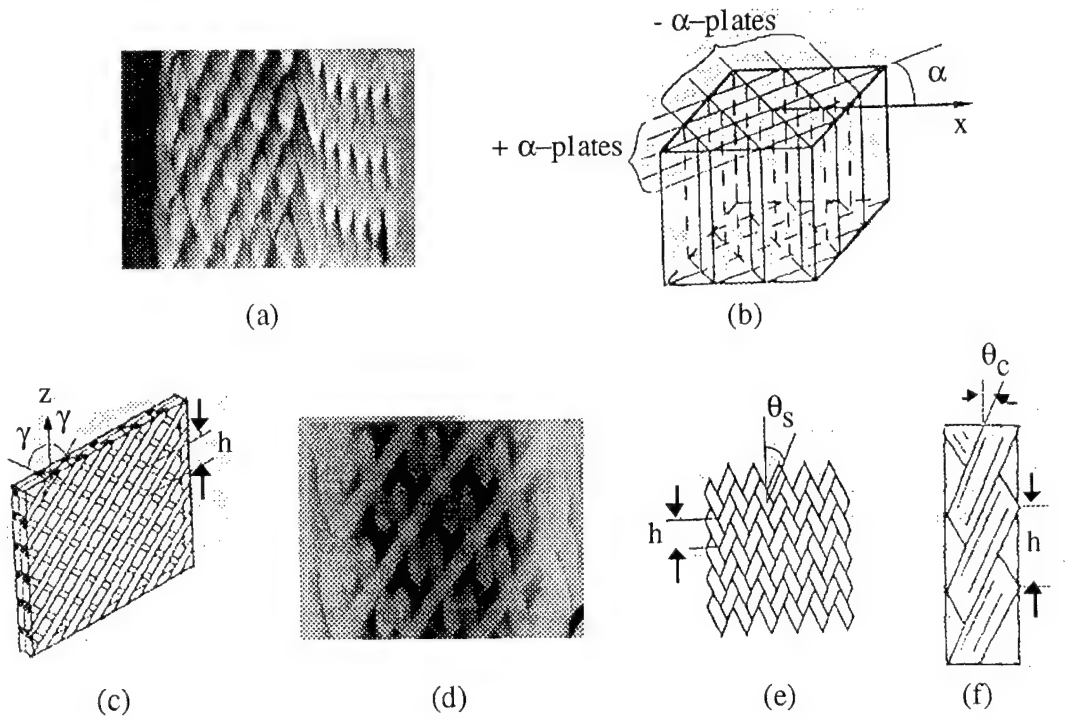

Fig. 1: (a) Exterior look of the braided specimen; (b) Interior intersecting plates structure; (c) Yarn topology of the α-plate; (d) An actual section of the α-plate; (e) Yarn topology of the braided surface; (f) Yarn topology of the braided corner.

Once the preform is consolidated, the braiding pitch h is measured from the exterior surface; so are the dimensions of the cross-section: W_x and W_y as denoted in the sketched in Fig.2. Then, we can define:

$$\Delta x = W_x/(M+1) \qquad \Delta y = W_y/(N+1) \tag{3}$$

where M and N are, respectively, the number of yarn carriers in the x-track and the y-track of the original braiding setup (see [1]). It follows that the surface yarn angles are defined by:

$$\tan\theta_x = \Delta x/h \qquad \tan\theta_y = \Delta y/h \tag{4}$$

Consequently, the interior angles α and γ are found by (1) and the corner angle θ_c by (2).

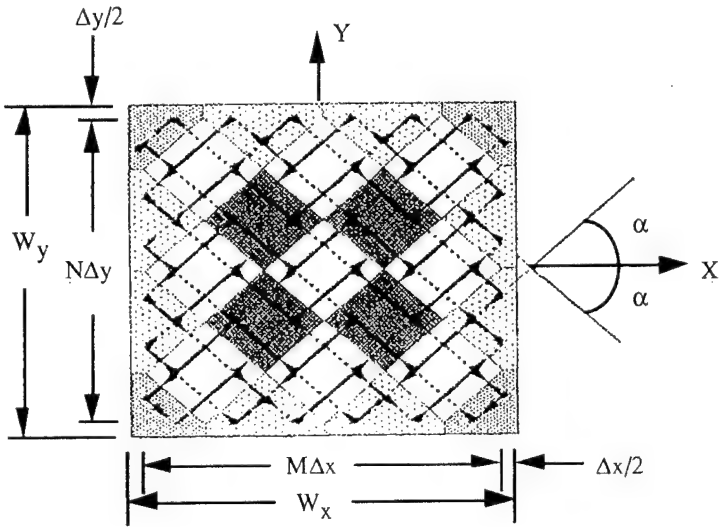

Fig. 2: Rectangular cross-section of the braided specimen, showing the geometric relationships among the interior, surface and corner areas.

Fiber Volume Fractions.

From Fig.2, we approximate the interior core area as (N-1)(M-1)$\Delta x\Delta y$; the corner area as (3/2)$\Delta x\Delta y$; the surface layer areas as 2(M-1)$\Delta x\Delta y$ and 2(N-1)$\Delta x\Delta y$ with the normal in x-axis and the y-axis, respectively. Then, the fiber volume fractions of the interior (V_i), the surface layers (V_x and V_y) and the corner area (V_c) can be determined as:

$$V_i=A_f/(\Delta x\Delta y\cos\gamma) \quad V_x=[A_f\sqrt{(h^2+\Delta x^2)}]/(h\Delta x\Delta y) \quad V_y=[A_f\sqrt{(h^2+\Delta y^2)}]/(h\Delta x\Delta y)$$
$$V_c = [2A_f\sqrt{(9h^2+\Delta x^2+\Delta y^2)}]/(9h\Delta x\Delta y) \tag{5}$$

where A_f is the solid cross-sectional area of the yarn.

Elastic Property Models.

The interior core is composed of the $\pm\alpha$ plates as explained before. One simple approach is to

model the plates individually as a [±γ] angle-plied laminate: the [+γ] lamina is modeled first as an off-axis unidirectional (UD) ply with the fiber volume fraction V_i. Given the properties of the fiber and the matrix, the elastic constant of the UD ply can be found, for instance, by the model of Chamis [2] who considers the UD ply as a transversely isotropic material. In its principal coordinates (L,T,z), the five independent elastic constants of the UD ply are:

$$E_L=V_iE_f+(1-V_f)E_m \quad E_T(=E_z)=E_m/[1-(1-E_m/E_f)\sqrt{V_i}] \quad G_{LT}=G_m/[1-(1-G_m/G_f)\sqrt{V_i}$$
$$\nu_{LT} = V_i\nu_f + (1-V_i)\nu_m \quad \nu_{Tz} = [E_T/(2G_{LT}) -1] \qquad (6)$$

The elastic constants of the [±γ] angle-plied laminate can subsequently be found by a model such as given by Pagano [3] (the detail of which is omitted here); the elastic constants of the the +α or -α plate in the global coordinates (x,y,z) are found by a proper rotation about the z-axis. This last step furnishes the elastic constants for the interior core. Similarly, the surface layers can individually be modeled as cross-plied [$\pm\theta_S$] laminates, using the proper fiber volume fraction V_S. As for the corners, they are modeled as an off-axis lamina with the off-axis angle θ_c and the fiber volume fraction V_c. All constants must be properly transformed to the global coordinates (x,y,z) of the total specimen.

With the above, any global response of the composite under a given load can, at least logically, be forecasted by treating the beam as one composed of the core, surface layers and corner areas according to Fig.2. By the rule of mixture, the fiber volume content of the whole composite is:

$$V_{fc}=(V_iA_i+V_SA_S+V_cA_c)/A \qquad (7)$$

where A_i is the core area, A_S is the surface layers area and A_c, the corners area; $A = A_i+A_S+A_c$.

If the composite is under axial tension in the z-direction, for instance, the axial tensile modulus E_{tz} can be estimated as:

$$E_{tz} = (E_iA_i+E_SA_S+E_cA_c)/A \qquad (8)$$

If the composite is under pure bending, the flexural modulus E_{fl} of the beam is:

$$E_{fl} = (E_iI_i+E_SI_S+E_cI_c)/I \qquad (9)$$

where I_i, I_S, I_c are the area moments of inertia (with respect to the bending axis) of the core, surface and corner areas, respectively; and $I=I_i+I_S\ I_c$.

EXPERIMENT AND ANALYSIS RESULTS.

Braiding, Preform Consolidation and Test Specimens.

Six preforms were braided by the 4-step 1x1 method; three were braided using the AS4-G2 12K graphite yarn with the respective braiding sizes of [11x11], [11x7] and [11x3]; three were braided using a 12K E-glass yarn with the braiding sizes of [11x11], [8x8] and [4x4], respectively. The relevant properties of the yarns are:

Yarn	E_f (axial)	ν_f	A_f
Graphite	235.0 GPa	0.22	0.48 mm^2
E-glass	72.4 GPa	0.20	2.12 mm^2

These preforms were all RTM-processed with the PR-500 epoxy. The epoxy in the bulk has the base-line properties:

$$E_m = 4.5 \text{ GPa} \quad \text{and} \quad \nu_m = 0.38.$$

The consolidated preforms were cut into 16 specimens suitable for 4-point bending test: the E-glass [11x11] and [8x8] each yielded two specimens of 305 mm in length; the E-glass [4x4] and all the graphite ones each yielded three specimens of 203 mm in length. For each of the 16 specimens, the braiding pitch h and the cross-section W_x, W_y were measured; the characterizing parameters α and γ were computed using (1-4), and the fiber volume fractions of the core, surface and corner areas via (5). The average over 2 or 3 replicates in each case is listed below:

Specimen	W_x, mm	W_y, mm	h, mm	α	γ	V_i, %	V_s, %	V_c, %
GR. [11x11]	12.17	12.33	3.41	45.4°	40.2°	60	48	31
GR. [11x7]	14.61	7.90	3.81	39.1	39.5	52	42	27
GR. [11x3]	13.70	4.60	3.61	45.2	41.9	49	38	25
GL. [11x11]	26.63	23.51	8.30	41.5	35.6	60	50	32
GL. [8x8]	18.92	17.50	7.77	42.8	36.4	64	53	35
GL. [4x4]	11.07	10.50	6.36	43.5	43.8	63	48	31

In the above, it is noted that the computed $V_x \approx V_y \approx V_s$.

Each specimen was strain-gaged with a pair of 90°-rosettes in the pure bending section, one mounted on the tensile side and one on the compression side. Load-responses were recorded in real-time, including strain-gage readings up to 1.5% strain on the compressive surface of the beam, the maximum bending defection up to 6 mm by a dial gage located at the center of the beam, and the video recording taken by a CCTV camera zoomed (up to 200x) at the center section of the beam during the entire test.

Global Responses.

The global response of the beam under loading is first studied from it's load-deflection (F-δ) curve recorded from the dial-gage. Fig.3a is the F-δ curve taken from a graphite [11x11] specimen and Fig.3b is one taken from an E-glass [11x11] specimen. The curves show a linear elastic regime up to the critical load (point A), whereby a sudden drop in the load occurs. Beyond this point, the beam continues to bear load and undergoes a prolonged inelastic deformation. From the CCTV video recording and other in-situ inspections, it was found that the beam is essentially damage-free in the linear regime. At the critical load, however, spontaneous damages suddenly occur in the compression zone of the entire pure bending length. This rather proliferate damage state is associated with the observed load-drop at point A.

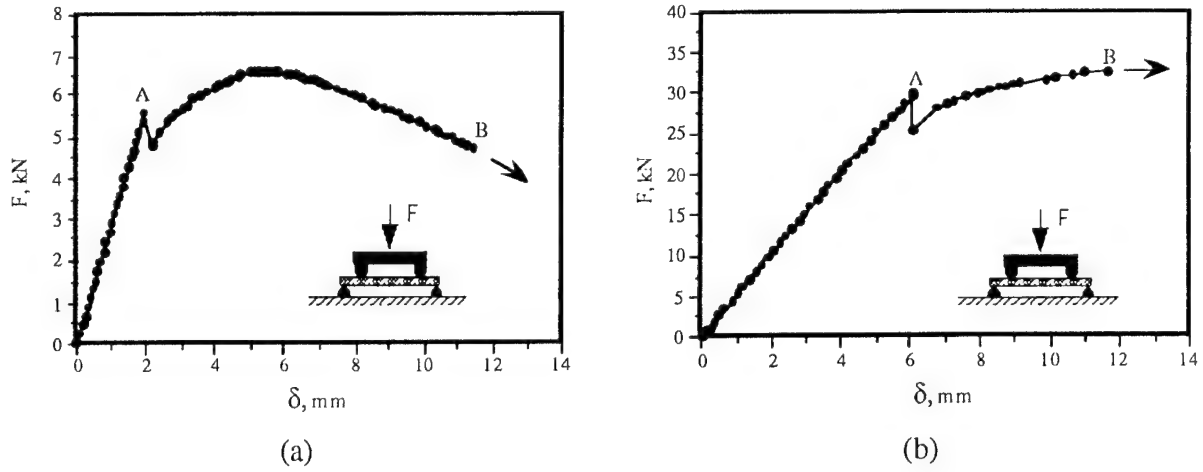

Fig.3: Load-deflection data for (a) graphite [11x11]; (b) E-glass [11x11].

In the linear response regime, the strain-gage readings provide a more accurate measure of the flexural strain ε_{fl} and the Poisson ratio ν_{zx} on the specimen's top and bottom surfaces. These measurements (average of 2 or 3 replicates) are listed below:

Specimen	ε_{fl}(+), με/(N-m)	ε_{fl}(-), με/(N-m)	ν_{zx}(+)	ν_{zx}(-)
GR. [11x11]	76.70	83.91	0.66	0.67
GR. [11x7]	179.00	165.86	0.80	0.80
GR. [11x3]	655.56	717.24	0.52	0.50
GL. [11x11]	14.31	15.35	0.43	0.40
GL. [8x8]	39.01	38.68	0.43	0.40
GL. [4x4]	234.83	232.37	0.46	0.46

In the above, $\mu\varepsilon = 10^{-6}$; the (+) sign refers to the tensile side and (-), the compressive side of the beam.

From the measured surface strain ε_{fl}/(N-m), the flexural modulus E_{fl} of the beam can be estimated by means of the property models outlined previously, that the beam is composed of a core, four surface layers and four corner areas. Omitting the details in the calculation, we simply state that the surface stress corresponding to the surface strain ε_{fl} per unit applied moment (N-m) is:

$$\sigma_{fl}/(\text{N-m}) = W_y/2I \tag{10}$$

where $I=I_i+I_s\ I_c$ as before. It then follows that $E_{fl} = \sigma_{fl}/\varepsilon_{fl}$.

Independently, the linear portion of the F-δ curves from the dial-gage reading also provides an estimate for the flexural modulus E_{fl}. At the same time, a theoretical estimate for E_{fl} is provided by (9). Thus, omitting the detailed calculation, a comparison between the experimental (average over 2-3 replicates) and the theoretical E_{fl} is given below:

Specimen	E_{fl}, strain-gage	E_{fl}, dial-gage	E_{fl}, theoretical
GR. [11x11]	41.3 GPa	37.2 GPa	38.0 GPa
GR. [11x7]	36.6	31.4	37.2
GR. [11x3]	30.5	23.7	29.8
GL. [11x11]	27.6	25.5	25.4
GL. [8x8]	26.7	26.0	27.1
GL. [4x4]	21.3	25.4	23.2

Note the relative range of disagreements in the above results.

Damage Modes and Mechanisms.

For each beam loaded to it's critical load, the compressive zone along the pure bending length suffers a sudden collapse. The associated damage modes can be explained from the photographs in Fig.4. Fig.4a is a video frame of the damaged surface taken from an E-glass specimen; note the surface of the pure bending length has suffered inter-yarn debonding. Fig.4b is a video frame of the frontal surface of the beam; the compression zone (top) has suffered similar damage while the tension zone (bottom) remained damage-free.

A magnified view (under the SEM) of the beam cross-section is shown in Fig.4c, Note the inter-yarn debonding in the compression zone; the debonding cracks follow the $\pm\alpha$-planes of the interior core. Recall that the $\pm\alpha$-plates intersect each other at $\approx 90^{o}$; the observed zigzagging debonding lines are in fact following the interface planes of the $[\pm\gamma]$ laminates.

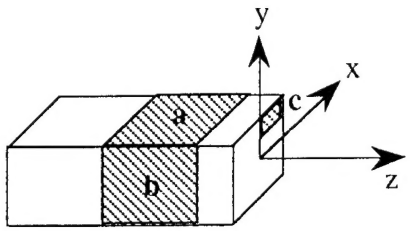

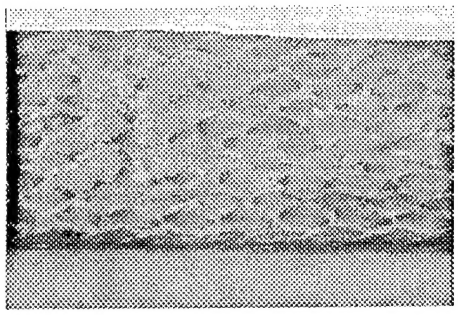

(a)

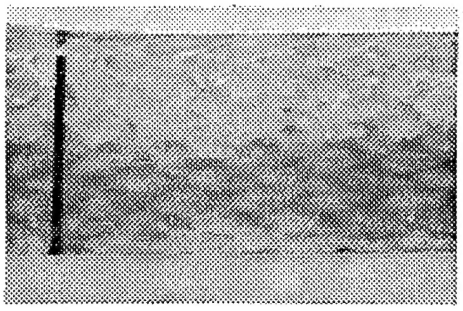

(b)

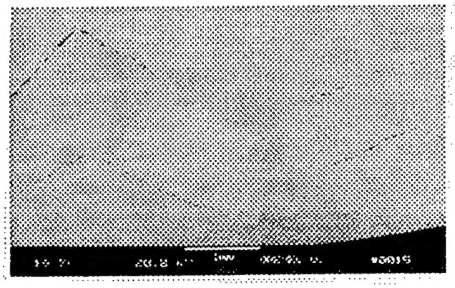

(c)

Fig. 4: Damage modes in tested specimens. (a), (b), (c): top, side and cross-sectional views of an E-glass [11x11] specimen.

Fig.4d, e and f are photographs taken from a graphite [11x11] specimen. They show, respectively, the damaged compressive surface of the beam where a thin epoxy-grazed layer has spalled, thus exposing the damaged yarn cells underneath; the damaged side surface in the compression zone near the top, revealing the familiar inter-yarn debonding pattern; and the damaged cross-section showing the zigzagging debonding cracks along the $\pm\alpha$-planes. These observations indicate that the core area in the compression zone fails suddenly due to interface shearing of the $\pm\alpha$-plates.

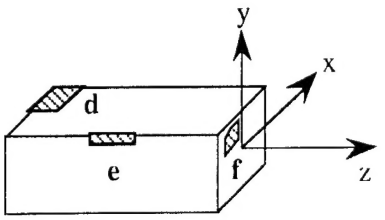

(d)

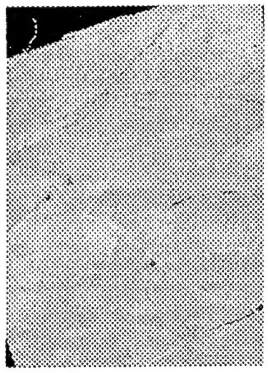

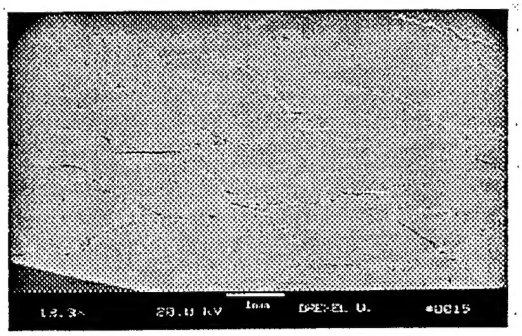

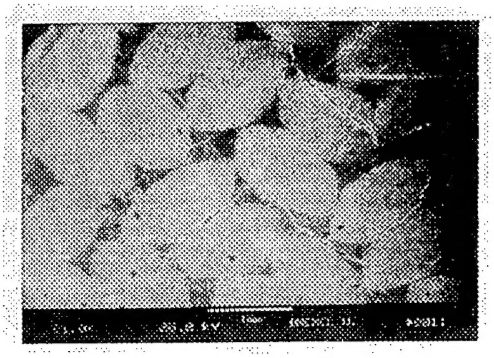

(e) (f)

Fig. 4 (continued):Damage modes in tested specimens. (d), (e), (f): top, side and cross-sectional views of a graphite [11x11].

Inter-yarn Shear Debonding Criterion.

The premise of the criterion is that the $\pm\alpha$-plates, being angle-plied laminates, suffered interface shear debonding as illustrated in Fig.5. Here, the α-plate be compressed axially with the strain ε_z; a lateral (tensile) strain $\nu_\alpha\varepsilon_z$ is induced due to Poisson effect. The in-plane shear strain in the α-plate is estimated as:

$$\gamma_\alpha \approx (1+\nu_\alpha)\,\varepsilon_z \qquad (11)$$

where ν_α is the Poisson ratio of the α-plate when subjected to the axial strain ε_z.

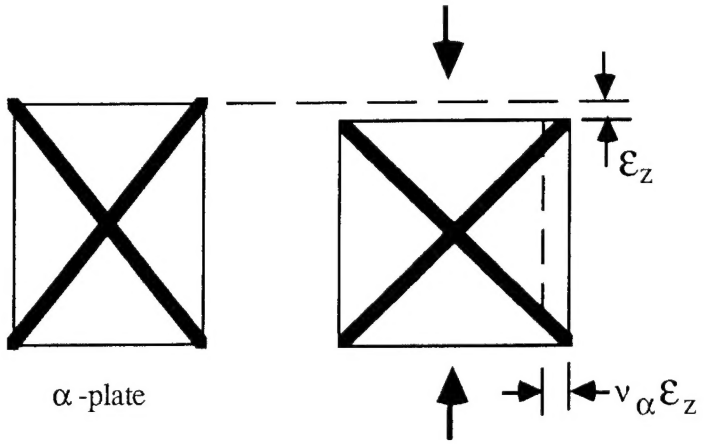

Fig.5: Local deformation of the α-plate under compression

Now, ε_z is also the bending strain of the interior core near the compression surface of the beam; and it is computed by:

$$\varepsilon_z = (Md)/(E_{fl}I) \qquad (12)$$

where M is the applied bending moment and $d \approx (W_y - \Delta y)/2$, the distance from the bending axis to the interior core near the compression surface.

At the critical load F_{cr} or the critical moment M_{cr}, the shear strain γ_α in the $\pm\alpha$-plates reaches the critical value $(\gamma_\alpha)_{cr}$. The latter is considered a material condition governing the onset of interface debonding of the $\pm\alpha$-plates. Since the moment is uniform in the pure bending length, the α-plates near the compressive surface collapse spontaneously. Calculations of the critical $(\gamma_\alpha)_{cr}$ for the specimens tested have yielded the following values (average over 2-3 replicates):

Specimen	M_{cr},N-m	$(\gamma_\alpha)_{cr}$ Range (Average)
GR. [11x11]	54.61	0.58-0.83% (0.68%)
GR. [11x7]	18.36	0.46-0.48% (0.47%)
GR. [11x3]	7.65	0.55-0.62% (0.58%)
GL. [11x11]	580.54	1.16-1.21% (1.20%)
GL. [8x8]	315.18	1.48-1.53% (1.51%)
GL. [4x4]	56.41	0.93-1.66% (1.33%)

Note that the $(\gamma_\alpha)_{cr}$ values do exhibit the sort of scatter normally found in fracture and strength properties in composites. If the nominal value of $(\gamma_\alpha)_{cr} = 0.6\%$ for the graphite and 1.35% for the E-glass specimens are used to predict the critical F_{cr} or M_{cr} in conjunction with (11-12), the predicted values would be fairly agreeable with the experimental values. Clearly, independent validations are necessary in order to ascertain the applicability of the proposed criterion in a wide range of loading conditions. Some works related to the latter work are in progress.

Acknowledgments: The results reported in this paper were obtained during the course of research supported by the U. S. Air Force Office of Scientific Research and by Boeing Defense & Space Group, Helicopters Division.

REFERENCES

1. Wang, Y. Q. and Wang, A. S. D., "On the Topological Yarn Structure in 3-D Rectangular and Tubular Braided Preforms", *J. Composites Science & Technology* , Vol. 51, p. 575.

2. Chamis, C. C., "Simplified Composite Micromechanics Equations for Hygral, Thermal and Mechanical Properties," *SAMPE Quart.* April, p.14.

3. Pagano, N. J., "Exact Moduli of Anisotropic Laminates," in *Mechanics of Composite Materials,* Ed. G. P. Sendeckyj. Academic Press, New York, p.23.